CHEMICAL REVIEWS

Review

pubs.acs.org/CR

Chemistry of Atmospheric Brown Carbon

Alexander Laskin,*[,†] Julia Laskin,*[,‡] and Sergey A. Nizkorodov*[,§]

[†]Environmental Molecular Sciences Laboratory and [‡]Physical Sciences Division, Pacific Northwest National Laboratory, Richland, Washington 99352, United States

[§]Department of Chemistry, University of California, Irvine, Irvine, California 92697, United States

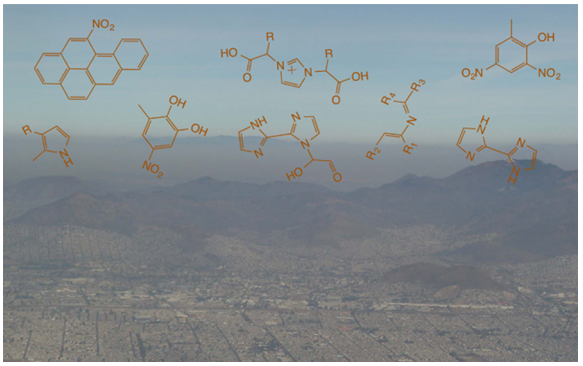

CONTENTS

1. INTRODUCTION

Organic carbon (OC) accounts for a large fraction of atmospheric aerosol and has profound effects on air quality, atmospheric chemistry, and climate forcing. The molecular composition of OC and its evolution during various processes of atmospheric aging have been the subject of extensive research over the past decade (see reviews of Ervens et al.,[1] Hallquist et al.,[2] Herckes et al.,[3] Carlton et al.,[4] Kroll and Seinfeld,[5] Rudich et al.,[6] and Kanakidou et al.[7]). Although many fundamental advances have been reported in these studies, our understanding of the climate-related properties of atmospheric OC still is incomplete, and the specific ways in which OC impacts atmospheric environment and climate forcing are only beginning to be understood. This review covers one topic of particular interest in this area: the environmental chemistry of light-absorbing OC aerosol and its impact on radiative forcing.

There are two major aerosol effects on the propagation of radiation through Earth's atmosphere. The cloud albedo effect,

Special Issue: 2015 Chemistry in Climate

Received: October 24, 2014
Published: February 26, 2015

DOI: 10.1021/cr5006167
Chem. Rev. 2015, 115, 4335−4382

or indirect effect, arises from nucleation of cloud droplets and the formation of ice crystals on atmospheric particles. The direct effect refers to direct absorption and scattering of solar and terrestrial radiation by aerosols. Most organic aerosols (OA) can be characterized as "white" because they efficiently scatter visible radiation. However, a significant and highly variable fraction of carbonaceous and organic aerosols absorbs radiation.[8−12] The best-known type of light-absorbing carbonaceous aerosol is "black carbon" (BC), which represents soot-like particulates generated by fossil fuel combustion and biomass burning.[12] BC absorbs solar radiation over a broad spectral range, from ultraviolet (UV) all the way into infrared (IR). The effects of BC are especially significant in areas that rely on burning biomass and coal.[12−14] Most OC compounds absorb IR and UV radiation strongly but are relatively transparent to visible (vis, 400−700 nm) and near-IR (700−2500 nm) wavelengths. However, certain types of OC absorb radiation efficiently in the near-UV (300−400 nm) and vis ranges. A new term, "brown carbon" (BrC), has emerged in recent scientific literature to describe this type of aerosol, characterized by an absorption spectrum that smoothly increases from the vis to UV wavelengths.[11,15−17] In addition to their direct effects on vis radiation, both BC and BrC immersed in cloud droplets absorb light and facilitate water evaporation and cloud dispersion, an additional indirect effect that counteracts the cooling effect of cloud droplet nucleation by aerosols.[18]

Figure 1[19] shows a range of atmospheric carbonaceous compounds subdivided into operationally defined classes on the basis of the most common methods of bulk particulate matter (PM) analysis. At the top of the chart, BC compounds have the lowest volatility and strongest light-absorption properties. While BC is inherently complex,[11,12,20] its basic chemical structure and optical properties are reasonably well-known. In BC, carbon atoms are organized in two-dimensional honeycomb graphitic layers stacked together perpendicular to the planes of the layers. A large number of electrons delocalized along the extended network of graphitic layers defines the strong broadband absorption properties of the BC material with only weak (λ^{-1}) spectral dependence of the absorption coefficient.[11,21] The bottom of the chart corresponds to volatile organic compounds with characteristic absorption in the UV spectral range. These organic species are highly relevant to atmospheric photochemical processes, but they have nearly no direct implications for radiative forcing determined by the absorption of visible radiation. Between the two extremes of the chart, there is a broad range of moderately volatile (refractory) organic compounds with different and poorly characterized molecular structures. Among them, a subset corresponds to colored compounds with optical properties relevant to the BrC material. In contrast to BC, the light-absorption coefficient of BrC has strong wavelength dependence (λ^{-2}–λ^{-6}) with absorption increasing sharply from the vis to the UV range.[17,21,22] The complexity of light-absorbing organic compounds and variations in their relative concentrations make it difficult to characterize the molecular composition and determine which types of molecules or molecular aggregates dictate the optical properties of BrC. One goal of this review is to assess the current state of knowledge regarding the molecular structures of these BrC compounds on the basis of analysis of recent field and laboratory measurements.

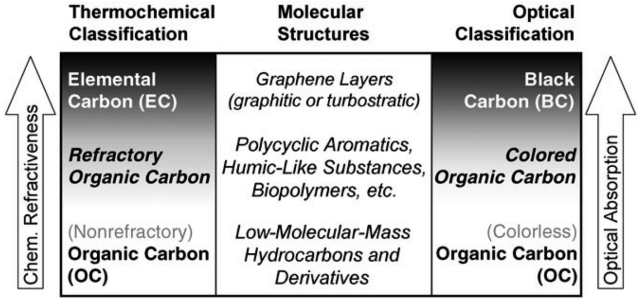

Figure 1. Optical and thermochemical classification of atmospheric carbonaceous particulate matter. BrC material is an ensemble of light-absorbing (colored) organic compounds with a variety of molecular structures and molecule-specific optical properties. (Reprinted with permission from ref 19. Copyright 2005 Wiley-VCH Verlag GmbH & Co.).

Quantifying BrC contribution to light absorption is critically important for the accurate interpretation of the aerosol optical depth (AOD), the atmospheric column's light extinction due to both scattering and absorption. AOD data are retrieved from ground-based and satellite measurements and used in climate model predictions. Retrieval modeling requires knowledge of the key optical properties, specifically the extinction coefficient and single-scattering albedo (SSA). These quantities depend on the wavelength, particle size distribution, spatial distribution of different light-absorbing materials within individual particles, and optical properties of these materials. Current climate modeling approaches often assume that BC and mineral dust are the only two significant types of light-absorbing aerosols on the global scale, and they treat OA as a purely scattering component that leads to climate cooling.[23,24] However, there is a growing amount of data indicating that BrC is widespread in specific geographic areas and urban environments, where it may contribute substantially or even dominate the total aerosol absorption at specific wavelengths.[15,16,23−28] These reports highlight the need for improved understanding of OA absorption properties, providing motivation for numerous laboratory, test facility, and field studies focused on fundamental understanding of the chemical composition and absorption properties of BrC.

Despite these efforts, our understanding of the relationship between the chemical composition and optical properties of BrC remains limited. BrC sources are not well characterized, and little is known about the mechanisms and rates of its atmospheric transformations. Emissions of "primary BrC" have been attributed to forest fires and biomass burning,[15,29,30] residential heating by wood and coal,[31] and biogenic release of fungi, plant debris, and humic matter.[32−34] In addition, recent laboratory studies have demonstrated that high molecular weight (high-MW) light-absorbing compounds can be produced in atmospheric multiphase reactions between the gas-phase, particulate, and cloud microdroplet constituents.[35−42] Thus, this type of BrC produced in the atmosphere as a result of chemical processes can be categorized as "secondary BrC". Because ambient particles are transported over long distances, both primary and secondary BrC may play an important role in the atmospheric environment, thereby affecting the accuracy of satellite data retrieval and climate model predictions.

This review focuses on the current understanding of the chemistry of atmospheric light-absorbing organic compounds relevant to BrC formation and is organized as follows: after the

DOI: 10.1021/cr5006167
Chem. Rev. 2015, 115, 4335−4382

Introduction, section 2 presents a summary of field observations and modeling studies describing trends in air pollution and climate forcing attributed to BrC at different geographic locations and regional variations of BrC concentrations. In the same section, we summarize the primary and secondary sources of BrC inferred from field observations and factors affecting the evolution of its physicochemical properties. Section 3 describes optical measurements and analytical chemistry approaches used for molecular characterization of BrC aerosols and individual chromophores. Section 4 presents a comprehensive account of past and ongoing studies regarding the molecular characterization of BrC constituents and understanding the fundamental relationship between aerosol chemistry and its effects on the optical and chemical properties of this important class of complex atmospheric particles. Section 5 summarizes the known aspects of BrC chemistry and presents the authors' outlooks and perspectives on selected topics for future research in this area.

2. EVIDENCE AND IMPACT OF LIGHT-ABSORBING ORGANICS IN THE ATMOSPHERE

2.1. Attribution of BrC Based on the Wavelength Dependence of Light Absorption and Estimates of Its Global and Regional Impact

Approximately a decade ago, BrC was first described in the literature in a number of experimental studies[11,17,27,31] where carbonaceous aerosols were distinguished on the basis of the spectral dependence of their light-absorption with respect to the empirically defined power law relationship described by eq 1

$$\mathrm{MAC_a}(\lambda) = K\lambda^{-\mathrm{AAE}} \quad (1)$$

where $\mathrm{MAC_a}$ is an effective mass absorption coefficient attributable to particles in an aerosol, measured in units of $\mathrm{cm^2\ g^{-1}}$; K is a factor that includes aerosol mass concentration; λ is the wavelength (nm); and AAE is the absorption Angström exponent. The reason for introducing the subscript "a", as well as other common parameters used in aerosol absorption measurements and relevant experimental methods, is discussed in Section 3 of this review. Here, we summarize the most important experimental observations and modeling studies that made the distinction between BC and BrC aerosols, largely based on the observed AAE values.

When absorption is dominated by graphitic-like BC aerosols, the corresponding AAE values are close to 1, which is typical for areas with abundant soot emissions from engineered high-temperature-combustion processes, such as energy production by power plants or motor vehicles.[11,42,43] The steep increase of absorption toward shorter wavelengths with characteristic values of AAE in excess of 1 was attributed to aerosol organic constituents from inefficient combustion at lower temperatures, such as biomass burning. In one of the early studies, Kirchstetter et al.[27] distinguished the BC and BrC components of biomass smoke by separating organic constituents from insoluble soot-like carbon using solvent extraction. As illustrated in Figure 2, the overall spectral dependence of the untreated samples showed a strong wavelength dependence with AAE = 2.2, which, after solvent extraction of the organic constituents, was reduced to AAE = 1.3. The authors concluded that organic components of aerosol contribute substantially to light absorption at wavelengths shorter than 600 nm with AAE > 2. Following this seminal work, deconvolution of the spectral

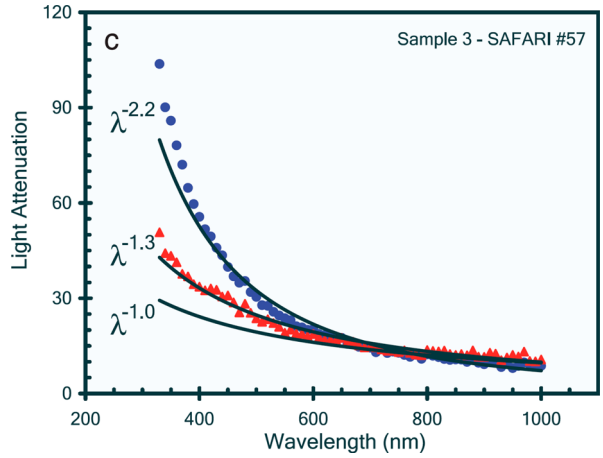

Figure 2. Measured light attenuation from an untreated sample of biomass-burning aerosol from savanna fires in Africa (SAFARI 57 is the sample ID tag). Circles (blue) indicate an untreated sample, and triangles (red) denote a sample with organic constituents removed by acetone extraction. Angström exponents were determined by fitting the data with a power law equation. The λ^{-1} trend line expected for BC is shown for comparison. (Reprinted with permission from ref 27. Copyright 2004 Wiley-Blackwell)

dependence of aerosol light absorption became a common method for attributing light absorption to BC and BrC components. However, because of multiple effects related to external versus internal mixing of BC, OC, and BrC in airborne particles, the threshold value of AAE that distinguishes BC and BrC in field samples is somewhat uncertain.[21,44] For instance, coating BC particles with nonabsorbing OC materials results in a lensing effect that focuses more photons on the strongly absorbing BC core.[45,46] The extent of this effect is determined by the wavelength-dependent refractive index of the OC material, particle morphology, coating thickness, and ratio between the core/shell dimensions.[44,47] Lack and Cappa's recent modeling study showed that AAE values, ranging from 1−1.6, can be observed for internally mixed OC/BC particles and suggested that aerosols with AAE exceeding 1.6 should be classified as BrC.[44]

The importance of wavelength-dependent absorption by BrC has been highlighted in a number of recent climate modeling studies,[16,26,48] as well as demonstrated via assessment of the satellite-based remote sensing retrievals[49] and analysis of AOD data from Aerosol Robotic Network (AERONET) spectral measurements.[25,48,50,51] The magnitude of BrC contribution to radiative forcing of climate by absorption of incoming solar radiation on a planetary scale is estimated to be in the range of 0.1−0.25 W $\mathrm{m^{-2}}$, which is approximately 25% of the radiative forcing by BC (1.07 W $\mathrm{m^{-2}}$).[16] Regional effects of BrC over major areas of biomass burning and biofuel combustion, such as South and East Asia, South America, and subtropical Africa, may be substantially higher than 0.25 W $\mathrm{m^{-2}}$, suggesting that BrC may be the dominant atmospheric light-absorbing material in these regions.[16] The BrC warming effect is comparable to typical estimates of cooling by nonabsorbing OA (−0.1 to −0.4 W $\mathrm{m^{-2}}$). However, it is not clear if these effects compensate each other or compete to a different extent,[26] depending on the chemical composition, optical properties, and atmospheric concentrations of BrC and nonabsorbing OA. Considering the strong spectral dependence of BrC absorption, its wavelength-specific effects may be even more substantial. Spectral analysis

DOI: 10.1021/cr5006167
Chem. Rev. 2015, 115, 4335−4382

of AERONET data from summer months in Southern California showed that light absorption by BrC at 440 nm is ~40% of the light absorption by BC at this wavelength, while BrC contributes only 10% to the light absorption at 675 nm.[25] Lin et al.[52] modeled the effects on radiative forcing by anthropogenically influenced OA, including the effects of its deposition on snow. Their work showed that absorption by BrC corresponds to between 27% and 70% of the BC absorption predicted in the model and accounts for a measurable fraction of the overall forcing by OA.[52] A recent scientific assessment of the role of BC in climate by Bond and co-workers[12] indicated that a fraction of presently used BC estimates inferred from AOD observations may in fact be attributable to BrC. A later global modeling study of Wang et al.[48] corroborated this assertion and showed that explicit inclusion of the wavelength-dependent absorption by BrC and the absorption enhancement attributed to the lensing effect in mixed OC/BC particles reduces the model bias in prediction of absorption aerosol optical depth (AAOD) measurements at AERONET sites worldwide. The same study reported BrC contributions of 25%, 20%, and 15% of the total AAOD at 440 nm simulated globally for the US, Europe, and East Asia, respectively. However, while inclusion of BrC in models improves predictions of AAOD observations and especially its wavelength dependence (AAE values), the modeling results largely underpredict the AERONET observations.[16,48,52]

Significant light absorption by BrC in the UV spectral range may lead to substantial reduction of photolysis rates for photochemically active gaseous compounds, affecting concentrations of atmospheric oxidants. For example, a modeling study by Jiang et al.[53] showed that suppression of downward solar radiation by BrC formed during large-scale forest fires in the western United States resulted in reduced isoprene emissions, reduced $J(NO_2)$ photolysis rates, and a consequent drop in O_3 concentrations by more than 15%. Similar reductions of O_3 and OH concentrations in Mexico City, by up to 17% and 9%, respectively, were attributed to BrC impact on photolysis rates.[54] The sensitivity analysis reported in that study showed that, under certain conditions, the O_3 reduction effects could be as high as 40%. All of the aforementioned modeling studies indicated large uncertainties and a lack of fundamental data about BrC variability with respect to its sources, chemical composition, optical properties, formation mechanisms, atmospheric evolution, and scavenging processes. This increasing evidence of BrC effects on climate and the atmospheric environment has motivated a range of focused analytical and physical chemistry studies, summarized in this review.

2.2. Sources and Physicochemical Properties of BrC

On a global scale, BrC is consistently observed in geographic areas influenced by biomass and biofuel burning. BrC emissions are usually caused by uncontrolled, disastrous events, such as large-scale forest and savanna fires; prescribed smoldering fires used in forest management; and extensive use of wood and other biofuels for heating, cooking, and energy production in developing countries with high population densities.[15] Typical emissions contain internal and external mixtures of BC, BrC, nonabsorbing OA, and inorganic materials in different proportions that depend, in a complicated way, on the biomass/biofuel types and burning conditions.[17] Because of this variability, corresponding emission factors (EF) are quite uncertain, even for a broadly defined BrC type based on the AAE > 2 criterion. Most studies report EF values for $PM_{2.5}$ emissions, which typically range from 10 to 20 g/kg fuel for the combustion of biomass from North America.[55−59] BrC emissions are only a fraction of those, but estimates of their EF values are rarely reported. We are aware of only one study where EF values for BrC emissions from forest fires in the southeastern United States were reported. In that study, BrC emissions were estimated at the level of 1−1.4 g/kg fuel, which was ~50% of BC emissions (1.2−2.1 g/kg fuel) in this area.[59] However, little is known about BrC EFs from different types of sources or from other geographic locations. Most existing reports attribute BrC to primary organic aerosols (POA) in these emissions. However, recent studies indicate that secondary organic aerosols (SOA) that form from the oxidation of volatile organic compounds (VOCs) present within biomass smoke also may be a source of BrC.[60]

Atmospheric humic-like substances (HULIS) formed by aqueous in-cloud processing and oligomerization of water-soluble organics have been recognized as an important component of BrC.[17,61] In one of the early studies, Mukai and Ambe[62] reported that the humic acid extracts were very similar in composition to extracts from biomass smoke particles. This led the authors to suggest that HULIS in atmospheric aerosols were mostly compounds containing polycyclic ring structures with hydrocarbon side chains containing hydroxyl, carboxyl, and carbonyl groups. In later studies, the term "poly(carboxylic acid)s" was introduced to denote atmospheric HULIS.[63] More recent studies[64−68] of the chemical composition of atmospheric HULIS reported the abundant presence of relatively small organic molecules, such as nitrocatechols, aromatic carboxylic acids, terpenoid acids, and nitrooxy organosulfates, that cannot be categorized as "macromolecules" or "poly(carboxylic acid)s". They are rather low-MW compounds of different chemical nature that resemble SOA constituents formed through atmospheric oxidation of anthropogenic and biogenic VOCs.[61]

Atmospheric HULIS formation occurs during cloud processing of smoke from biomass burning.[64,66,69−72] However, even in areas impacted by forest fires, HULIS structures may incorporate additional organics from natural biogenic emissions, leading to the formation of different molecular structures. Furthermore, biomass burning is not the only source of HULIS in the atmosphere. HULIS are also produced through multiphase chemistry of organic constituents derived from other anthropogenic and natural sources,[3,68,73,74] such as vehicle exhaust and fossil fuel combustion in urban areas[75,76] and biogenic[77] and marine[78] emissions.

Optical properties of BrC from different emission sources are highly variable. A number of studies[27,34,79−86] have examined the differences in light absorption by BrC produced from burning different types of biofuels under varied combustion conditions. A detailed survey of these studies is outside the scope of this review. Here, we provide only a qualitative summary of the most consistent observations (readers interested in more specific quantitative data can refer to the original reports). Characteristic UV−vis spectra of ambient BrC are mostly featureless because they contain a variety of individual chromophores and supramolecular aggregates with different absorptivities and concentrations. Remarkable variability in the spectral dependence has been reported for BrC with AAE values ranging from just greater than 2 to as high as 11. This extensive range is inherent to the chemical variability of BrC constituents and implies that no single AAE value can

DOI: 10.1021/cr5006167
Chem. Rev. 2015, 115, 4335−4382

be selected as an intrinsic parameter describing BrC in models. BrC constituents exhibit characteristics of polar molecules and contain both water-soluble and insoluble components. The water-soluble fraction of BrC is usually below 70%, while nearly 90% of BrC can be extracted into polar organic solvents, such as methanol and acetonitrile. Of note, the water-insoluble fraction of BrC has greater absorption per unit of mass than the water-soluble fraction.[69,84,86] In biomass-burning emissions, the relative abundance of BrC and its light-absorption properties are strongly affected by the temperature of the combustion process and moisture content, while the type of fuel itself is less important.[69,84,86]

Depending on its composition and atmospheric conditions at a specific geographic location, the physical form of airborne BrC can be quite different. For example, BrC formed in aqueous media of deliquesced particles and cloud droplets is a complex mixture of fully dissolved molecules and colloidal aggregates that can change properties upon evaporation and hydration cycles. Typically, water-soluble and water-insoluble (colloidal) OC are referred to in the literature as "WSOC" and "WIOC", respectively. Depending on the solubility of WSOC components and the presence of WIOC and other nonsoluble heterogeneous inclusions, evaporation of these droplets may lead to core−shell, engulfed, and homogeneous mixing states of particles, which, in turn, can have profound effects on their optical properties.[87] Similarly, in biomass-burning events, BrC is coemitted with BC, inorganic salts, and fly ash, producing internally and externally mixed particles where BrC components are present in different relative abundance. This inherent complexity of airborne particles presents a challenge for extraction and chemical analysis of BrC materials.

Figure 3 shows electron microscopy images of so-called "tar balls", a prominent type of largely homogeneous BrC particles commonly detected in smoke emissions from smoldering burns of biofuels.[29,88−94] X-ray spectro-microscopy analysis of these particles showed that their spectral and chemical characteristics were remarkably different from those of BC but quite similar to the characteristic properties of HULIS: an amorphous carbon composition with a very modest degree of sp^2 hybridization (tar balls, 10%; HULIS, 7%−30%); a high extent of oxygenation (tar balls, O/C = 45/55; HULIS, O/C ∼ 40/60); and the absence of any elements other than C, O, H, and N.[95,96] The unique spherical morphology of these particles, very low volatility of their components, and unusual stability under the electron beam of a transmission electron microscope (TEM) afforded direct measurements of their optical properties at a single-particle level. The approach employed electron energy loss spectroscopy (EELS) of individual tar ball particles followed by quantitative analysis of EELS spectra to derive complex dielectric constants and refractive indexes for a broad optical range of 380−1000 nm.[89] The retrieved imaginary refractive index values for this type of BrC are comparable to those of BC for most of the UV−vis spectral range and even exceed them at shorter wavelengths. In this case, relative contributions of BrC and BC in the aerosol-containing mixed tar balls and soot particles cannot be discriminated using optical measurements over ensembles of airborne particles or via collected bulk samples. While the molecular composition of tar balls is not known, indirect observations[97] suggest they are composed of extremely low volatility organic compounds, or ELVOCs (defined, on the basis of the volatility basis set,[98] as chemical compounds with saturation concentrations less than 10^{-4} $\mu g\ m^{-3}$). Tar balls probably are the most absorbing and most refractory BrC material that can be easily observed under the vacuum conditions of an electron microscope (although results of Saleh et al.[97] suggest that the imaginary refractive indexes reported by Alexander et al.[89] could be too high due to partial volatilization of the less-absorbing organics from the particles). Other BrC materials have higher volatilities, characteristic of common SOA (10^{-1}−10^{1} $\mu g\ m^{-3}$), and are much more susceptible to electron beam damage, limiting application of the TEM/EELS approach for particle-specific detection and characterization of the more common BrC particles.

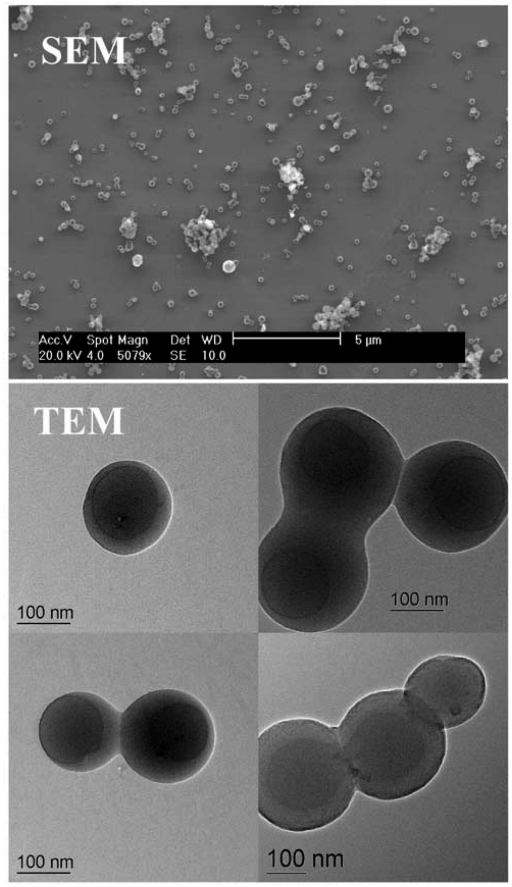

Figure 3. Electron microscopy images of tar balls, a special type of BrC, shown as individual spherical particles (TEM images) and their large agglomerates (SEM image). (Reprinted with permission from ref 92. Copyright 2005 Wiley-Blackwell.)

Either in primary emissions or during secondary aerosol formation, BrC coexists with a multitude of other materials, comprising complex mixtures of externally and internally mixed particles. Notably, depending on the particle mixing state, substantially different absorption properties of particle ensembles may be observed in the presence of the same amount of BrC. Modeling particle optical properties based on Mie theory suggests that absorption by core−shell mixed particles composed of absorbing/nonabsorbing materials may be a factor of 2−5 times larger than by particles with a homogeneous distribution of the same materials.[97] Experimental detection of the BrC mixing state and its effect on the overall optical properties is quite challenging, especially in field studies. Nevertheless, novel photoacoustic optical measurements, employing comparisons between measured properties of original and thermo-denuded particles, have allowed assess-

DOI: 10.1021/cr5006167
Chem. Rev. 2015, 115, 4335−4382

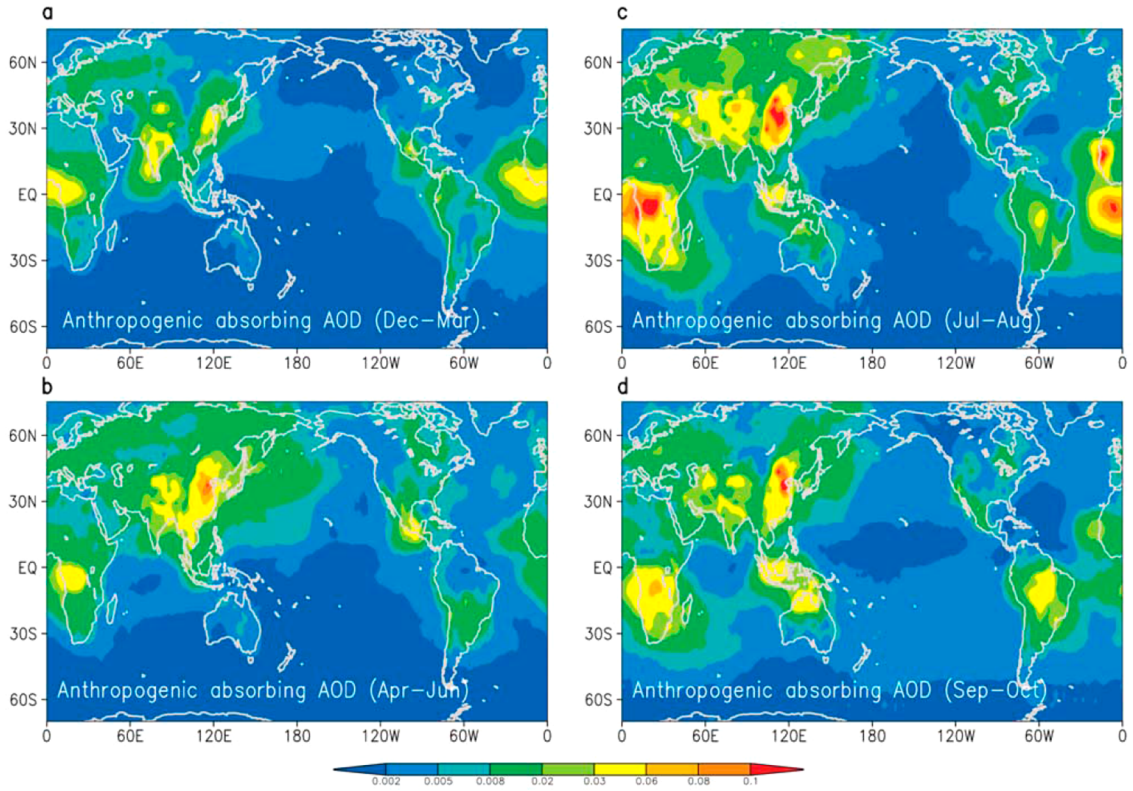

Figure 4. Calculated global distribution of anthropogenic absorbing aerosol optical depth (AAOD), in the Northern Hemisphere during (a) the dry season, December–March; (b) a transition period, April–June; (c) the monsoon season, July–August; and (d) a transition period, September–October 2001–2003. (Reprinted with permission from ref 15. Copyright 2007 Wiley-Blackwell).

ment of BrC variability in particle mixing states.[30,99] The results indicate that MAC_a values at 405 nm observed for internal mixtures of ambient BrC can increase by 50% compared to MAC_a values of the BrC material itself, if it was present as an external component.[100]

As already noted, BrC is closely related to atmospheric HULIS in that they are either water-soluble or can form colloidal micelle-like aggregates suspended in atmospheric water.[61,79] Hydration experiments using an environmental scanning electron microscope (ESEM) showed that even tar balls (the most refractive BrC material) begin to absorb water at 92%–99% relative humidity (RH) and are subsequently fully dissolved in water droplets growing under supersaturation conditions (cloud processing).[92] On the basis of these observations, it is reasonable to assume that BrC materials deposited on particles can "wet" surfaces of insoluble particles by forming a film of aqueous BrC brine at high RH, making them sufficiently hygroscopic to nucleate cloud droplets. Consequently, hydration cycles and cloud processing of particles containing BrC material and its precursors may induce physical changes in particle morphology and redistribute its BrC and other components, modifying the particle mixing state and causing different effects on optical properties.[101–103] The same processes may induce the formation of new chromophores from nonabsorbing precursors.[35,38,104] The large molecular size of BrC components and the presence of oxygen-containing functional groups make those species surface active, which may facilitate chemical transformations of BrC material via reactions at gas–water interfaces. Furthermore, either at the interface or dissolved inside cloud and fog droplets, BrC species are susceptible to atmospheric aging processes, such as direct photolysis and photochemical oxidation by NO_2, O_3, H_2O_2, OH, and other oxidants. It follows that during the atmospheric lifetime of BrC, its physicochemical properties are not static and may exhibit dynamic changes that are insufficiently understood—even at the phenomenological level.

The effects of atmospheric aging are complex and can either enhance or reduce light absorption by BrC. For example, aqueous-phase aging of organic material may form light-absorbing oligomeric products, as indicated in studies where increased O/C ratios of OA were found to correlate with enhanced light absorption.[60,105] Conversely, direct photolysis by sunlight may efficiently photobleach BrC with different photolysis rates highly specific to certain types of chromophores.[106,107] Additional complications stem from the fact that the overall absorption properties of some BrC materials may be determined by the very minor presence of highly absorbing chromophores with unique molecular structures and precursor-specific chemistry in their formation and evolution.[35,108,109] Combined, the complexity of BrC and dynamic changes in its physicochemical properties make it especially challenging to investigate factors governing the relationship between the continuously evolving BrC composition and its absorption properties.[47,103,110–112] A number of excellent comprehensive reviews have been published describing BrC optical properties,[11] figures of merit and applications of novel broadband techniques for BrC measurements,[8,87] and the fundamental theory of light absorption by complex multicomponent particles.[22,113] However, understanding the effects of BrC molecular composition and chemistry on its optical properties still is in its early stages. This review presents the first

DOI: 10.1021/cr5006167
Chem. Rev. 2015, 115, 4335–4382

comprehensive account of BrC chemistry based on knowledge accumulated to date.

2.3. BrC at Different Geographic Locations

Anthropogenic emissions produce both BrC and BC materials as a complex blend of externally and internally mixed particles. These particles contribute collectively to a phenomenon called "atmospheric brown clouds" (ABC), observed on both global and regional scales. The term "ABC" was first introduced by Ramanathan et al.[15] in a study that focused on a global-scale integrated analysis of various satellite and surface network (AERONET) data sets, assisted with observationally constrained models simulating aerosol basic composition, radiation, and transport. Figure 4 shows season-specific calculated values of the anthropogenic AAOD color-coded over the world map. On the basis of the criteria of AAOD > 0.03 and AOD > 0.3, the following regions were categorized as the regional hot spots and identified on the map: (1) South Asia−Indo-Gangetic Plain, (2) Eastern Asia, (3) Amazon basin, (4) the Indonesian region, and (5) Southern Africa. Remarkably, the geographic areas of ABC identified in that study and seasons when AAODs exhibit the highest values match those regions that are heavily influenced by either regional forest fires or enhanced consumption of biomass fuels in densely populated developing countries. The original Ramanathan et al.[15] study and a number of additional global modeling studies[52,114−117] recognized significant contributions from the BrC component to the observed AOD and AAOD values and emphasized the critical need for a quantitative breakdown of the BrC and BC contributions and advanced characterization of BrC for improved climate predictions. Despite many studies focused on the characterization of atmospheric BC in these areas and quantitative assessment of radiative forcing by BC,[28,118−123] a detailed characterization of BrC was not pursued because of its inherent chemical complexity. Still, a number of very recent reports have focused on the description of BrC relevant to the identified hot spots and provided a number of interesting area-specific observations. The majority of these studies have been conducted in the first three areas (South Asia, East Asia, Amazonia), where infrastructure for atmospheric field research is sufficiently supported by local governments and authorities.

2.3.1. South Asia−Indo-Gangetic Plain. Srinivas and Sarin reported measurements of BrC in field samples of aerosols collected at a ground site in northeast India and aboard the research ship *Sagar Sampada* during its cruise in the Bay of Bengal and Arabian Sea.[124−126] These field experiments were designed to collect and characterize aerosols typical for the wintertime (December−March) transport of atmospheric pollutants from the Indo-Gangetic Plain to the Bay of Bengal areas. Analysis of atmospheric concentrations and absorption properties of WSOC extracts indicated the presence of abundant water-soluble BrC in the air transported from the Indo-Gangetic Plain to the Bay of Bengal. Notably, reported atmospheric mass concentrations of OC consistently were 3−11 times higher than BC. In turn, the WSOC fraction of OC was leveled at 30%−100% with net concentration values of WSOC = 3−30 μg m^{-3} (10%−23% of $PM_{2.5}$ mass). The measured absorbance of WSOC was in the range of MAC_{bulk} = 0.2−1.2 × 10^4 cm^2 g^{-1} between 700 and 300 nm (AAE = 8.3 ± 2.6) with the upper end of the reported values lower than those of BC (~10^5 cm^2 g^{-1}) by a mere factor of 10. (Here and below, the subscript "bulk" emphasizes the fact that the primary measured quantity is absorbance of a bulk PM extract from a filter; a subscript "a" will be used for more direct measurements on aerosols.) Considering that reported mass concentration of OC was higher than that of BC by the same factor of 10, these results presented convincing evidence that BrC is an important climate-forcing contributor in this area. Additional studies of WSOC collected in Delhi reported even higher values of the BrC absorption, MAC_{bulk} = (1.1−2.7) × 10^4 cm^2 g^{-1} (AAE = 3.1−9.3), and attributed BrC sources to modern carbon from both biomass-burning and biogenic SOA based on dual carbon isotope (^{13}C and ^{14}C) signatures.[127,128] A few other studies discussed specific optical properties and the significance of BrC sources unique to the South Asia region, including region-specific agricultural crop residue burning[129] and traditional religious rituals unique to the area.[90,130]

2.3.2. East Asia. Field studies of BrC optical properties and composition in East Asia indicate that biomass burning is not the only source of BrC in that region. Thermochemical analysis and classification of WSOC fractions of aerosols sampled at the Korea Climate Observatory in Gosan in 2005 showed that a major fraction of WSOC were high-MW secondary products likely produced through fossil fuel combustion.[131] Recently, these conclusions were corroborated by radiocarbon isotope analysis of WSOC samples collected at the same site during the polluted air outflow events from northern China in 2011.[127] The study showed high fractions (30%−50% of OC) of fossil carbon sources characteristic for this area. The reported 365 nm absorption values of WSOC for air masses during the outflow episodes were MAC_{bulk} = (0.2−1.1) × 10^4 cm^2 g^{-1} and AAE = 5.6−7.7. In a separate study of aerosol samples from the same site collected in 2010, Chung et al.[132] reported substantially higher values of light absorption at 530 nm by the overall OC (both WSOC and WIOC) with values of MAC_a = (0.8−2.0) × 10^4 cm^2 g^{-1} and AAE = 1.6−1.8, exceeding those typical for BrC from biomass burning. The authors proposed that the strongly absorbing BrC might be related to photochemically aged SOA produced from anthropogenic emissions of VOC with fossil carbon. Similar observations of fossil-derived BrC were reported in a year-long study of WSOC collected in Beijing.[133−137] Cheng et al. found that organic fractions extracted from PM samples in Beijing using a mixture of hexane, methylene chloride, and acetone were light-absorbing, with MAC_{bulk} at 632 nm as high as 1.4 × 10^4 cm^2/g.[137] The presence of BrC with such unusually high absorption most likely affects filter-based measurements of BC. These studies attributed BrC in Beijing to both biomass-burning primary emissions and light-absorbing photochemical SOA formed from anthropogenic precursors. Seasonal variations in the relative contributions of these two types of BrC were reported, with the biomass-burning BrC dominating over the winter period and photochemical BrC dominating in summertime.

2.3.3. Amazon Basin. The ABC area over the Amazon basin is unique in the sense that it does not have the major influence of pollutants associated with rapidly developing industries and energy production for large populations. The Amazon basin is covered with thousands of acres of tropical forest with only one single spot source of urban pollution: Manaus, a city with a population of 2 million located in the middle of the region. Long-term atmospheric measurements in this area identified regional forest fires as the major source of BrC with more substantial impact during the dry season.[33,34,138] Characteristic absorption properties of BrC in this region are reported as MAC_a = 4 × 10^3 cm^2 g^{-1} at 532 nm and AAE = 1.5−1.2 with strong seasonal variability. The overall absorption

DOI: 10.1021/cr5006167
Chem. Rev. 2015, 115, 4335−4382

in the Amazon basin is dominated by BC, while BrC contribution is leveled at 6%−8%, which is somewhat marginal but still not negligible. Measurements of HULIS in WSOC extracts from the Amazon basin suggest that organics from both biomass-burning and natural biogenic emissions from forest metabolism may contribute to the buildup of HULIS macromolecules.[71,139]

2.3.4. Urban Areas in North America and Europe. In addition to the large-scale ABC discussed earlier, local urbanized areas in North America and Europe also are affected by BrC, an issue that has prompted many recent and ongoing field studies. For instance, Marley et al.[140] conducted systematic measurements of AAE for urban aerosols collected in Mexico City in April 2003 and March 2006. To better constrain their source, they also determined the fraction of modern carbon for the same aerosol samples. The measured AAE values ranged from 0.63 to 1.6, indicating the dominance of BC in the aerosol samples. However, the afternoon AAE values were systematically higher than the morning ones, strongly suggesting contributions from photochemically generated aerosols to the observed light absorption. Moreover, a positive correlation between the modern fraction of carbon and AAE indicates that even in this heavily urbanized area, biogenically derived SOA were dominant contributors to the afternoon increase in AAE. In the United States, Weber and co-workers conducted a number of studies describing BrC particles present in the Los Angeles basin and Atlanta areas.[69,72,86,141−144] Radiocarbon isotopic analysis of WSOC from Los Angeles showed that BrC in that area likely is an anthropogenic SOA formed from fossil carbon precursors, while chemical analysis suggested that nitroaromatics were important BrC chromophores in these samples. In contrast, analysis of the Atlanta samples showed the presence of BrC related to biomass-burning sources and to SOA from biogenic precursors in this area. Comparison of the characteristic absorption properties per soluble carbon between the two regions showed that BrC from Los Angeles is 4−6 times more absorbing than that from the Atlanta area. In another study by the same group, Liu et al.[145] presented aircraft-based measurements of the total aerosol absorption coefficient at 365 nm over the continental United States and estimated its fraction attributable to BrC. Their measurements confirmed that BrC is ubiquitous in the troposphere, and its relative contribution to the absorption coefficient increases with altitude, suggesting that secondary sources may contribute to BrC formation. An estimation of the direct radiative forcing at the top of the atmosphere indicated that BrC absorption reduced forcing by about 20%, which clearly is a significant contribution to the overall radiative forcing. Residential heating by wood and biomass burning also is an important source of BrC and BC in many parts of Europe.[146] In Europe, BrC measurements (mostly optical data) were reported for areas of central Europe,[147,148] Switzerland,[82] Italy,[149] Spain,[150,151] Portugal,[152] and the United Kingdom.[153]

2.3.5. Arctic Areas. BrC occurrence in the Arctic and its contribution to the Arctic haze phenomenon are particularly important to climate forcing. During the polar day, low solar elevation angles and highly reflective surfaces of airborne and surface ice increase optical depths and associated radiative effects resulting from both light scattering and absorption. Summertime boreal fires and long-range transport of anthropogenic emissions from midlatitudes are the major sources of BC and BrC in the Arctic.[154] In addition to their direct and indirect atmospheric radiative effects, deposition of light-absorbing materials on snow decreases surface albedo and accelerates melting of snow and ice.[155] In turn, melted brine formed at the ice surface modifies the kinetics and mechanisms of snow photochemistry[156,157] with consequent impacts on the release of halogen atoms pertinent to ozone decomposition. Recent aircraft-based measurements conducted in the spring and summer of 2008 showed that BrC contributes substantially to the total light absorption by aerosols in the Arctic across all wavelengths.[154,158] During selected research flights, when biomass-burning plumes were encountered, the BrC contribution to total absorption was reported at the level of ∼57% over the integrated spectral range of 350−550 nm, 10%−12% at the fixed wavelength of 470 nm, and 4%−6% at the wavelength of 530 nm, respectively. The corresponding MAC_a values were $(0.7−1.0) \times 10^4$ cm^2 g^{-1} at 470 nm and $(2.0−3.5) \times 10^3$ cm^2 g^{-1} at 530 nm with AAE values in the range of 1.5−3[154] and 5−7.[158] Analysis of the aerosol chemical composition based on the onboard measurements by an aerosol mass spectrometer (AMS) indicated a strong correlation between the higher oxidation of BrC constituents and its enhanced absorption.[158] These findings suggest that either differences in the initial molecular composition of BrC or the possible effects of its atmospheric oxidation (aging) had a primary influence on the light-absorption properties. Results of these aircraft-based measurements were consistent with separate studies that examined light-absorbing compounds deposited in Arctic snow.[159,160] Specifically, chemical and optical analysis of deposits in more than a thousand snow samples taken at different Arctic locations showed widespread occurrence of BrC. The overall contribution of BrC chromophores to total light absorption was in the range of 25%−50%.[159]

3. OVERVIEW OF METHODS FOR PHYSICOCHEMICAL CHARACTERIZATION OF BrC AEROSOLS AND CHROMOPHORES

3.1. Measurements of Optical Properties

In this section, we briefly review common definitions used in measurements of absorption and scattering properties of aerosols. Our overview is by no means comprehensive. We only include information directly relevant to our discussion regarding the optical properties of BrC. However, it should be helpful to the researchers who are new to the field and not necessarily familiar with the overwhelming amount of literature on interactions between radiation and particles. For more comprehensive accounts of theory, methods, and techniques relevant to measuring aerosol light absorption and scattering, we refer readers to a classic text[161] and a number of excellent recent reviews focused on aerosol optical properties.[8,11,22]

3.1.1. Optical Properties of Bulk Aerosol Materials and Aerosol Extracts. From a conceptual point of view, it is easier to start with a description of bulk measurements. The wavelength-dependent extinction (ext) coefficient of a bulk material, $\alpha_{bulk}^{ext}(\lambda)$, can be defined in the context of the Beer−Lambert law, which relates the attenuation of radiation propagating through the material to the propagation path length, l, as shown in eq 2:

$$\frac{I(\lambda)}{I_0(\lambda)} = \exp[-\alpha_{bulk}^{ext}(\lambda) l] \quad (2)$$

The extinction coefficient of a bulk film can be measured with commercial UV−vis spectrometers, which typically are configured to provide base-10 absorbance, A_{10}, given by eq 3:

DOI: 10.1021/cr5006167
Chem. Rev. 2015, 115, 4335−4382

$$A_{10}^{\text{film}}(\lambda) = \frac{\alpha_{\text{bulk}}^{\text{ext}}(\lambda) l_{\text{film}}}{\ln(10)} \quad (3)$$

The extinction results from both absorption and scattering of radiation by molecules in the material. The scattering component, as well as loss of light due to surface reflections, can be eliminated by acquiring the spectrum relative to a nonabsorbing film with a similar real refractive index. Under such conditions, the scattering contribution cancels out and absorption (abs) makes the dominant contribution to the measured extinction coefficient [$\alpha_{\text{bulk}}^{\text{ext}}(\lambda) \approx \alpha_{\text{bulk}}^{\text{abs}}(\lambda)$].

For homogeneous materials with a known density, ρ, it is convenient to define a quantity called "mass absorption coefficient of the material," or MAC_{bulk}, which is measured in the units of area per mass (such as cm^2/g) as shown in eq 4:

$$\text{MAC}_{\text{bulk}}(\lambda) = \frac{\alpha_{\text{bulk}}^{\text{abs}}(\lambda)}{\rho_{\text{bulk}}} \quad (4)$$

If a known mass of OA is collected and pressed into a homogeneous film of known area (which arguably is very challenging)[162,163] MAC_{bulk} can be calculated from the measured absorbance through this film using eq 5:

$$\text{MAC}_{\text{bulk}}(\lambda) = \frac{A_{10}^{\text{film}}(\lambda) \times \text{Area}_{\text{film}} \times \ln(10)}{\text{mass}_{\text{film}}} \quad (5)$$

Absorption properties of atmospheric aerosols are typically described in terms of the real (n, responsible for scattering) and imaginary (k, responsible for absorption) refractive index, $m = n + ki$, where i is the imaginary unit. The imaginary refractive index can be calculated from the absorption coefficient,[161] molar absorptivity (ε), or MAC_{bulk} using eq 6:

$$k(\lambda) = \frac{\alpha_{\text{bulk}}^{\text{abs}}(\lambda)\lambda}{4\pi} = \frac{1000 \ln(10)\varepsilon(\lambda)\rho_{\text{bulk}}\lambda}{4\pi} = \frac{\text{MAC}_{\text{bulk}}(\lambda)\rho_{\text{bulk}}\lambda}{4\pi} \quad (6)$$

This equation is commonly used to convert the measured MAC_{bulk} data into k, and vice versa.

Liu et al.[163] described a novel method for measurements of both real and imaginary refractive indexes of secondary organic material (SOM). The method relies on collecting a uniform film of SOM using an electrostatic precipitator followed by spectroscopic ellipsometry measurements. The method's advantage is that it provides n and k with high wavelength resolution in a range as wide as 220−1200 nm (limited by the available instrument). The method's major limitation is that it is only applicable to aerosols that can produce a homogeneous film, such as SOA generated in a smog chamber in the absence of seed particles. However, optical properties of inhomogeneous films, such as SOM containing embedded inorganic particles, would be difficult to determine using this method.

The same concepts are also useful for solution extracts of complex organic materials. For a solution of a material with mass concentration C_{mass} (measured in units of grams of dissolved material per cubic centimeter of solution)—assuming that the dissolution process does not affect the molecular absorption properties of the chromophores—MAC_{bulk} is given by eq 7:

$$\text{MAC}_{\text{bulk}}(\lambda) = \frac{A_{10}^{\text{solution}}(\lambda) \ln(10)}{l_{\text{solution}} C_{\text{mass}}} \quad (7)$$

Using mass concentration is a natural choice for solutions of OA because the overall mass of the dissolved organics can be measured or estimated, whereas the distribution of individual organic compounds in the sample is often unknown, making molar concentrations less useful. Normally, the solution is placed in a standard cuvette, but hollow optical fibers are also used to increase the path length and decrease the solution volume requirements. Once again, the experiments can be designed to eliminate contributions from scattering by the solution and from reflections at the cuvette surfaces, for example, by measuring A_{10} with respect to a matched cuvette filled with the same solvent. A sound example of MAC_{bulk} measurements from BrC filter extracts can be found in the work of Chen and Bond,[84] who reported the density normalized absorption coefficients for several solvents over a range of wavelengths. Hecobian et al.[72] described an elegant online method in which water-soluble compounds are extracted from aerosol with a particle-into-liquid sampler (PILS).[164] The extract is sent into a liquid waveguide capillary cell to measure absorbance and a total organic carbon (TOC) analyzer to measure the organic mass concentration in the extract (shown in Figure 5a). The instrument has sufficient sensitivity for measuring the absorption coefficient at 365 nm for directly sampled aerosols and full wavelength-resolved spectra for filter extracts (shown in Figure 5b). We note that the reported absorption spectra show "classic" BrC behavior with the power law dependence of the wavelength (eq 1) and large AAE values in the range of 6−8 for both biomass (higher levels of levoglucosan) and nonbiomass burning (lower levels of levoglucosan) periods.

Although aerosols contain a number of different compounds, it sometimes is convenient to estimate the average base-10 molar absorptivity ε ($\text{L mol}^{-1}\ \text{cm}^{-1}$) or average base-e molecular absorption cross section σ ($\text{cm}^2\ \text{molecule}^{-1}$) for the aerosol components given by eqs 8 and 9, respectively

$$\varepsilon_{\text{effective}}(\lambda) = \frac{MAC_{\text{bulk}}(\lambda) \times \text{MW}}{\ln(10) \times 1000} \quad (8)$$

$$\sigma_{\text{effective}}(\lambda) = \frac{\text{MAC}_{\text{bulk}}(\lambda) \times \text{MW}}{N_{\text{A}}} \quad (9)$$

where N_{A} is Avogadro's number in mol^{-1}. A reasonable effective molecular weight, MW (g mol^{-1}), must be assumed for such conversions. The values of ε and σ are useful for comparing absorption spectra of aerosol compounds with those of pure organic compounds, which are commonly reported in the form of molar absorptivities.

As previously indicated, the absorption coefficients of ambient aerosols often follow a power law dependence on wavelength given by eq 10:

$$\alpha_{\text{bulk}}^{\text{abs}}(\lambda) = \alpha_{\text{bulk}}^{\text{abs}}(\lambda_0)\left(\frac{\lambda_0}{\lambda}\right)^{\text{AAE}} \quad (10)$$

where λ_0 is a reference wavelength and AAE is the absorption Angström exponent. Ideally, AAE values should be determined from a fit of $\alpha_{\text{bulk}}(\lambda)$ to λ using eq 10. In practice, wavelength-resolved aerosol spectra are rarely available, and AAE values are estimated from absorption coefficient measurements at two selected wavelengths using eq 10.

DOI: 10.1021/cr5006167
Chem. Rev. 2015, 115, 4335−4382

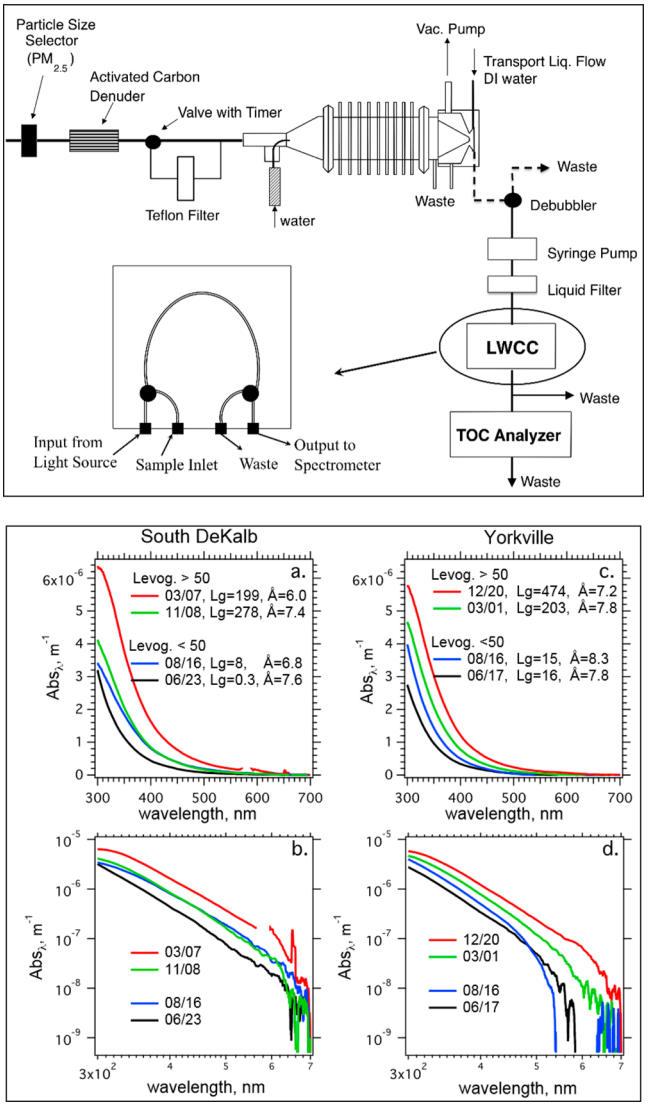

Figure 5. The upper panel shows the particle-into-liquid-sampler instrument reported by Hecobian et al. (2010) for online wavelength-resolved measurements of the absorption spectra of WSOC in aerosols. Data plots in the lower panels show examples of absorption spectra from filters collected at representative urban (South Dekalb, GA) and rural (Yorkville, GA) sites for both biomass burning (higher levels of levoglucosan) and nonbiomass burning (lower levels of levoglucosan) periods. (Reprinted with permission from ref 72. Copyright 2010 Copernicus Publications.)

Equation 10 is convenient, but it is purely empirical. Sun et al. evaluated the applicability of a band gap relationship given by eq 11 for describing absorption spectra of BrC and humic-like materials[165]

$$\alpha_{\text{bulk}}^{\text{abs}}(E) = \frac{B^2(E - E_g)^2}{E} \tag{11}$$

where B is a fitted constant, E is the photon energy, and E_g is the band gap energy. The band gap relationship, commonly used to describe absorption spectra of amorphous organic semiconductors, worked reasonably well for BrC with B^2 of 2.89×10^4 cm^2 g^{-1} eV^{-1} and an effective band gap of $E_g = 2.5$ eV. The agreement with water-soluble, humic-like OC could be further improved by including the so-called "Urbach tail", which describes the absorption coefficient at energies below the band gap using eq 12

$$\alpha_{\text{bulk}}^{\text{abs}}(E) = \alpha_{\text{cr}} \exp\left(-\frac{E_{\text{cr}} - E}{E_0}\right) \tag{12}$$

where α_{cr} and E_{cr} are the values at the band gap and E_0 determines the Urbach tail width. On the basis of analysis of the available atmospherically relevant data, Sun et al. recommend E_0 of 0.4 eV.[165] The band gap treatment is a useful alternative for representing the wavelength dependence of BrC absorption spectra compared to the largely empirical power law parametrization relying on AAE. A further discussion of this model and its applications to BrC can be found elsewhere.[22]

3.1.2. Optical Properties of Air Containing Aerosols. The quantitative description becomes more complicated for airborne particles because the extinction coefficient of an aerosol depends not only on the mass concentration of the dispersed material but also on the size distribution, shapes, and mixing state of the particles. The extinction coefficient of aerosol-laden air typically is represented as the sum of the absorption and scattering coefficients for aerosolized particles (denoted by subscript "a") and gases (subscript "g") as shown in eq 13:

$$b_{\text{air}}^{\text{ext}}(\lambda) = b_{\text{a}}^{\text{abs}}(\lambda) + b_{\text{a}}^{\text{sc}}(\lambda) + b_{\text{g}}^{\text{abs}}(\lambda) + b_{\text{g}}^{\text{sc}}(\lambda) \tag{13}$$

Note that we use letter b to denote the base-e extinction, absorption, and scattering coefficients, as commonly done in the literature, to highlight the distinction with α used for denoting the absorption coefficient of the bulk aerosol material. Because of the high air transmittance, even under moderately polluted conditions, the common units for b are inverse megameters (Mm^{-1}) instead of inverse centimeters (cm^{-1}). Under typical urban conditions, the overall extinction at visible wavelengths is dominated by particle scattering.[166] Contributions from absorption by particles and gases increase significantly in the UV range. Integration of the extinction coefficient due to particles over the entire column of air from the ground up produces what is known in the remote sensing literature as "aerosol optical depth" (already denoted as AOD herein), which can be subdivided into absorption (AAOD) and scattering components (SAOD), as shown in eq 14:

$$\begin{aligned}\text{AOD}(\lambda) &= \text{AAOD}(\lambda) + \text{SAOD}(\lambda) \\ &= \int_{z=0}^{\infty} b_{\text{a}}^{\text{abs}}(z, \lambda)\, \text{d}z + \int_{z=0}^{\infty} b_{\text{a}}^{\text{sc}}(z, \lambda)\, \text{d}z\end{aligned} \tag{14}$$

The mass-normalized absorption cross section of aerosol particles, MAC_{a}, can be used to relate the particle mass concentration in air, C_{PM}, and absorption coefficient using eq 15:

$$b_{\text{a}}^{\text{abs}}(\lambda) = \text{MAC}_{\text{a}}(\lambda) \times C_{\text{PM}} \tag{15}$$

For example, air containing 10 μg/m^3 of strongly absorbing PM with $\text{MAC}_{\text{a}} = 7.5 \times 10^4$ cm^2/g (a value characteristic of BC at 550 nm)[11] would have an absorption coefficient of 75 Mm^{-1}. We should note that the MAC notation is not universally accepted. Some authors use MAE (mass absorption efficiency) to denote the same quantity.

The mass-normalized scattering absorption cross section of MSC_{a} can be defined in a similar manner to MAC_{a}. With the exception of very strongly absorbing particles, such as soot, MSC_{a} is considerably larger than MAC_{a}. More quantitatively,

DOI: 10.1021/cr5006167
Chem. Rev. 2015, 115, 4335−4382

the relationship can be expressed with the help of SSA, defined as a fraction of light scattered by aerosol, as shown in eq 16:

$$\mathrm{SSA} = \frac{b_a^{sc}}{b_a^{abs} + b_a^{sc}} = \frac{\mathrm{MSC_a}}{\mathrm{MSC_a} + \mathrm{MAC_a}} \quad (16)$$

Nonabsorbing OA and major inorganic aerosols, such as ammonium sulfate, have SSA ∼ 1 at visible wavelengths. For strongly absorbing aerosols, SSA is lower, but it never approaches zero, even for the strongest absorbers. For example, aerosolized nigrosine, a mixture of strongly absorbing dyes commonly used for calibrating aerosol absorption spectrometers,[167] has SSA ∼ 0.5 and a refractive index of 1.67+0.26i. Typical values of SSA for fresh combustion aerosol can be as low as 0.2.[11]

The use of the same abbreviation for the mass absorption coefficient of bulk material, $\mathrm{MAC_{bulk}}$, and the mass-normalized absorption cross section of aerosol, $\mathrm{MAC_a}$, has resulted in some confusion in the literature. Although both quantities have the same units, they have different meanings. For example, as explained by Sun et al.,[165] in the small particle limit, where scattering by particles can be approximated with Rayleigh theory, the two MAC values are related through eq 17

$$\mathrm{MAC_a}(\lambda) = \frac{6\pi}{\rho_{\mathrm{bulk}}\lambda} Im\left[\frac{m(\lambda)^2 - 1}{m(\lambda)^2 + 2}\right] = \xi(\lambda) \times \mathrm{MAC_{bulk}}(\lambda) \quad (17)$$

where m is the wavelength-dependent complex refractive index. For a spherical homogeneous particle of radius r, the small particle limit applies when the particle size parameter, $2\pi nr/\lambda$, is much smaller than unity. The parameter ξ weakly depends on k (the imaginary part of the refractive index) and is about 0.7 for n = 1.5 particles (n is the real part of the refractive index). Quantitative comparisons between experiments relying on direct measurements of aerosol absorption coefficients and bulk measurements of absorption spectra of aerosol extracts should always take the difference between $\mathrm{MAC_{bulk}}$ and $\mathrm{MAC_a}$ into account. A good example of applying such corrections has been presented by Nakayama et al.[168] To avoid the naming ambiguity between $\mathrm{MAC_{bulk}}$ and $\mathrm{MAC_a}$, Sun et al. recommended reporting wavelength-dependent $\alpha_{\mathrm{bulk}}^{\mathrm{abs}}(\lambda)/\rho_{\mathrm{bulk}}$ in bulk measurements and discontining the use of the name "MAC".[165] In this review, we opted for using subscripts "bulk" and "a" to emphasize the difference between the mass absorption coefficient of bulk material and the mass-normalized absorption cross section of aerosolized particles, as well as the different methods used to measure these quantities. Specifically, all MAC values obtained from solution extracts and SOM films are designated as $\mathrm{MAC_{bulk}}$, while those retrieved from direct aerosol and filter-based measurements, which are described below, are designated as $\mathrm{MAC_a}$.

The preceding parameters have been used to evaluate the impact of aerosols on visibility and climate. The extent of radiative forcing exerted by aerosols can be roughly estimated from the simple forcing efficiency (SFE) defined by Bond and Bergstrom[11] and shown in eq 18:

$$\mathrm{SFE} = -\frac{1}{4} S_0 \tau^2 (1 - F_c)[2(1 - a)^2 \beta \times \mathrm{MSC_a} - 4a \times \mathrm{MAC_a}] \quad (18)$$

This equation describes the effect of a uniform, optically thin layer of aerosol in the lower atmosphere on radiative forcing. The parameters in this equation and their typical values correspond to the solar constant S_0 = 1370 W m^{-2}, atmospheric transmission $\tau \sim 0.79$, cloud fraction $F_c \sim 0.6$, surface albedo $a \sim 0.19$, and backscatter fraction $\beta \sim 0.17$. SFE has units of W g^{-1} and represents the energy added to the atmosphere by a given mass of aerosols. As the scattering term in parentheses normally dominates, SFE is usually negative, which corresponds to the cooling effect by aerosols. The presence of BC and BrC makes SFE less negative compared to the case of a scattering-only aerosol with $\mathrm{MAC_a}$ = 0 and, for (unrealistically) strongly absorbing aerosol, may even invert the sign of SFE to positive (warming). In the wavelength-dependent form of this equation, SFE and S_0 are replaced by their density distribution functions of wavelength, $\mathrm{dSFE}/\mathrm{d}\lambda$ and $\mathrm{d}S_0/\mathrm{d}\lambda$, and parameters τ, a, β, $\mathrm{MSC_a}$, and $\mathrm{MAC_a}$ are treated as wavelength-dependent. Dinar et al.[80] used a related quantity, called "radiative-forcing efficiency" (RFE), to estimate radiative forcing by BrC. RFE is measured in W m^{-2}, and it represents the net *change* in the solar flux at the top of the atmosphere normalized to the AOD, i.e., RFE = ΔFlux/AOD. The value of ΔFlux (and RFE) is negative with scattering aerosols present in the atmosphere and becomes less negative when aerosols are absorbing. In evaluating the climate effect of light-absorbing aerosols, it is common to initially evaluate SFE or RFE for a base-case scenario, such as an aerosol composed of only ammonium sulfate (k = 0), and then compare it to the case for an absorbing aerosol (k > 0), such as BC or BrC.

3.1.3. Transmission Measurements with Aerosol Filters. Measurements of transmission through filters loaded with aerosol particles have been used historically for quantifying aerosol absorption properties. The best known examples of filter-based instruments include a particle soot absorption photometer (PSAP)[167] and aethalometer.[169] However, a number of other filter-based instruments have been reported, including ones that simultaneously measure the scattering and absorption coefficients. For example, Petzold and Schönlinner described a multiangle absorption photometer (MAAP),[170] which measures transmission and backward scattering from two angles at a single wavelength of 550 nm. Massabo et al. introduced a multiwavelength absorbance analyzer (MWAA)[171] for filter-collected PM. The MWAA records transmission and backward scattering at two fixed angles, just like the MAAP, but it does so for three wavelengths (405, 635, and 850 nm), enabling measurements of the BC and BrC content from the wavelength dependence. In general, all these instruments measure the effective absorption coefficient by comparing the transmission, I, through a particle-laden filter to that of a clean filter, I_0 (usually the same filter measured at an earlier time), after sampling a certain amount of air volume, as shown in eq 19:

$$b_{\mathrm{filter}}^{\mathrm{ext}} = \frac{\mathrm{Area_{filter}}}{\mathrm{Volume_{air}}} \ln\left(\frac{I_0}{I}\right) \quad (19)$$

As described, for example, by Bond et al.,[167] due to the possibility of multiple scattering events prior to absorption, transmission through a particle-loaded filter depends not only on the absorption coefficient of the collected aerosol but also on the scattering coefficient, as shown in eq 20

$$b_{\mathrm{filter}}^{\mathrm{ext}} = K_1 b_a^{sc} + K_2 b_a^{abs} \quad (20)$$

DOI: 10.1021/cr5006167
Chem. Rev. 2015, 115, 4335−4382

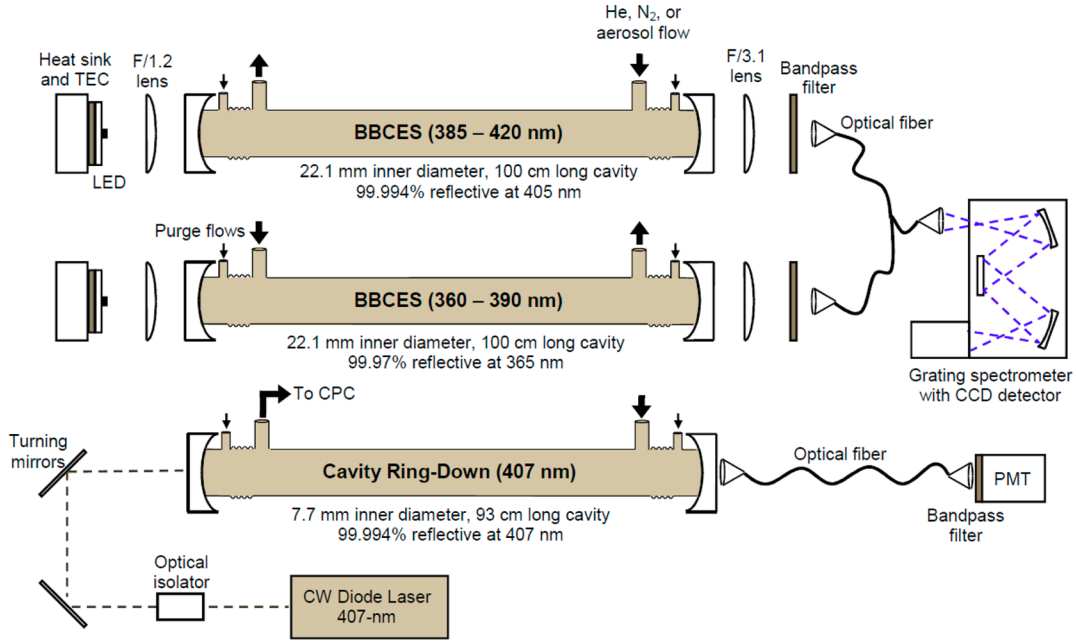

Figure 6. BBCES instrument designed by Washenfelder et al. (2013). Two independent cavities with different sets of LEDs and CRD mirrors are used to provide a combined wavelength coverage from 360 to 420 nm. For calibration purposes, a CRD system is used in series with BBCES. (Reprinted with permission from ref 183. Copyright 2013 Copernicus Publications.)

where the calibration constant K_1 is typically small and the calibration constant K_2 is greater than 1. The formula makes an implicit assumption that aerosol particles do not change their morphology when they stick to the filters. Subramanian et al.[172] pointed out that this assumption breaks down for the BrC aerosol produced by nonflaming combustion. They found that this type of BrC aerosol tends to coat quartz filter fibers and form liquid-like elongated beads. This has significant consequences for the interpretation of filter absorption data and data obtained in thermal–optical analysis used to apportion aerosols into elemental (absorbing) and organic (nonabsorbing) carbon. Indeed, measurements by Cappa et al.[173] showed that as a result of this effect, even nonabsorbing aerosols, such as α-pinene SOA, may appear to be absorbing on filters.

Hitzenberger et al.[174] developed and later refined the integrating sphere method for measuring absorption coefficients of BrC. The method relied on a single wavelength measurement at 550 nm for a filter or a suspension of PM in a solvent placed in the middle of an integrating sphere. At the time of development, BC was assumed to be the sole contributor to absorption of visible light by aerosols. To separate the contributions of BC and BrC to the overall light absorption, Wonaschütz et al.[175] extended the integrating sphere method to measurements at three wavelengths (450, 550, and 650 nm). They additionally found that thermal methods tend to overestimate the amount of BrC on days with large contributions of wood smoke. Recently, the filter-based integrated sphere methods were further extended to measure the full absorption spectrum.[176,177] Examples of such wavelength-resolved measurements are still rare, but they are definitively more useful as they provide a better quantitative description of the spectrum than what is possible on the basis of measurements at isolated wavelengths, which rely on the assumed power law dependence of the absorption coefficient on the wavelength.

3.1.4. Direct Measurements of Aerosol Optical Properties. Multiple approaches have been developed to directly measure the absorption, scattering, and extinction coefficients of aerosols, either independently or in combination. The overall extinction coefficient can be sensitively and accurately measured using multiple variations of cavity-based methods. Cavity ring-down (CRD) spectroscopy, which is by far the most common method in this category, was originally developed for sensitive measurements of absorption spectra of gaseous molecules.[178] The method relies on sending a pulse of radiation into an optical cavity formed by two carefully aligned, high-reflectivity mirrors and observing the radiation decay from the cavity using a fast detector, such as a photomultiplier tube, placed behind the cavity. The extinction coefficient is obtained from the measured exponential decay time for a cavity containing aerosols (τ) and a cavity containing just the buffer gas (τ_0) using eq 21

$$\alpha_a^{ext}(\lambda) = \frac{1}{c}\left(\frac{1}{\tau} - \frac{1}{\tau_0}\right) \quad (21)$$

where c is the speed of light. The first applications of CRD to measurements of extinction coefficients of particles were reported more than 10 years ago by Sappey et al.[179] and Smith and Atkinson,[180] and the method has been adopted by many research groups that have developed numerous CRD-based instruments for field and laboratory work. The field has since advanced so rapidly that even spectrometers capable of detecting extinction from a single trapped particle now exist.[181] The most common CRD configuration relies on the first (532 nm) or second (355 nm) harmonic of a pulsed Nd:YAG laser as a light source. However, fast switchable continuous laser diodes are becoming increasingly common, especially the blue diode at 405 nm made widely available by the development of Blu-ray technology.

Similar to CRD, cavity-enhanced spectroscopy (CES) also uses a cavity formed by two highly reflective mirrors to measure

DOI: 10.1021/cr5006167
Chem. Rev. 2015, 115, 4335–4382

the overall transmitted power instead of the cavity decay time constant. Moosmüller et al.[182] demonstrated that CRD and CES measurements for aerosols give nearly identical results. Broadband cavity-enhanced spectroscopy, or BBCES, relies on coupling a broadband light source into a cavity and recording a spectrally resolved transmission through the cavity using a monochromator and a multichannel detector, such as a charge-coupled device (CCD). Although less sensitive compared to the single-wavelength methods, BBCES provides extinction coefficients over a broad range of wavelengths. For example, as described by Washenfelder et al.,[183] the extinction coefficient can be derived from BBCES measurements using eq 22

$$\alpha_a^{ext}(\lambda) = \frac{l_{cell}}{l_{sample}}\left(\frac{1 - R(\lambda)}{l_{cell}} + \alpha_{Rayleigh}(\lambda)\right)\left(\frac{I_0(\lambda) - I(\lambda)}{I(\lambda)}\right) \quad (22)$$

where R is the wavelength-dependent mirror reflectivity, l_{cell} is the distance between the mirrors forming the cavity, l_{sample} is the length of the portion of the cavity occupied by the aerosol flow, $\alpha_{Rayleigh}$ is the scattering coefficient for the buffer gas (typically nitrogen), $I_0(\lambda)$ is the reference spectrum recorded for the cavity containing just the buffer gas, and $I(\lambda)$ is the measured spectrum recorded in the presence of particles. With the instrument depicted in Figure 6, Washenfelder et al.[183] showed that BBCES can be used to determine both the real and imaginary refractive indexes for aerosols with a substantial spectral dependence of the refractive index by doing measurements on particles of multiple diameters. Because of the limitations in the wavelength range over which the mirrors remain highly reflective and the bandwidth of the light-emitting diode (LED) sources, the setup shown in Figure 6 incorporates two separate cells: one optimized for the 385−420 nm range and the other for the 360−390 nm range. A third cell, configured as a 407 nm CRD instrument, is also included. The sampled aerosol passes in series through all three cells. Zhao et al.[184] developed a related instrument, calling their approach "incoherent broadband cavity-enhanced absorption spectroscopy" or IBBCEAS. The BBCES and IBBCEAS instruments have a somewhat different overall wavelength coverage of 360−420 and 445−480 nm, respectively, determined by the laser diodes used in their construction. Varma et al.[185] compared optical measurements obtained with three CES instruments—IBBCEAS, a broadband cavity ring-down spectrometer (BBCRDS), and a cavity-enhanced differential optical absorption spectrometer (CE-DOAS)—and found close agreement between real refractive index (n) retrievals obtained for the β-pinene + NO_3 SOA.

Using integrating nephelometry, a well-established technique,[186] the scattering coefficient can be measured independently from the overall extinction. In the past, the absorption coefficient commonly was derived from the difference between the extinction and scattering coefficients. However, because a small value has to be determined as a difference of two large values, this method is not reliable for weakly absorbing BrC aerosols. The "albedometer"[187,188] offers a definitive improvement by simultaneously measuring the 355 nm extinction coefficient with CRD and the scattering coefficient with an integrating sphere nephelometry in the same instrument. Using this approach, the SSA can be measured with higher precision than from combining independent extinction and scattering measurements. The albedometer has been tested for various types of aerosols, measuring SSA ∼ 1 for ammonium sulfate and α-pinene SOA at 532 nm wavelength, as expected for purely scattering aerosols, and SSA ranging from 0.75 to 0.84 for biomass-burning aerosol and soil dust. The SSA for SOA produced from OH-induced oxidation of toluene in the presence of NO_x was ∼0.95, also measured at 532 nm.

Photoacoustic spectroscopy (PAS) enables direct measurement of the absorption coefficient.[189,190] PAS relies on detection of a sound wave generated by absorption of pulsed (or modulated continuous wave) radiation by molecules or particles. Under appropriate conditions, the sound intensity measured with a microphone is directly proportional to the absorption coefficient. Typically, a gaseous species with well-known absorption spectrum is used for calibration. Examples of instruments that combine PAS and CRD into an integrated system can be found in refs 184, 191, and 192. Although PAS is a powerful technique, it has its limitations. For example, Langridge et al.[193] showed that because a portion of the absorbed energy is used up by the water evaporation from particles, instead of generating the acoustic signal, PAS underestimates the absorption coefficient under high RH conditions.

To simplify conversion of the measured extinction and absorption coefficients into a refractive index using Mie theory, CRD, CES, PAS, and other optical measurements are typically carried out for size-selected particles. However, even for size-resolved spherical particles, the conversion of the measured extinction coefficients into the refractive indexes is not always straightforward. Lang-Yona et al.[87] and Riziq et al.[194] examined the effect of the particles' internal mixing state on the measured extinction. They found, for example, that for aerosols consisting of a strongly absorbing core coated by a nonabsorbing shell, the Mie theory prediction deviated from the measurements by up to 10%. In addition, the absorption coefficient may be affected by the particle's internal mixing state. For instance, a nonabsorbing or weakly absorbing organic coating is known to amplify absorption by a strongly absorbing BC core. Shiraiwa et al.[46] used Mie theory to estimate the amplification factor for such core−shell particles and found that the factor can be as large as 2. The interpretation of optical measurements becomes even more challenging when both internally and externally mixed particles are present in the sample, as often is the case of biomass-burning plumes. However, Lack et al.[21,100] developed an approach that helps account for the simultaneous presence of internally and externally mixed particles and apportions the absorption coefficient measured by PAS into separate contributions from BC, amplification of the absorption of BC by the nonabsorbing OC coating, and intrinsic absorption by the BrC compounds.

In summary, a number of methods for measuring the absorption, scattering, and extinction coefficients of aerosols have been developed, and with help of modeling, the measurements can be converted into intrinsic properties for the aerosol materials, namely, the refractive indexes.

3.2. Molecular-Level Characterization of BrC Compounds

The complexity of OA imposes significant analytical challenges on the molecular characterization of its light-absorbing constituents. Mass spectrometry (MS) has been used extensively to characterize the chemical composition of OA. For detailed descriptions of MS techniques and their application to both on- and off-line OA chemical analysis, readers are referred to several recent reviews.[195−203] Because of its ability to provide molecular-level information, offline OA

DOI: 10.1021/cr5006167
Chem. Rev. 2015, 115, 4335−4382

characterization using high-resolution mass spectroscopy (HR-MS) is of particular interest to this review and is briefly described in this section. HR-MS experiments normally rely on soft ionization of analyte molecules in OA with or without prior chromatographic separation. Several ionization techniques have been used for OA analysis. Electrospray ionization (ESI)[204] is the most popular ionization technique by far. In ESI experiments, OA is dissolved in an appropriate solvent and ionized at a mass spectrometer inlet by generating a mist of charged droplets. Subsequent droplet evaporation in the instrument's vacuum manifold generates bare ions of analyte molecules (M), carrying positive or negative charge. Positive mode OA spectra are dominated by the singly charged $[M + H]^+$ and $[M + Na]^+$ ions (even small amounts of Na^+ leached into the solution from laboratory glassware are sufficient to generate $[M + Na]^+$ ions), whereas $[M - H]^-$ species are typically observed in negative mode spectra. The formation of native radical cations ($M^{+\bullet}$) and anions ($M^{-\bullet}$) through ESI, while possible, is quite rare. As ESI traditionally is used to analyze polar molecules in complex mixtures, atmospheric pressure chemical ionization (APCI)[205] and photoionization (APPI)[206] provide better alternatives for efficient ionization of less-polar components, which are not ionizable by ESI. Soft ionization techniques (e.g., ESI, APCI, APPI) are readily coupled with liquid chromatography (LC) separation but also can be used for direct infusion experiments. The latter provides the advantage of rapid analysis—important for experiments that require high throughput but suffer from the so-called "matrix effects" (signal suppression of certain ions in ionization of complex mixtures of analytes). Chromatographic separation prior to MS reduces the complexity of the sample eluting at a given time, thereby increasing the sensitivity and facilitating quantification at the expense of analysis speed. Furthermore, as discussed below, a spectrophotometer can be readily integrated into an LC−MS system, making it possible to simultaneously record mass spectra and absorption spectra of the separated BrC components.

Chemical characterization of substrate-deposited OA has been performed using several ambient surface ionization techniques. These techniques provide the advantage of rapid analysis of molecules on surfaces that do not require any sample pretreatment but cannot be coupled to LC. As a result, these techniques suffer from the matrix effects mentioned earlier. Desorption electrospray ionization (DESI)[207] produces ions through bombardment of substrate-deposited OA with charged primary droplets that generate secondary charged droplets containing desorbed OA material.[208−210] The final ionization step in DESI is similar to ESI, generating intact ions of OA constituents. However, the short residence time in analyte molecules in the solvent of DESI experiments has been shown to be important for analysis of chemically labile components of OA that may not survive the solvent extraction necessary for ESI analysis.[208] Atmospheric solids analysis probe mass spectrometry (ASAP-MS)[211] has been used for chemical analysis of laboratory-generated and field-collected OA.[212] This technique relies on thermal desorption of the sample followed by gentle APCI ionization and, as such, is well-suited for analyzing thermally stable compounds in OA.

Nanospray desorption electrospray ionization (nano-DESI) relies on localized liquid extraction of analyte molecules into a liquid bridge formed between two glass capillaries.[213] The first capillary supplies the extraction solvent, while the second capillary removes the dissolved analyte and transfers it to a mass spectrometer inlet. Similar to DESI and ASAP, nano-DESI analysis does not require any sample pretreatment. Gentle liquid extraction, along with precise control and independent optimization of desorption and ionization processes, results in improved sensitivity. Nano-DESI generates a stable analyte signal necessary for MS/MS analysis. Although sensitivity also depends on mass spectrometer performance, good-quality nano-DESI MS spectra can be obtained with <10 ng of OA material using modern commercial instruments.[214] Localized liquid extraction also provides the basis for the liquid extraction surface analysis (LESA) technique that has been used recently for characterizing ambient aerosol samples collected using a rotating drum impactor.[215] In LESA, a drop of the extraction solvent deposited onto the substrate using a micropipette subsequently is aspirated and introduced into MS using nanospray ionization. Similar to DESI and nano-DESI, this enables spatially resolved analysis of complex samples on substrates.

Although soft ionization techniques have been used traditionally for offline OA analysis, recent studies by Doezema et al.[216] and Gallimore and Kalberer[217] have introduced an approach for online analysis of laboratory-generated and ambient particles using extractive electrospray ionization (EESI). In EESI, the particle beam is intercepted with a mist of charged solvent droplets produced by ESI. Analyte molecules extracted into the electrospray plume droplets are subsequently ionized and analyzed using MS. This approach has been used for OA characterization with a sampling rate of several seconds and a dynamic range of 0.2−600 $\mu g/m^3$.

HR-MS of OA samples typically produces complex spectra containing hundreds or even thousands of peaks. Annotation of such complex spectra relies on data clustering using mass defect transformation, such as Kendrick analysis.[218] This approach enables efficient clustering of homologous compounds, differing only by the number of base units (e.g., O, CH_2O, C_2H_2O) with the base choice determined by a common building block in a particular sample. Additional data clustering prior to formula assignment may be performed using a higher-order mass defect transformation described in detail by Roach et al.[220] Subsequent identification of one group member identifies all members of the homologous series. Formula assignments can be performed using a variety of freely available and commercial calculators. An unconstrained formula search typically generates many unreasonable candidate formulas that should be later filtered using valence rules and other constraints.[219] Typically, more than 70% of the observed peaks are unambiguously assigned within reasonable constrains on the number of C, H, O, N, and S atoms.

Despite significant advances in OA characterization using MS, only a few studies focused on the analysis of BrC species. Because MS is not selective toward light-absorbing molecules, chemical characterization of BrC has been performed using two approaches. In the first approach, laboratory-generated white OA is subjected to chemical aging under controlled conditions to generate secondary BrC. Both white and BrC samples are analyzed under the same conditions using HR-MS.[108,208] A comparison between HR-MS spectra of the white and brown samples identifies new or significantly enhanced peaks in the chemically aged OA sample, generating a list of potential chromophores. Although this comparative approach cannot unambiguously identify light-absorbing species, it enables rapid screening of candidate elemental compositions.

DOI: 10.1021/cr5006167
Chem. Rev. 2015, 115, 4335−4382

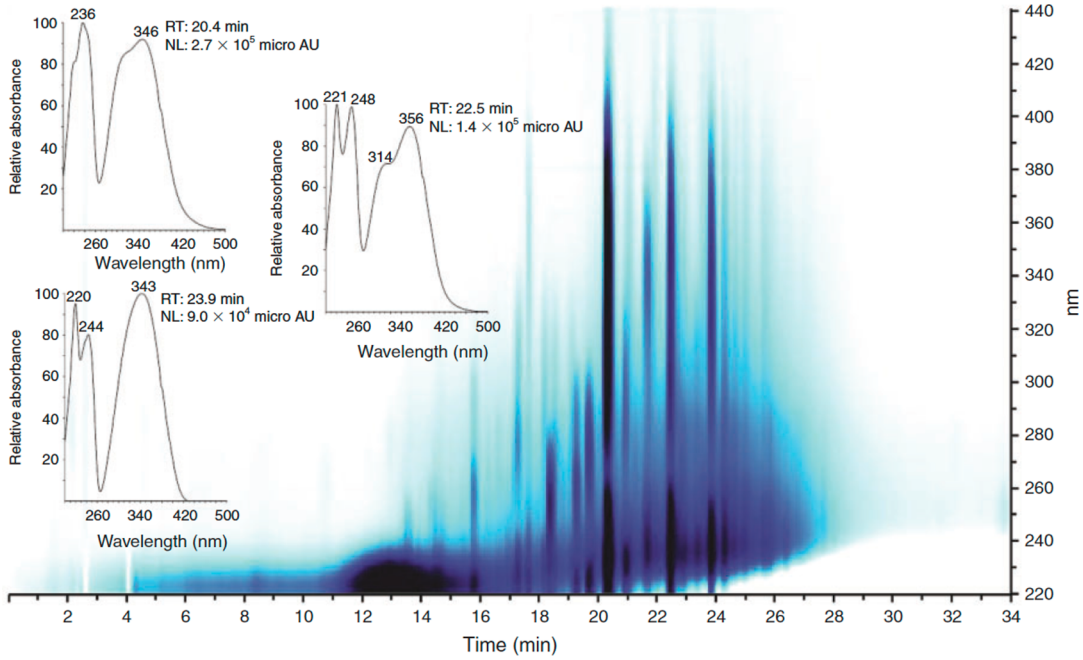

Figure 7. Photodiode array detection density map for HULIS in a sample of biomass-burning aerosol. Several UV−vis-active bands are present. The most intense ones (retention time = 20.4, 22.5, and 23.9 min) correspond to 4-nitrocatechol and two isomeric methyl nitrocatechols. Their tailing absorption in the 400−420 nm range is consistent with the HULIS sample's yellow appearance. The insets show the corresponding UV−vis absorption spectra. (Reprinted with permission from ref 64. Copyright 2012 CSIRO Publishing.)

Unambiguous identification of BrC chromophores requires correlative UV−vis and MS measurements. Lack et al.[102] presented one example of such correlative measurement for online OA characterization. In that study, the light absorption properties of biomass-burning aerosol examined using a PAS instrument were correlated with the chemical information obtained using AMS. The mass absorption efficiency at 404 nm was found to correlate with the ratio of the fragment at m/z 60 (f_{60}) to the fragment at m/z 44 (f_{44}), while no correlation was found for light absorption at 532 nm. The formation of the f_{60} fragment was attributed to levoglucosan and its derivatives, while the f_{44} fragment originated from dissociation of oxidized organic molecules in AMS. The results of this study indicated that organic compounds are the major contributors to the observed light absorption at 404 nm. This approach enabled online characterization of the overall BrC composition produced during forest fires. However, AMS relies on rapid vaporization of aerosols followed by an electron ionization of the resulting gas plume, leading to extensive fragmentation of the aerosol compounds.[221] Chemical characterization of individual BrC chromophores requires techniques that are more selective to individual components than those commonly used for online OA analysis.

A vast majority of studies focused on the characterization of individual BrC chromophores utilized high-performance liquid chromatography (HPLC) coupled with UV−vis detection of eluting species and electrospray ionization mass spectrometry (HPLC/UV−vis/ESI-MS) for offline analysis of BrC collected on substrates or into liquids.[64,86,222−224] Claeys et al.[64] examined the composition of BrC material in samples of biomass-burning aerosols collected at different locations. Figure 7 shows an example of HPLC/UV−vis data with pronounced absorption in the 300−440 nm range. LC−MS analysis enabled identification of the major BrC chromophores by comparison of the corresponding LC elution times and the MS features with those of reference compounds. Methyl nitrocatechols, formed through photooxidation of lignin degradation products in the presence of NO_x,[225] have been identified as the major light-absorbing molecules in these samples.

It is recognized that sample collection and extraction may have a significant effect on the quantitative analysis of BrC compounds in the atmosphere. Zhang et al. compared the amount of water-soluble fraction of BrC in aerosol samples collected using PILS with the amount of BrC extracted into methanol.[86] HPLC/UV−vis/MS analysis indicated that water-insoluble nitroaromatic BrC chromophores were more abundant than water-soluble chromophores in the studied samples. Kitanovski et al. established a protocol for accurate quantification of nitroaromatic compounds in complex OA samples (collected in Ljubljana, Slovenia) using LC−MS/MS experiments performed under carefully optimized conditions.[223,226] In particular, the mobile phase composition was optimized to eliminate matrix effects and to ensure good chromatographic separation, as well as the symmetric LC peak shapes necessary for accurate quantification. The extraction procedure was optimized to ensure complete extraction of the OA material prior to analysis. Quantification was performed by selective reaction monitoring of NO and CH_3 losses as markers of methyl nitrocatechols and nitroguaiacols, respectively. Methyl nitrocatechols and 4-nitrocatechol were quantified in these aerosol samples at concentrations up to 134 and 152 ng/m^3, respectively, corresponding to ∼1% of the total aerosol mass. Nitrophenol derivatives were also identified as major BrC components in cloudwater samples collected near agricultural biomass-burning sites in China,[222] in wood-burning smoke from residential heating in the United Kingdom,[153] and in aerosol samples from a rural site impacted by biomass burning in Flanders, Belgium.[65]

DOI: 10.1021/cr5006167
Chem. Rev. 2015, 115, 4335−4382

3.3. Chemical Characterization of BrC in Individual Particles

As already discussed, understanding the internal composition and lateral distribution of absorbing and nonabsorbing materials (mixing state) within individual particles is critical for interpreting the optical measurements, which are most often conducted over either large ensembles of particles or bulk samples collected on substrates. Therefore, an ideal analytical method should combine detection of light extinction by an individual particle and simultaneous measurement of its internal composition with sufficient chemical and lateral specificity. The only measurement that has approached these ideal characteristics was the TEM/EELS study of tar balls[89] (discussed in section 2.2). However, as mentioned earlier, TEM/EELS experiments are limited to particles that are stable under vacuum and electron beam, have spherical shape, and are transparent to the electron beam. As a result, this technique cannot be used for routine characterization of atmospheric particles. Other approaches for studying the effect of particle internal composition on its optical properties rely on complementary and independent measurements of these properties. Specifically, optical measurements on airborne particles are often followed by particle collection and offline characterization using various analytical techniques on a single-particle level.[110,227,228]

TEM is the most commonly used technique for examining the morphology and internal structures of submicron atmospheric particles with subnanometer lateral resolution.[229,230] The elemental composition of particles in TEM can be probed by energy-dispersive X-ray spectroscopy (EDX), while chemical bonding, coordination, and valence states of elements can be further investigated using EELS. Both EDX and EELS can be used to obtain high-resolution elemental particle maps.[92,94,231,232] However, TEM analysis of organic particles and inclusions does not provide sufficient molecular specificity to distinguish between BrC and other organic materials.

Better specificity of the chemical characterization of different forms of organic material within individual particles can be achieved using synchrotron-based soft X-ray microspectroscopy, a method that combines scanning transmission X-ray microscopy (STXM) at fixed energies of X-rays and near-edge X-ray absorption fine structure (NEXAFS) spectroscopy with lateral specificity.[233] Compared to TEM, STXM particle analysis provides substantially lower lateral resolution (>20 nm) but higher chemical specificity. Because organic material in atmospheric particles is less sensitive to the beam damage by soft X-rays, STXM enables acquisition of characteristic carbon K-edge NEXAFS spectra for each pixel in the image. Figure 8a shows an example of the NEXAFS spectrum of an individual organic particle. Different carbon functionalities of the organic material that compose this particle are assessed by a peak-fitting procedure that provides chemically resolved information on bonding and structural ordering of carbon within this particle.[95] Furthermore, selected features of carbon K-edge NEXAFS spectra, indicative of specific carbon functionalities, can be used to construct component maps outlining chemical differences of carbon within individual particles (illustrated by Figure 8b).[234] These maps are used for grouping and classification of particle ensembles based on their "mixing states".[231,235] The appearance of a specific particle class in samples collected at different times can be correlated with concurrent optical measurements to evaluate the relationship between the organic particles' composition and their optical properties.

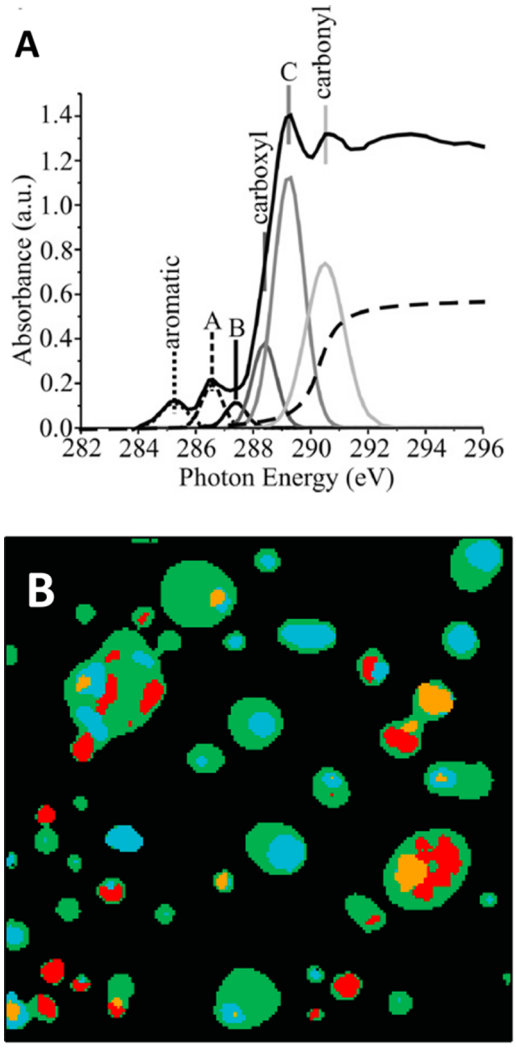

Figure 8. Panel A: An example of a carbon K-edge NEXAFS spectrum of an individual atmospheric particle and assignments of the deconvoluted peaks. Gray shades and line styles indicate specific peak assignments in the spectral fit. The labels indicate the following carbon bonding: A, phenolic/ketone C═O; B, aliphatic/aromatic carbonyl; C, alcohol/O-alkyl-C/carbonyl. (Reprinted with permission from ref 95. Copyright 2007 Elsevier). Panel B: A component map of field-collected atmospheric particles based on characteristic features of laterally resolved NEXAFS spectra. Different colors correspond to particle areas with characteristic signatures of OC (green), BC (red), potassium-containing salts (orange), and other inorganic (cyan) constituents. (Reprinted with permission from ref 234. Copyright 2010 American Chemical Society.)

Hopkins et al. used X-ray microspectroscopy analysis of individual biomass-burning particles to correlate in situ optical measurements of SSA and AAE with the characteristic chemical signatures of particles, such as carbon-to-oxygen ratios and the extent of carbon sp^2 hybridization.[236] Figure 9 illustrates the correlation plots of SSA (panel A) and AAE (panel B) with averaged values of carbon sp^2 hybridization for particles emitted from 12 test burns of different biomass fuels. While substantial scatter of the data points indicates the analyzed particles' diverse chemical and optical properties, the overall trend is consistent with the assumption that particles with a high extent of carbon sp^2 hybridization (>80%) exhibit absorption

DOI: 10.1021/cr5006167
Chem. Rev. 2015, 115, 4335−4382

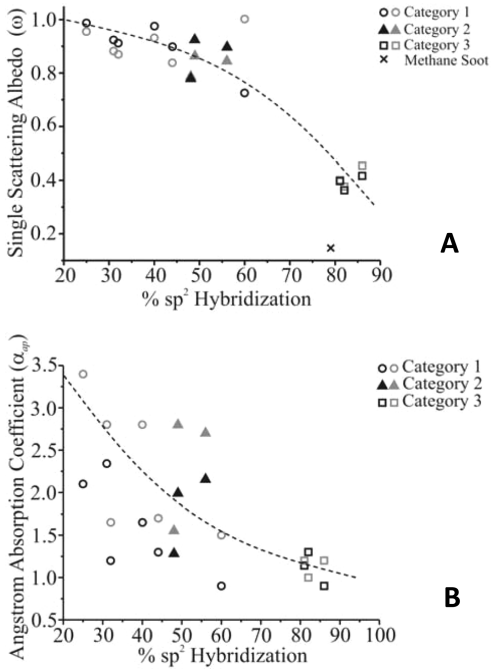

Figure 9. Correlation plots of measured SSA (A) and AAE (B) as a function of the percent of sp^2 hybridization determined from STXM/NEXAFS data for ensembles of individual particles sampled from the biomass-burning smoke of 12 biofuels and soot from methane combustion. Black and gray symbols represent optical measurements at 532 and 405 nm, respectively. The dashed lines are visual guides. (Reprinted with permission from ref 236. Copyright 2007 Wiley-Blackwell.)

properties of BC (AAE = 1, SSA = 0.4) and that particles containing more aliphatic carbon (20%−60% of sp^2 hybridization) show optical properties of BrC (AAE = 1.5−3.5, SSA = 0.8−1). Although both TEM and STXM/NEXAFS may provide useful information on the mixing state of BrC, the inherent variability and chemical complexity of BrC, the lack of known molecular signatures, the molecular selectivity, and the low concentrations of BrC chromophores preclude applications of these techniques as primary analytical tools for BrC characterization. Another limitation of these methods is that particle sampling by impaction onto the impaction substrates may alter the morphology of the collected particles versus that when they were airborne. Nevertheless, these chemical imaging techniques provide complementary information toward the molecular-level analysis of particle ensembles discussed in the previous section.

3.4. EEM Fluorescence Experiments

Fluorescence-based methods have been used extensively to characterize dissolved organic matter,[237] marine and terrestrial humic compounds,[238] and bioaerosols.[239] Liquid-phase fluorescence measurements can be performed in a three-dimensional mode with the emission intensity recorded as a function of both the excitation and emission wavelength, as done using excitation−emission matrix (EEM) spectroscopy. In EEM spectroscopy, the aerosol is extracted into a suitable solvent, and its EEM spectra are measured with a fluorometer. Examples of EEM applications to ambient aerosols can be found in refs 240−243. Time- and wavelength-resolved fluorescence spectra at a fixed excitation wavelength have been recorded for PM samples collected on a drum impactor,[244] resulting in a time resolution of several hours, as well as for single particles[245−247] in real time. Thus far, the fixed-wavelength excitation measurements have resulted in an empirical clustering of fluorescence spectra into groups based on the shape of the emission spectra with only tentative correlations between the observed clusters and the molecular identities of the fluorophores.[248,249]

Although the exact molecular identities of the BrC chromophores are not always known, they are expected to have a high degree of conjugation across the molecular skeleton and large-absorption cross sections. As fluorescent compounds often have the same characteristics, the compounds found in BrC aerosols potentially could act as efficient fluorophores. Although not as direct as absorption measurements, which classify BrC on the basis of the shape of absorption spectra, fluorescence measurements have the advantage of much higher detection sensitivity. However, only a few studies have relied on fluorescence as an indirect indicator of BrC compounds. Hegglin et al.[250] examined fluorescence of organic impurities in sulfuric acid aerosol, i.e., under highly acidic conditions known to promote BrC formation (see section 4). Rincon et al.[251] found that irradiation of aqueous pyruvic acid followed by dark aging of the solution produces BrC that can be repeatedly bleached by radiation and re-formed by dark aging with the concurrent loss and gain of fluorescence. Upon irradiation of solutions of phenolic compounds in the presence of H_2O_2 (a photochemical source of aqueous OH), Chang and Thompson[252] observed the formation of light-absorbing products. They also observed bathochromic shifts in fluorescence spectra of the solutions upon irradiation, which can be associated with increasing the size of the ring system and/or increasing conjugation in the products compared to the starting phenolic compounds. Using EEM spectroscopy, Lee et al.[253] found that α-pinene/O_3 SOA and d-limonene/O_3 SOA are weakly fluorescent. The fluorescence intensity increased significantly upon exposure of these aerosols to ammonia vapor, which converts initially colorless d-limonene/O_3 SOA into BrC material.[254] The fluorescence yield remained low, a fraction of a percent, and the fluorescence intensity increase was attributed to stronger absorbance by the aerosol at the excitation wavelengths. In a separate study, Lee et al.[255] found that aqueous solutions of BrC produced by high-NO_x photooxidation of naphthalene are fluorescent. The fluorescence intensity increased upon irradiation of the solution, even though the absorption coefficient decreased, suggesting either decreased fluorescence quenching or increased fluorescence quantum yields. In contrast, the d-limonene/O_3 + NH_3 brown material almost completely lost its ability to absorb visible radiation or fluoresce after irradiation. Zhong and Jang[111] observed fluorescence of OA from biomass burning during its photochemical aging in a smog chamber and found that the fluorescence intensity rapidly decreased with aging time, most likely resulting from reactions between fluorescent polycyclic aromatic hydrocarbons (PAH) and oxidants in the chamber. Phillips and Smith recorded EEM spectra of aqueous extracts of ambient particles collected in Atlanta, GA.[243] They interpreted the substantial Stokes shifts (~100 nm) and the lack of sensitivity of the high-wavelength tail of the emission spectrum to the excitation wavelength as a confirmation of the charge-transfer model for the absorption by organic matter.[256] In combination, these studies suggest that fluorescence is not only a sensitive probe of BrC but also is sensitive to the molecular (or supramolecular) identity of BrC compounds. Therefore, we

DOI: 10.1021/cr5006167
Chem. Rev. 2015, 115, 4335−4382

anticipate that fluorescence-based methods will play an increasingly important role in BrC studies.

4. LABORATORY STUDIES OF MODEL BrC SYSTEMS

4.1. BrC from Primary Fossil Fuel Combustion and Biomass Burning

Sun et al.[165] compared wavelength-dependent MAC_{bulk} for BrC from measurements by Havers et al.,[257] Varga et al.,[258] and Hoffer et al.[71] They found reasonable quantitative agreement between these measurements and MAC_{bulk} values reported for the humic fraction from pulp mill effluent by Duarte et al.[259] Measured values from Kirchstetter et al.[27] were significantly higher, most likely because of the experimental artifacts associated with filter optical measurements (discussed in section 3.1.3). To determine what types of organic molecules could be responsible for light absorption, Sun et al.[165] examined 550 UV−vis absorption spectra tabulated in the Perkampus atlas,[260] focusing on 200 spectra of compounds containing C, H, and O atoms. They cautioned that the molecule selection could be biased because the atlas contained information about molecules of synthetic rather than environmental interest and probably omitted weakly absorbing compounds. They concluded that molecules that contribute to BrC absorption of biomass-burning aerosol are likely to be large (18+ carbon atoms), have a large degree of unsaturation, and contain three or more oxygen atoms and/or one or more nitrogen atoms. Furthermore, they proposed that BrC absorption is controlled by a small fraction of strongly absorbing molecules with the remaining BrC components being nonabsorbing. Orthoquinones were cited as one example of potential chromophores consistent with the experimental observations.

Chakrabarty et al.[29] collected smoke from smoldering ponderosa pine duff and Alaskan duff in a chamber and probed their optical properties. A large fraction of the particles (>95%) were "tar balls," as suggested by their SEM images. These tar balls conformed to the definition of BrC, as the absorption coefficient increased quickly toward shorter wavelengths with an effective AAE of 6.4. They estimated the RFE of the tar balls (the definition of RFE is introduced near eq 18) and compared it to that of a "traditional organic carbon". The magnitude of RFE decreased when the imaginary refractive index was increased from zero (the base case scenario of nonabsorbing aerosol) to the value they observed in tar balls, although the effect was not dramatic. For example, the predicted RFE at 405 nm for the ponderosa pine duff aerosol (1.78 + 0.015i) and the traditional organic carbon (1.55 + 0i) were −22.7 and −26.0 W nm^{-1} m^{-2}, respectively (the negative sign means a cooling effect). The effect of BrC on the optical properties at 532 and 780 nm, where tar balls absorb weakly, was insignificant.

Chen and Bond[84] reported careful measurements of absorption coefficients from filter extracts of aerosols from solid fuel pyrolysis. They showed that methanol and acetone were much better solvents for extracting light-absorbing compounds from filters compared to water (polar solvent) and hexane (nonpolar solvent). This suggests that BrC chromophores in biomass smoke have some polar character, but they are not polar enough to make them sufficiently water soluble for efficient extraction from the filter. They calculated the simple forcing efficiency, defined by Bond and Bergstrom,[11] as a measure of the wavelength-integrated climate effect of absorption by BrC. They concluded that absorption by BrC investigated in their studies has a relatively small effect on the forcing efficiency and stated "Unless absorption by real ambient aerosol is higher than that measured here, it probably affects global average clear-sky forcing very little, but could be important in energy balances over bright surfaces."

Smog chamber experiments by Saleh et al.[60] have provided useful constraints on the relative contributions from fresh BC emissions, fresh POA emissions, and SOA formed by photochemical aging of residential hardwood to the overall absorption coefficient. This study provided conclusive evidence that both POA and SOA absorbed light to a significant extent. The optical measurements could not be explained by the absorption of BC alone. SOA was found to be less absorptive than POA in the visible range. However, it dominated the absorption coefficient in the near-UV range.

Zhong and Jang[111] conducted experiments on BrC produced by smoldering combustion of hickory hardwood in an outdoor smog chamber. They monitored the aerosol optical properties throughout the day to determine how photochemical aging of an aerosol affects its optical properties. They found that the MAC_a values of BrC material first increased in the morning and then gradually decreased in the afternoon. They interpreted these observations as evidence of competition between the formation of chromophores by photooxidation and photobleaching of chromophores by sunlight. These results suggest that BrC light absorption properties change significantly after a day of solar exposure, highlighting its highly dynamic nature.

Saleh et al.[97] carried out smog chamber aging experiments of airborne biomass-burning particles to characterize changes in the imaginary refractive index k as a function of fuel type and aerosol aging state. Figure 10 summarizes the major findings of that study. They found that k and AAE were strongly correlated with the BC-to-OA ratio for a broad range of experiments using a variety of biomass fuels, indicating that the aerosol absorption coefficient depends more on the burn conditions than on fuel type. Using thermodenuder-based measurements, where semivolatile organic compounds (SVOC) were stripped off aerosols, they were able to demonstrate that BrC compounds in biomass-burning aerosol can be classified as ELVOCs. They estimated that ELVOCs had an order of magnitude higher k than the rest of the organic compounds.

A comprehensive study by Lewis et al.[101] examined the role of the particle morphology and humidification-induced particle shape changes on the apparent absorption properties of biomass-burning aerosols. They generated aerosol by burning of several common types of biomass fuels and measured their scattering and absorption coefficients at 530 and 870 nm at different RH levels using nephelometry and PAS, respectively. The scattering coefficients increased as a result of water uptake by inorganic compounds in particles (larger particles are generally more efficient in light scattering than smaller ones). However, the absorption coefficients decreased as a result of the RH exposure, despite expectations that the presence of an aqueous shell on the particles should increase absorption due to lensing effects. A particle collapse (i.e., significant change in particle morphology from extended fractal to a significantly more compact round shape) induced by high RH was presented as a possible explanation for this discrepancy. However, these results could be also explained by an experimental artifact of the PAS measurements, resulting from a decrease in the photoacoustic signal due to the loss of energy to water evaporation from particles. This study highlights the difficulty in measuring absorption coefficients for realistic BrC particles under humid conditions. In a related

DOI: 10.1021/cr5006167
Chem. Rev. 2015, 115, 4335−4382

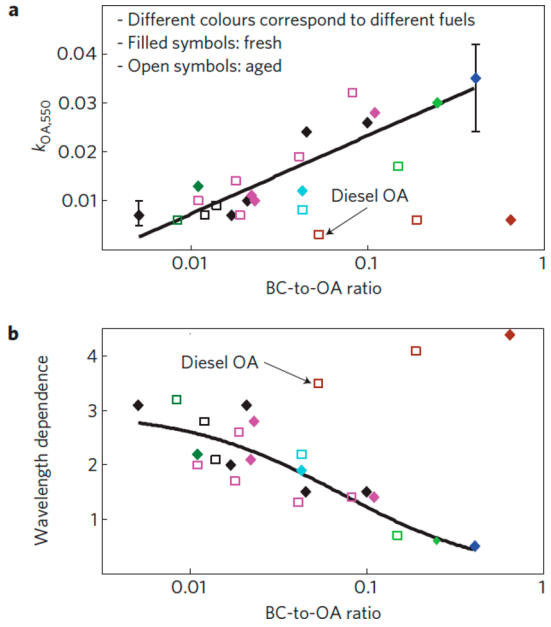

Figure 10. Panel a: Experimentally determined dependence of the effective OA absorptivity k_{OA} on the BC-to-OA ratio in biomass-burning aerosols. k_{OA} is quantified as an imaginary part of the refractive index, excluding contribution from BC. Panel b: Experimentally determined wavelength dependence of OA absorptivity on the BC-to-OA ratio in biomass-burning aerosols. Wavelength dependence (w) is defined as w = AAE − 1, which offsets the absorptivity of BC to w = 0 value. Filled diamonds and open squares correspond to measurements of fresh and chemically aged emissions, respectively. Colors correspond to different biomass fuels. Black lines are least-squares fits to the data. (Reprinted with permission from ref 97. Copyright 2014 Nature Publishing Group.)

study, Hand et al.[261] showed that the observed increase in the scattering coefficient upon humidification can be fully explained by water uptake by the particle's inorganic constituents. For particles containing only organic components, the humidification factors, defined as the ratio of scattering coefficients under humid and dry conditions, were not significantly different from 1.

A study by Hoffer et al.[71] focused on HULIS contributions to the absorption and scattering coefficients of biomass-burning aerosols in the Amazon region. They collected aerosols at a tropical pasture site in Brazil during a biomass-burning season in September. They isolated HULIS via the method described by Varga et al.;[258] aerosolized the extract; and measured the size distribution, 545 nm scattering coefficient, and 532 nm absorption coefficient of the resulting aerosol. In addition, they acquired full absorption spectra of the extracts to measure the AAE. The absorption coefficient at 532 nm was quite low, $MAC_a \sim 300\ cm^2g^{-1}$, resulting in a negligible contribution of HULIS to the overall Amazonian biomass-burning aerosol absorption coefficient at this wavelength. However, because of the large measured AAE of 6.4−6.8, HULIS absorbed about 50% of radiation in the photochemically active near-UV region of the spectrum, potentially affecting the availability of photochemically generated oxidants.

Experiments by Dinar et al.[80] provided an important link between the optical properties of HULIS and their nominal molecular weight. They carried out careful CRD measurements at 390 and 532 nm for size-resolved particles containing different types of HULIS. These experiments enabled quantitative determination of both real and imaginary refractive indexes from Mie closure calculations. For the molecular weight fractionated Suwannee River fulvic acid particles, k at 532 nm increased with a rise in the nominal molecular weight (k = 0.003, 0.021, and 0.094 for MW = 520, 570, and 770 g/mol, respectively). The same trend was observed for ambient HULIS in extracts of PM collected during a biomass-burning episode in a moderately air-polluted and a rural area. The lowest n and k values were obtained for HULIS collected in a rural area. Dinar et al.[80] calculated SSA and RFE for the base-case scenario of an internal mixture of 98% ammonium sulfate (AS) and 2% BC and for the aerosol containing an internal mixture of AS, HULIS, and BC. In the presence of 20%−70% HULIS, SSA decreased by up to 30% depending on the wavelength and refractive indexes used for HULIS. This decrease resulted in significantly less negative values of RFE, representing less cooling by aerosols. The authors concluded that HULIS in biomass smoke and air pollution may contribute significantly to light absorption and radiative forcing by aerosols.

4.2. BrC from Gas-Phase Photooxidation of VOCs

Table 1 features a summary of studies that reported experimentally measured or estimated light absorption coefficients for SOA in the visible range of the spectrum. The table does not include a large body of studies that measured only the real refractive index of SOA; an overview of such data can be found in refs 262 and 263. Because it is typical to report data for more than one type of SOA, the table is organized by the experimental study with a secondary grouping by the SOA precursor.

4.2.1. Optical Properties of SOA from Biogenic Precursors. Because of their large contribution to the global SOA budget, monoterpenes represent the most studied SOA precursors. Not surprisingly, significant attention has been dedicated to characterizing the optical properties of SOA prepared from monoterpenes. For example, Nakayama et al.[264,265] examined SOA generated by high-NO_x photooxidation (α-pinene/OH/NO_x) and ozonolysis (α-pinene/O_3) of α-pinene. They found that both types of SOA absorbed negligibly (k < 0.003) at 355, 405, 532, and 781 nm wavelengths. Flores et al.[262] measured the refractive indexes for SOA produced from α-pinene, limonene, and humulene in the 360−420 nm wavelength range using BBCES. They summarized all of the previous measurements for these SOA and compared typical k values for different known sources of BrC. All three precursors were shown to produce SOA with very small absorption coefficients, which often fall below the detection limit of aerosol absorption spectrometers. The result is predictable, as SOA compounds produced by photooxidation of isoprene and monoterpenes are dominated by molecules with carbonyl, carboxyl, and hydroxyl functional groups, which, with the exception of the very weak n → π^* band in carbonyls around 280 nm, do not have low-energy electronic transitions.

Song et al.[266] investigated the effect of seed aerosol acidity on SOA produced by ozonolysis and NO_3 oxidation of α-pinene under dry and humidified conditions in the chamber. The absorption coefficients were quantified at 355, 405, 532, and 870 nm (the absorption coefficients at 532 and 870 nm were below the detection limit). Neutral and acidic seed particles were generated by atomization of $MgSO_4$ and $MgSO_4/H_2SO_4$ solutions, respectively. The SOA formed on neutral seed did not absorb. However, the absorption coefficient increased rather significantly when an acidic seed was used under dry

DOI: 10.1021/cr5006167
Chem. Rev. 2015, 115, 4335−4382

Table 1. A Summary of Studies That Reported Various Light Absorption Properties of Model SOA Produced in Smog Chambers or Flow Tubes[a]

study	SOA precursors used[b]	conditions[c]	reported optical parameters[d]	summary of key results
Liu et al. (2013)[163]	APIN, LIM, CAT	O_3	wavelength-dependent k and n in the 220−1200 nm range measured by spectroscopic ellipsometry	introduction and validation of the spectroscopic ellipsometry method; insignificant k measured at visible wavelengths for all three SOA
Song et al. (2013)[266]	APIN	O_3 and NO_3	MAC_a at 355, 405, 532, and 870 nm	no significant absorption for SOA formed on neutral seed; significant increase in absorption at 355 and 405 nm for acidic seed, especially for the APIN/NO_3 SOA, but only observed under dry conditions
Mang et al. (2008)[268]	LIM	O_3	visual observation and absorption spectrum	LIM/O_3 becoming brown upon storage in laboratory air (for an unknown reason at that time; later attributed to NH_3+ SOA carbonyl chemistry)
Bones et al. (2010)[254]	LIM, APIN, BPIN, MYR, TER	O_3	absorption spectra of aerosol extracts from 200 to 700 nm	No significant absorption over the visible range; large increase in absorbance upon aqueous reaction of LIM/O_3 and TER/O_3 with AS
Laskin et al. (2010)[208]	LIM	O_3	absorption spectrum	large increase in the absorbance upon exposure of LIM/O_3 SOA samples to gaseous NH_3; the chromophores proved to be highly conjugated, nitrogen-containing compounds
Updyke et al. (2012)[269]	LIM, ISO, APIN, CED, HUM, FAR, PLO, CLO, TET, TMB, NAP	O_3, OH, and OH/NO_x	MAC_{bulk} of aerosol extract from 300 to 700 nm	no significant absorption over the visible range except for NAP/OH and NAP/OH/NO_x; large increase in MAC_{bulk} upon exposure of SOA material to gaseous NH_3 for LIM/O_3, HUM/O_3, CED/O_3, CLO/O_3
Nguyen et al. (2012)[35]	LIM	O_3	MAC_{bulk} of aerosol extract from 300 to 700 nm	LIM/O_3 SOA undergoes highly efficient browning when its aqueous solution with AS or H_2O_4 is evaporated
Lee et al. (2013)[253]	LIM, APIN	O_3 and OH	MAC_{bulk} of aerosol extract from 300 to 600 nm; fluorescence yields	increase in MAC_{bulk} and in fluorescence intensity from SOA upon exposure to gaseous NH_3, especially for LIM/O_3 and LIM/OH
Flores et al. (2014)[262]	LIM, APIN, HUM	O_3	n, k over the 360−420 nm range	no measurable absorption (k < 0.001) for fresh SOA; k increased from <0.001 to 0.032 ± 0.019 for LIM/O_3 and from 0 to 0.029 ± 0.021 for HUM/O_3 after exposure to NH_3 vapor
Lin et al. (2014)[273]	ISO	reactive uptake of IEPOX	MAC_{bulk} of aerosol extract from 290 to 700 nm	BrC compounds formed on an acidic seed aerosol; evidence for extensively dehydrated oligomers of IEPOX containing linked tetrahydrofuran rings
Sato et al. (2012)[292]	BEN, TMB	OH/NO_x	visual observation	yellow filters with BEN/OH/NO_x; white filters with TMB/OH/NO_x; major products of oxidation identified
Jaoui et al. (2008)[291]	TOL, APIN, ISO	OH/NO_x and OH/NO_x/SO_2	visual observation	yellowish TOL/OH/NO_x with color becoming darker with added SO_2 and lighter with added ISO (see Figure 14)
Nakayama et al. (2010),[264] (2012),[265] and (2013)[168]	TOL, TMB, APIN	OH/NO_x and O_3	n, k at 355, 405, 532, and 781 nm	zero k at all measurement wavelengths within experimental precision for APIN/O_3; measurable k at 405 and 355 nm for TOL/OH/NO_x likely due to absorption by nitrocresols with an increase in k with the initial NO_x concentration; negligible k at all measurement wavelengths for TMB/OH/NO_x, consistent with the lower yield of nitrocresols from TMB compared to TOL
Ma and Thompson (2012)[187]	TOL, APIN	OH/NO_x and O_3	extinction cross section, scattering cross section, and SSA at 355 nm	SSA ∼ 1.00 for APIN/O_3 (extinction and scattering cross section indistinguishable from each other); SSA ∼ 0.95 for TOL/OH/NO_x
Zhong and Jang (2011)[176]	TOL, APIN, LIM	OH/NO_x	wavelength-dependent mass-normalized absorbance recorded with an integrating sphere	higher absorbance for LIM/OH/NO_x and TOL/OH/NO_x SOA formed in the presence of AS neutral or acidic seed; reduced absorbance upon exposure of SOA to UV radiation
Zhong et al. (2012)[274]	TOL, APIN	OH/NO_x	wavelength-dependent mass-normalized absorbance recorded with an integrating sphere	increase in absorbance with the NO_x level for TOL/OH/NO_x; reasonable agreement between the measurements and semiempirical quantum calculations of absorption spectra of SOA components for both SOA
Liu et al. (2014)[277]	TOL, MXYL	OH and OH/NO_x	wavelength-dependent k (250−600 nm) and k (250−1200 nm) measured by spectroscopic ellipsometry	systematic increase in k with NO_x at all wavelengths; values of k for TOL/OH/NO_x approaching those from biomass-burning aerosol; lower values of k for MXYL/OH/NO_x despite the larger precursor's molecular size
Liu et al. (2012)[275]	TMB	OH and OH/NO_x	MAC_a at 467 nm	an increase in MAC_a under high-NO_x relative to the low-NO_x conditions; lower MAC_a under higher RH conditions, possibly due to hydrolysis of N-containing chromophores
Li et al. (2014)[278]	BEN, TOL, EBEN, MXYL	OH, OH/NO_x, and $h\nu$/NO_2	n at 532 nm	different n values observed under OH/NO_x and $h\nu$/NO_2 conditions possibly due to the chemistry switch from the RO_2 + HO_2 to RO_2 + NO control
Lambe et al. (2013)[105]	NAP, GUA, JP10, APIN	OH/NO_x	k at 405 nm and MAC_{bulk} of extracted SOA	MAC_{bulk} for all SOA increases with SOA age (increasing O/C ratio from an exposure to high OH levels); large MAC_{bulk} for NAP/OH/NO_x; complicated dependence of MAC_{bulk} for GUA/OH/NO_x on wavelength/age; good agreement for measured MAC_{bulk} with that calculated from independently measured k

Chem. Rev. 2015, 115, 4335−4382 DOI: 10.1021/cr5006167

Table 1. continued

study	SOA precursors used[b]	conditions[c]	reported optical parameters[d]	summary of key results
Lee et al. (2014)[106]	NAP	OH/NO_x	MAC_{bulk} of SOA extracts from 240 to 540 nm	large MAC_{bulk} values; reduction in MAC_{bulk} upon aqueous irradiation of SOA extracts accompanied by significant changes in molecular level composition; contribution of nitrophenols to the absorption spectrum deduced from the pH dependence.
Lu at al. (2011)[290]	BaP	NO_3	extinction coefficient at 355 and 532 nm; absorption coefficient at 532 nm	an increase in the extinction at both wavelengths and SSA at 532 nm dropping from 1 to 0.85 upon exposure of BaP-coated particles to NO_3
Ofner et al. (2011)[279]	GUA, CAT	O_3	absorption spectrum	spherical, absorbing particles produced on exposure of CAT and GUA to ozone
Ofner et al. (2012)[280]	GUA, CAT, APIN	O_3	absorption spectrum	exposure of SOA to Cl and Br atoms produces opposite changes on the SOA absorption for GUA/O_3 and CAT/O_3; no effect on APIN/O_3
Romonosky et al. (2014)[107]	GUA	OH/NO_x	effective molecular absorption cross section (see eq 9)	GUA/OH/NO_x is stable to irradiation, despite being more absorbing than SOA from APIN, BPIN, MYR, LIM, HUM, and TMB

[a]Measurements of real refractive indexes (k) of SOA are not included in this table. [b]Precursors are abbreviated as follows: APIN, α-pinene; BaP, benz[a]pyrene; BEN, benzene; BPIN, β-pinene; CAT, catechol; CED, α-cedrene; CLO, cedar leaf essential oils; EBEN, ethylbenzene; FAR, farnesene; GUA, guaiacol; HUM, α-humulene; IEPOX, isoprene epoxydiol; ISO, isoprene; JP10, tricyclo[5.2.1.$0^{2,6}$]decane; LIM, d-limonene; MYR, β-myrcene; MXYL, m-xylene; NAP, naphthalene; PLO, pine leaf essential oils; TER, γ-terpinene; TET, tetradecane; TMB, 1,3,5-trimethylbenzene; TOL, toluene. [c]Conditions for SOA preparation and aging: OH/NO_x, high-NO_x photooxidation; OH, low NO_x photooxidation; $h\nu/NO_2$, classic photooxidation done without explicitly adding an OH precursor; O_3, oxidation by ozone; NO_3, oxidation by NO_3 (sometimes with O_3 present). [d]See section 3.1 for definitions of various aerosol absorption properties.

conditions, especially when using NO_3 as the oxidant. The enhancement was not observed when RH in the chamber was elevated. On the basis of the analogy of the formation of brown organosulfates in evaporating limonene SOA (LSOA) solutions acidified with H_2SO_4[35] and the formation of light-absorbing compounds by carbonyl uptake into concentrated sulfuric acid,[267] the authors suggested that the highly acidic seed particles promote aldol condensation of the SOA compounds. Of note, Zhong and Jang[176] observed enhancement in the absorption coefficient for limonene/OH/NO_x and toluene/OH/NO_x SOA. They also attributed this effect to aldol condensation of carbonyl compounds in SOA. On the basis of the larger absorption coefficients in the presence of NO_3, Song et al.[266] hypothesized that chromophores are compounds possessing both the organosulfate and organonitrate groups. They argued that the acidity level experienced by the SOA material in their study is unlikely to occur under typical ambient conditions. The authors concluded that dark reactions of α-pinene with ozone and NO_x do not contribute to BrC formation. However, both field studies and laboratory experiments indicate that organosulfates formed in reactions of α-pinene oxidation products with acidic seeds[266] or nitrooxy organosulfates emitted[65] during biomass burning of coniferous wood may contribute to light absorption by α-pinene SOA.

Browning of the limonene/O_3 SOA (LSOA) has been examined in several studies (refs 35, 208, 253, 254, 268, and 269) with a special emphasis on BrC formation upon exposure to ammonia and amines. Table 1 summarizes the studies of LSOA optical properties, while a discussion about the underlying ammonia-driven chemistry is deferred to the next section. Following the initial qualitative observations that visible absorbance by limonene/O_3 SOA increases in the presence of ammonia, AS, and amines,[208,254,268] Updyke et al.[269] reported MAC_{bulk} values for several types of SOA produced from various biogenic (d-limonene, isoprene, α-pinene, α-cedrene, α-humulene, farnesene, and pine and cedar leaf essential oils) and anthropogenic [tetradecane, 1,3,5-trimethylbenzene (TMB), and naphthalene] precursors in the 300−700 nm range. Some of these precursors were oxidized by both OH and ozone to examine the effect of the oxidant on the SOA optical properties. No seed aerosol was used in these experiments. With the exception of naphthalene SOA produced under low-NO_x and high-NO_x conditions, none of the SOA examined by Updyke et al.[269] had significant absorption in the visible range. This observation is in agreement with other measurements discussed in this section. However, SOA from several precursors, including d-limonene, α-humulene, α-cedrene, and cedar leaf essential oils, exhibited a significant increase in MAC_{bulk} upon exposure to ammonia vapor. In a related study, Nguyen et al.[35] measured MAC_{bulk} values resulting from evaporation of limonene/O_3 SOA solutions in water containing AS or H_2SO_4. The evaporation was shown to be a quick and efficient way to trigger browning in both cases. Lee et al.[253] quantified MAC_{bulk} values, as well as fluorescence quantum yields, for SOA produced by ozonolysis and OH oxidation of limonene and α-pinene before and after exposure to ammonia. Finally, Flores et al.[262] conducted aerosol flow tube experiments to test if exposure to gaseous ammonia can increase the imaginary refractive index for SOA particles produced from limonene, humulene, and α-pinene. They observed a measurable increase in the imaginary refractive index for the limonene/O_3 and humulene/O_3 SOA but not for α-pinene/O_3

DOI: 10.1021/cr5006167
Chem. Rev. 2015, 115, 4335−4382

SOA, which is in quantitative agreement with the results of previous bulk measurements.[269]

Isoprene has attracted much attention as a major VOC precursor of global SOA. The formation of highly reactive isoprene epoxydiol (IEPOX) products from isoprene oxidation is a critical mechanistic step in isoprene SOA formation under low NO_x conditions.[270] IEPOX compounds have been shown to be efficiently taken up by acidic aerosols and are responsible for the enhanced yield of isoprene SOA under low-NO_x conditions.[271,272] A recent study by Lin et al. demonstrated that the reactive uptake of IEPOX into acidic aerosols leads to oligomeric products, which absorb UV and visible light with an average MAC_{bulk} (for the 300−700 nm range) of 300 cm^2/g.[273] The formation of these BrC products was observed upon uptake of IEPOX by dry acidified $MgSO_4$ seed aerosol (estimated aerosol pH = 0.6) and was efficiently quenched under humid conditions. No BrC products were observed on acidified AS seed (estimated aerosol pH = 2.3). They used HPLC/UV−vis/ESI-MS to probe the molecular composition of the IEPOX-derived BrC. The retention time of the absorbing products suggested they are relatively nonpolar compounds. The mass spectra of compounds eluting at these retention times corresponded to oligomeric structures containing up to 10 units of $C_5H_8O_2$ and C_5H_6O with values of double bond equivalents (DBE) ranging from 7 to 16. Using MS^n fragmentation analysis, the authors could identify tetrahydrofuran rings as elements of the oligomer structures and proposed that chromophores must be formed by extensive dehydration of the oligomers. Figure 11 shows the tentative mechanism for the initial stages of this dehydration. They suggested that such oligomers potentially may contribute to the source of HULIS in atmospheric aerosol. Similar light-absorbing oligomers were identified in aerosol samples collected in the rural southeastern United States, which is known to be strongly influenced by isoprene chemistry.

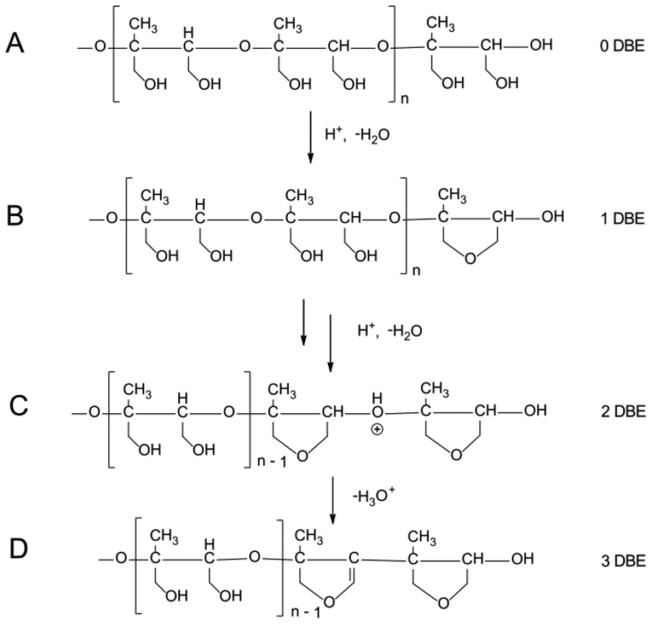

Figure 11. Tentative mechanism of dehydration of oligomeric species in IEPOX-derived SOA. (A) Initial oligomer derived from IEPOX, (B) tetrahydrofuran ring formation by cyclodehydration of the hydroxymethylene groups, and (C and D) proposed dehydration of ether linkages with the formation of dihydrofuran rings. (Reprinted with permission from ref 273. Copyright 2014 American Chemical Society.)

4.2.2. Optical Properties of SOA from Aromatic Precursors. Several groups have measured absorption and scattering coefficients of SOA produced by high-NO_x photooxidation of toluene (toluene/OH/NO_x SOA). Zhong and Jang[176] used an integrated sphere method to examine full absorption spectra of toluene/OH/NO_x, as well as SOA from high-NO_x photooxidation of limonene and α-pinene. Of the three aerosols, only the toluene SOA had an appreciable absorption coefficient at near-UV wavelengths. Nakayama et al.[168] compared results from Kim and Paulson,[263] Nakayama et al.,[264] and Zhong and Jang[176] with their own measurements for toluene/OH/NO_x SOA and detected no measurable absorption at 532 and 781 nm. However, the k values at 405 nm increased from 0.0018 to 0.0072 as the starting concentration of NO_x in the chamber changed from 110 to 570 ppb.[168] Nitrocresols were tentatively identified as the primary contributors to the absorption spectrum of toluene/OH/NO_x SOA. This assumption was corroborated by the negligible measured absorption coefficients for TMB + OH/NO_x SOA, which is known to contain lower amounts of nitrocresols than toluene SOA. Depending on the initial NO_x level, the estimated MAC_a at 405 nm ranged from 800 to 5200 cm^2/g, suggesting that toluene/OH/NO_x SOA could contribute to the radiation balance around 400 nm.

In a follow-up study, Zhong et al.[274] introduced a bottom-up approach for modeling SOA optical absorption properties. They combined a master chemical mechanism (MCM) model to estimate product distribution generated during oxidation of α-pinene and toluene with a gas-particle partitioning model to predict SOA composition. For each major particulate compound, they calculated the energy and oscillator strength of the lowest electronic transition using a semiempirical neglect of diatomic differential overlap (NDDO) method. The contributions from individual compounds were added together in proportion to their concentrations in the particles and then convoluted with an empirically chosen Gaussian band shape with the full width at half-maximum of 60−80 nm. Simulated spectra obtained using this approach were compared with experimental absorption spectra of the corresponding SOA obtained using the integrated sphere method. Despite the limitations of the electronic structure method used in that study and the rather approximate treatment of the band shapes, reasonable agreement was obtained between the experimental and calculated absorption spectra.[176] This type of bottom-up modeling approach could work reasonably well when individual SOA components contribute roughly equally to light absorption. The authors acknowledged that the method only works within MCM model limitations. For example, an accurate prediction of SOA absorption cannot be obtained for systems where absorption spectra are dominated by minor high-MW compounds absent in the MCM model or by molecular aggregates. The authors also noted that, in agreement with experimental observations, the model predicted an increase in the absorption coefficient of toluene SOA produced under high-NO_x conditions but no significant change in light absorption by α-pinene SOA in the presence of NO_x.

Liu et al.[275] examined the effect of hydrolysis on the composition and optical properties of SOA produced through photooxidation of TMB in humid air under low- and high-NO_x conditions. Using Fourier transform infrared (FTIR) spectroscopy functional group analysis, they estimated that 5%−20% of

DOI: 10.1021/cr5006167
Chem. Rev. 2015, 115, 4335−4382

organic compounds by mass in the TMB/high-NO_x SOA correspond to organonitrates. The fraction of organonitrates in the aerosol decreased for RH in excess of 20% with an effective rate constant of 4 day^{-1}, suggesting that even small amounts of aerosol water could affect SOA composition. MAC_a of SOA was measured by PSAP at 467 nm. In contrast to Nakayama et al.,[168] they found that TMB/high-NO_x SOA was reasonably absorbing and definitively more absorbing than the TMB/low-NO_x SOA system. Of note, photooxidation of TMB most likely produces both organonitrates, detected in abundance in the Liu et al. experiments, and nitro compounds. Simple aliphatic organonitrates have negligible light absorption at 467 nm,[276] while nitroaromatic compounds absorb radiation much more efficiently (related discussion follows). The decrease in the absorption coefficient for SOA produced under humidified conditions relative to dry conditions may imply that multifunctional, aromatic organonitrates produced from TMB have considerably higher absorption cross sections than their simpler aliphatic analogs.

Lambe et al.[105] investigated SOA optical properties as a function of aerosol age. In that study, model aerosols were prepared from various precursors (naphthalene, α-pinene, guaiacol, and tricyclodecane) and exposed to high OH concentrations for a controlled period of time in a potential aerosol mass (PAM) flow reactor. Upon exiting the PAM reactor, particle extinction and absorption were measured with a combined CRD/PAS instrument, and the particle composition and extent of oxidation (O/C ratio) were probed using AMS. In addition, absorption spectra of the particle extracts were measured to provide their wavelength-dependent MAC_{bulk} values. Several interesting observations emerged from their study. First, MAC_{bulk} calculated (using eq 6) from the PAS measurements of k at 405 nm were in good agreement with MAC_{bulk} values measured from the absorption spectra of the SOA extracts for all of the aerosol precursors and for different SOA ages (the 532 nm absorption coefficients measured with PAS were below the detection limit for all systems). Second, both the imaginary refractive index and MAC_{bulk} showed a clear positive correlation with aerosol age, suggesting that more oxidized organics in SOA absorb light more efficiently. Third, the reported MAC_{bulk} values at 405 nm of these SOA were relatively small (below 900 cm^2/g) compared to MAC_{bulk} values of BrC from biomass burning [typically $(0.2-3) \times 10^4$ cm^2/g]. However, because SOA global production rates are significantly higher than biomass-burning emissions, BrC produced by chemical aging of SOA may still compete with BrC from biomass burning for its effect on overall light absorption. Finally, the PAM measurements agreed reasonably well with previous chamber measurements for naphthalene SOA by Updyke et al.[269] and for α-pinene SOA by Zhong and Jang,[176] suggesting that the fast SOA aging in PAM under high OH concentration conditions and slower photooxidation by OH in a smog chamber may have a comparable effect on the optical properties.

Lee et al.[255] reported the wavelength-resolved MAC_{bulk} values of SOA produced by high-NO_x photooxidation of naphthalene. On the basis of the observed red-shift in the absorption spectrum of the SOA aqueous extracts at higher pH, they concluded that nitrophenols contribute to the large absorption coefficients in the naphthalene/OH/NO_x SOA. MAC_{bulk} values were shown to decrease following aqueous irradiation of SOA extracts. Furthermore, irradiation resulted in significant changes in molecular composition of SOA examined using direct-infusion ESI-HR-MS. Romonosky et al.[107] studied aqueous photodegradation involving a range of different SOA types. That study reported effective molecular absorption cross sections for guaiacol/OH/NO_x SOA, which was found to be the strongest-absorbing SOA and appeared yellow when collected on filters. Despite being the most absorbing, guaiacol/OH/NO_x SOA was more resilient to photodegradation compared to considerably less absorbing SOA from monoterpenes.

As described in section 3.1.1, Liu et al.[163] introduced an ellipsometry-based method for measuring both real and imaginary refractive indexes of SOM between 220 and 1200 nm. They validated their methods by recording refractive indexes of SOA produced by ozonolysis of α-pinene, limonene, and catechol. The α-pinene and limonene had negligible k values (<0.001) above ~310 nm. The catechol SOA absorbed about an order of magnitude more strongly, but its k values still dropped below 0.001 at visible wavelengths. In a follow-up study, Liu et al.[277] used the spectroscopic ellipsometry method to determine the complex refractive index of SOA material from photooxidation of toluene and *m*-xylene. They concluded that k values for toluene and xylene SOA are, at least, an order of magnitude greater than those for typical biogenic SOA materials. By varying the NO_x concentration during SOA preparation, they found that higher NO_x levels resulted in enhanced light absorption, which is in agreement with observations of Nakayama et al.[168] Despite its larger molecular size, *m*-xylene produced less-absorbing SOA compared to toluene, indicating that BrC formation is sensitive to subtle differences in molecular structures of SOA precursors. Figure 12 shows a comparison of the wavelength-dependent k values reported by Liu et al., along with k values reported for BrC from biomass burning and HULIS.[277] Under high-NO_x photooxidation conditions, the measured k values for toluene and xylene SOA are within a range of observations for atmospheric BrC (shaded area in the figure).

A recent set of laboratory experiments by Li et al.[278] compared classical photooxidation (NO_2 + VOC without an OH precursor); high-NO_x photooxidation with nitrous acid (HONO) used as an OH precursor; and low-NO_x photooxidation of benzene, toluene, ethylbenzene, and *m*-xylene. Although they only reported the real refractive index, they found significant differences in n for the classical and high-NO_x oxidation, attributing it to the predominance of RO_2 + HO_2 chemistry in the former case and RO_2 + NO chemistry in the latter. This study highlights the high sensitivity of the optical properties to NO_x levels in the chamber.

Ofner et al.[279] examined the products of ozonolysis of catechol and guaiacol as a model for the aromatic fraction of atmospheric HULIS. The ozonolysis produced cluster-like aggregates of nearly perfect spherical particles as revealed by electron microscopy imaging. Compared to the precursors, the resulting aerosols had considerably increased absorbance, extending all the way to 600 nm (the authors did not quantify the absorption coefficient). Of note, the absorption spectrum of the catechol ozonolysis products looked rather different from the one obtained by Liu et al.[163] At present, the reason for this difference is unclear. The same group later examined the effect of aging these SOA, as well as the α-pinene/O_3 SOA, by exposure to Cl and Br atoms.[280] The absorbance of the catechol/O_3 and guaiacol/O_3 SOA decreased following exposure to Cl, while exposure of the same SOA to Br resulted in enhanced light absorption. The effect of halogen atom

DOI: 10.1021/cr5006167
Chem. Rev. 2015, 115, 4335−4382

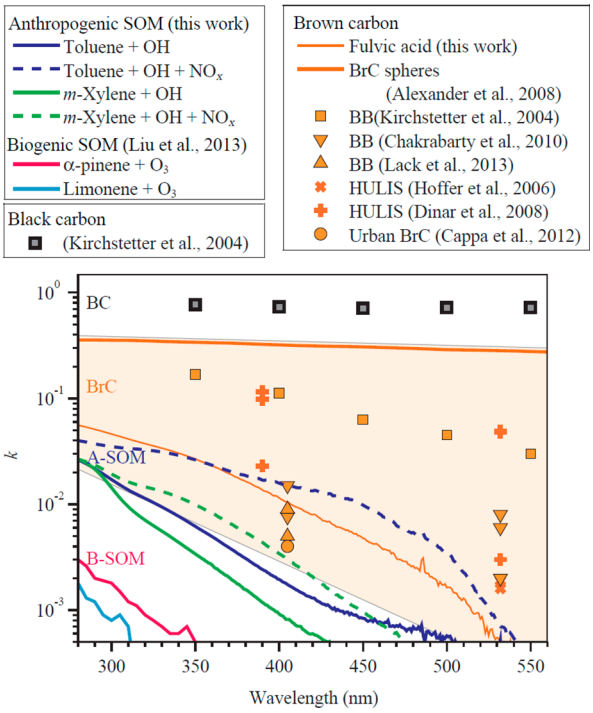

Figure 12. Comparison of a wavelength-dependent imaginary part of the refractive index (k) values for different types of atmospherically relevant light-absorbing materials. Dark blue and green lines show original data from the work of Liu et al. (2014), the source for this plot: anthropogenic SOM derived from reacting toluene or *m*-xylene at low- and high-NO_x conditions and a BrC surrogate (Suwannee River fulvic acid). Literature: α-pinene- and limonene-derived biogenic SOM (B-SOM), various atmospheric BrC in both biomass burning (BB) and urban plumes and BC. (Reprinted with permission from ref 277. Copyright 2014 Copernicus Publications.)

exposure on the absorbance of α-pinene/O_3 SOA was not significant.

4.2.3. Chromophoric Nitroaromatic Compounds in SOA. Jacobson proposed that light absorption by nitroaromatic compounds in the gas and aerosol phases may be responsible for a 25%−30% reduction of the near-UV (300−400 nm) irradiance within the boundary layer in Los Angeles.[281] Neutral nitroaromatic compounds, such as nitrobenzenes, nitrophenols, nitrocatechols, nitroguaiacols, and nitrosalicylic acids, have large absorption cross sections (>10^{-17} cm^2/molecule)[281,282] in the near-UV region extending into visible, while the corresponding deprotonated species are characterized by even stronger absorption at longer wavelengths. The relative yield of nitroaromatic compounds is rather independent of NO concentration[283] but increases with NO_2/NO_3 concentration.[284−286] Furthermore, the product distribution strongly depends on the structure of the aromatic precursor, which affects the efficiency of the OH-aromatic product formation and the subsequent reactivity of these products with O_2 and NO_2. For example, Nishino et al.[287] showed that the reactivity of the OH-aromatic products with NO_2 becomes prominent at NO_2 mixing ratios of ∼3.3 ppm for toluene, ∼0.06 ppm for naphthalene, and ∼0.6 ppm for biphenyl, indicating that OH-adducts of PAHs react more efficiently with NO_2 than their single-ring aromatic counterparts. Under typical atmospheric conditions, comparable reactivity toward NO_2 and O_2 is observed for OH-adducts of benzene, toluene, and *p*-xylene at NO_2 mixing ratio of around 1.25 ppm[288] and for OH-adducts of naphthalene and larger PAHs at NO_2 mixing ratios of 50−150 ppb.[287,289] These factors, along with the structures of the nitroaromatic products, may significantly affect light absorption by aromatic SOA formed under high-NO_x conditions.

To test Jacobson's prediction[281] that nitrated PAHs in aerosols contribute to the absorption of UV light, Lu et al.[290] examined how optical properties of PAH-containing particles change upon oxidation with NO_2 and NO_3. They measured the extinction coefficient for polystyrene latex (PSL) spheres coated with benz[*a*]pyrene using CRD and the absorption coefficient at 532 nm using PAS at 355 and 532 nm. Exposure of these particles to NO_3 increased both the overall extinction at both wavelengths and the absorption at 532 nm, with SSA at 532 nm dropping from 1 to 0.85. Using AMS, they could detect nitrobenz[*a*]pyrene as the main reaction product in particles. They also studied the reaction of benz[a]pyrene with NO_3 in a bulk solvent, but this resulted in a reduction (rather than an increase) of the 355 nm absorption, indicating that the reaction mechanism depends sensitively on the environment around benz[a]pyrene. In the atmosphere, nitroaromatic compounds are produced through oxidation of aromatic precursors in the presence of NO_2. It has been suggested that nitrocatechols and other nitroaromatic compounds formed through atmospheric oxidation of biomass-burning emissions are major contributors to atmospheric BrC.[64,222,223,225,291] Recent HPLC/UV−vis/MS studies unambiguously identified nitrophenols and nitrocatechols as dominant light-absorbing compounds in cloud-water samples impacted by agricultural biomass burning in Eastern China[222] and in $PM_{2.5}$ biomass-burning samples collected in Hungary.[64] Similar to terpenes, the browning capacity of SOA produced from aromatic VOCs strongly depends on the precursor structure. For example, Sato et al.[64,292] reported the light yellow color of benzene/OH/NO_x SOA collected on filters, while the TMB/OH/NO_x SOA was white. LC−MS analysis revealed the presence of nitrophenols in the benzene SOA but not in TMB SOA, which may explain the differences in the extent of browning observed for these materials.

Forstner et al.[286] reported a detailed study of the chemical composition of SOA formed from different aromatic precursors (e.g., toluene, *m*-xylene, *p*-xylene, 1,2,4-trimethylbenzene, ethylbenzene, *m*-ethyltoluene, and *p*-ethyltoluene) in the presence of NO_x. Gas chromatography−mass spectrometry (GC−MS) analysis indicated the presence of saturated and unsaturated anhydrides along with nitroaromatic compounds in SOA samples. However, the relative yield of nitroaromatics is strongly dependent on the structure of the aromatic precursor. The highest fraction of nitroaromatic compounds was observed in toluene SOA, while 1,2,4-trimethylbenzene SOA did not contain measurable amounts of nitroaromatic products.[286] Figure 13[286] shows a summary of reaction steps, resulting in the formation of nitroaromatic products from toluene. The reaction is initiated by adding OH to the ring. The resulting methylhydroxycyclohexadienyl radical reacts with NO_2 to produce cresols. Subsequent reactions of cresols with OH generate methylphenoxy radicals that react with NO_2 to form nitroaromatic products. Jang and Kamens[293] identified a large number of substituted aromatic, nonaromatic ring-retaining, and ring-opening products in toluene SOA. They found that methylnitrophenols and methyldinitrophenols were the dominant products formed under high-NO_x conditions. Sato et al. quantified 22 particle-phase products of toluene oxidation using LC−MS.[285] The mass ratio of the aromatic products (e.g.,

DOI: 10.1021/cr5006167
Chem. Rev. 2015, 115, 4335−4382

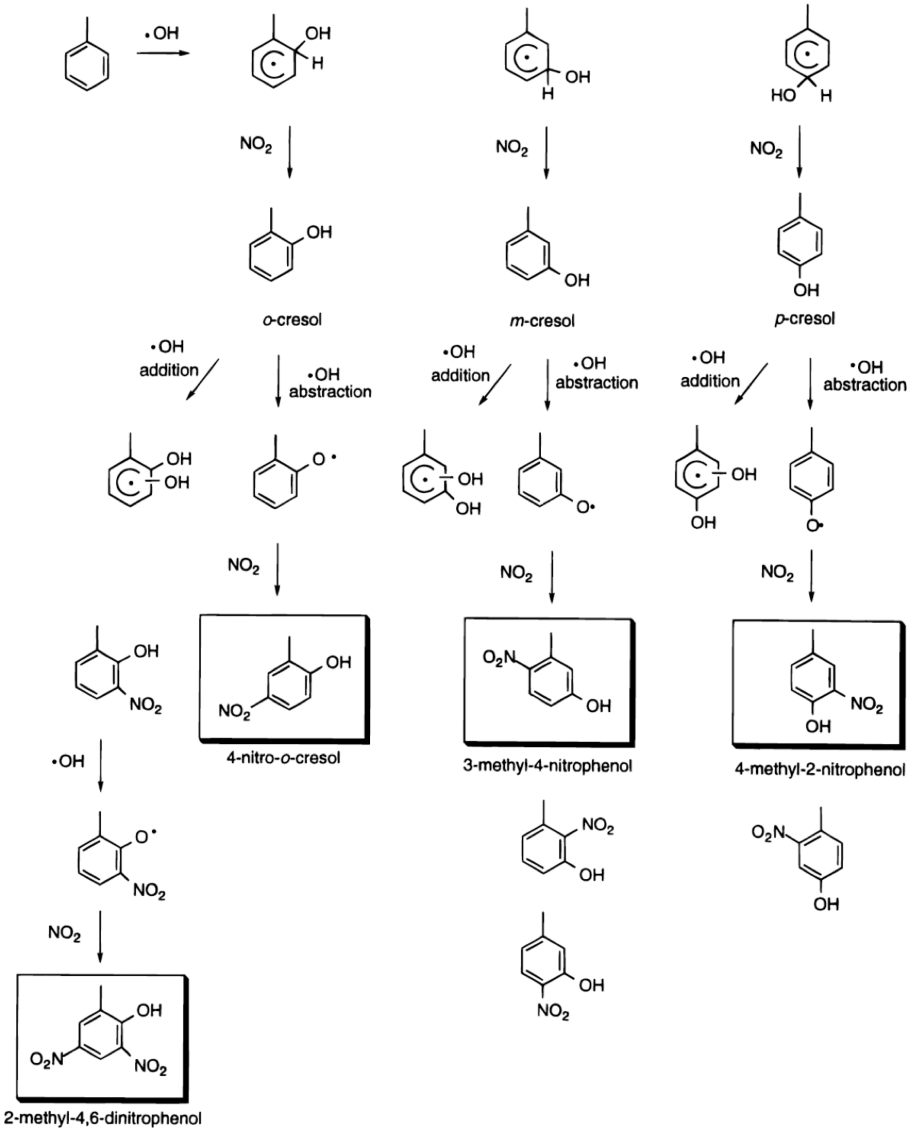

Figure 13. Atmospheric oxidation of toluene with OH in the presence of NO_2. The initial reactions of NO_2 with the methylhydroxycyclohexadienyl radicals resulting from toluene−OH reaction lead to cresols, which then result in nitroaromatic products. (Reprinted with permission from ref 286. Copyright 1997 American Chemical Society.)

Figure 14. Colored appearance of SOA material generated from different combinations of α-pinene, toluene, and isoprene precursors mixed with variety of oxidants, including NO_x and SO_2. (Reprinted with permission from ref 291. Copyright 2008 Wiley-Blackwell.)

nitrocresols, nitrotoluene, and dinitrocresol) increased, while the yield of ring-opening products decreased with NO_x concentration. This result is consistent with the recent study by White et al., in which fewer nitroaromatic compounds were detected in toluene SOA produced under intermediate NO_x concentrations.[294]

Jaoui et al. observed that SOA generated by mixing biogenic and anthropogenic precursors had different color, indicating differences in composition.[291] Figure 14 showcases photographs of the filters containing SOA produced from α-pinene and toluene in the presence of NO_x. SOA produced from the α-pinene/toluene mixture (filter labeled F1) has a light-yellow color, while the addition of SO_2 produces brown SOA (F3). A

DOI: 10.1021/cr5006167
Chem. Rev. 2015, 115, 4335−4382

substantially lighter color is observed when isoprene is added to the mixture (F2 and F4). The addition of isoprene was shown to efficiently sequester NO_2, thereby reducing the amount of nitroaromatic products generated through oxidation reactions. The addition of SO_2 was shown to have a minor effect on gas-phase reactions and a modest effect on the particle-phase reactions of α-pinene, which may contribute to the browning observed for the α-pinene/toluene/SO_2 mixture (F3).

4.3. BrC from Aqueous-Phase Photochemical Processes

There is mounting evidence that aqueous-phase chemistry in cloud and fog droplets contributes to the formation and aging of SOA compounds. For a comprehensive summary of the current state of knowledge about the aqueous atmospheric chemistry, readers are referred to recent reviews by Ervens et al.[1] and Herrmann et al.[295] In this context, the term "cloud/fog processing" encompasses various processes where aerosols and clouds/fog closely interact with each other. For example, some of the cloud condensation nuclei (CCN)-active particles in an ascending air parcel may activate into clouds droplets. The cloud droplets then might scavenge some of the water-soluble gases, as well as particles that did not nucleate droplets. The dissolved compounds may participate in aqueous chemical and photochemical reactions during the droplet lifetime. The liquid water from cloud droplets eventually evaporates, leaving residual atmospheric particles that have been "processed by the cloud." In addition to the obvious physical effects of evaporation leading to the reshuffling of the water-soluble material, droplet evaporation has been recognized as a mediator of chemical reactions. The evaporation processes increase concentrations of solutes, lower the pH, and promote reactions where water acts as an explicit product (i.e., condensation reactions). Examples of the evaporation-driven chemistry, along with key references, will be provided in section 4.4.

The cloud/fog processes that convert smaller water-soluble organic compounds into larger low-volatility products, which remain in the condensed phase upon droplet evaporation (a SOA produced by this pathway is called an "aqSOA" to emphasize its origin), are of particular interest in BrC chemistry. The most important process that contributes to aqSOA formation is oxidation of organics by OH. However, under certain conditions, metal-catalyzed chemistry, photolysis, and various nonradical processes may compete with OH oxidation. For example, section 4.4 will discuss the extensively studied chemistry of α-dicarbonyls that result in imidazole-based light-absorbing products through aqueous processes catalyzed by an ammonium ion. In this section, we will overview photochemical and free radical aqueous reactions that lead to the production of BrC compounds. Aqueous processes that result in BrC photobleaching (i.e., reduction in the visible absorption coefficient) will be discussed as well.

Aqueous oxidation of phenolic compounds by OH has been shown to result in products that have characteristic BrC absorption spectra. Early work in this area was done by Gelencser and co-workers, who were the first to demonstrate that aqueous OH oxidation of 3,5-dihydroxybenzoic acid, a water-soluble compound released in biomass burning, results in strongly light absorbing organic matter.[296] The authors attributed light absorption to the formation of HULIS and proposed that HULIS observed in these experiments may have secondary (rather than primary) origin in the form of aqueous photooxidation products of phenolic compounds. A follow-up study by Hoffer et al.[297] compared different properties of 3,5-dihydroxybenzoic acid oxidation products with those of typical HULIS. They showed that the UV−vis absorption spectra, ESI mass spectra, thermally assisted hydrolysis, methylation GC−MS, and thermograms of the aqueous photolysis products and HULIS looked quite similar, lending support to the aqueous photooxidation mechanism of HULIS production.

The experiments of Gelencser et al.[296] relied on Fenton chemistry initiated by the addition of $FeCl_3$ + H_2O_2 to the solution of 3,5-dihydroxybenzoic acid as a dark source of OH. Fenton chemistry contributes to OH production but it is not the major source of OH in cloud/fog droplets. Chang and Thompson[252] showed that an alternative method of OH generation through photolysis of H_2O_2 produces qualitatively similar results. They conducted a systematic study of the photooxidation of a number of phenolic compounds (Figure 15 features a complete list of compounds) under irradiated conditions using H_2O_2 as an OH source. The reaction products were examined using UV−vis, ESI-MS, nuclear magnetic resonance (NMR), and FTIR. For all compounds, aqueous photooxidation resulted in a significant buildup of colored products and the formation of high-MW compounds. When the hydroxyl or methoxy group was in the ortho position with respect to the phenolic OH, reactions proceeded more rapidly. In contrast, para substitution slowed the formation rate of light-absorbing products.

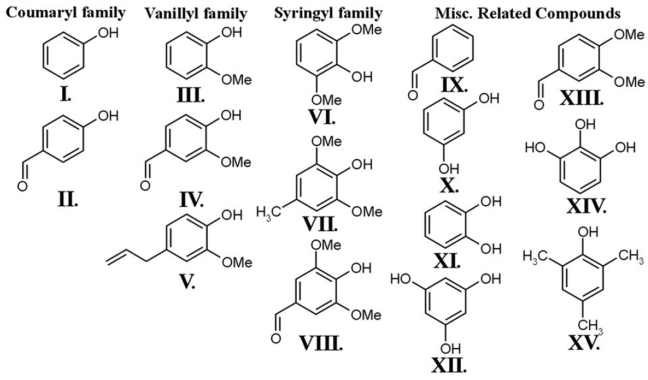

Figure 15. Compounds examined by Chang and Thompson (2010) with respect to their aqueous-phase reaction with OH: **I**, phenol; **II**, *p*-hydroxybenzaldehyde; **III**, guaiacol; **IV**, vanillin; **V**, eugenol; **VI**, syringol; **VII**, 4-methylsyringol; **VIII**, syringaldehyde; **IX**, benzaldehyde; **X**, resorcinol; **XI**, catechol; **XII**, phloroglucinol; **XIII**, veratraldehyde; **XIV**, pyrogallol; and **XV**, 2,4,6-trimethylphenol. (Reprinted with permission from ref 252. Copyright 2010 Elsevier Ltd.)

Sun et al. studied the mechanism of aqueous oxidation of phenol, syringol, and guaiacol by OH, produced through H_2O_2 photolysis as shown in Figure 16.[298] Using AMS, they were able to detect dimeric reaction products, as well as larger oligomers, formed by phenoxy radical chemistry. Recently, Kitanovski et al. investigated the aqueous photonitration of guaiacol in irradiated solutions containing hydrogen peroxide and nitrite anion to investigate its possible transformation in fog waters.[299] Using HPLC coupled with UV−vis and ESI-MS/MS detectors, they identified a number of guaiacol photonitration products, including 4-nitroguaiacol, 6-nitroguaiacol, and 4,6-dinitroguaiacol. They also identified two of these compounds in PM samples from Slovenia. All of the products, especially 4,6-dinitroguaiacol, had significant absorbance. In addition, they observed a large peak in the UV−vis chromatogram due to

DOI: 10.1021/cr5006167
Chem. Rev. 2015, 115, 4335−4382

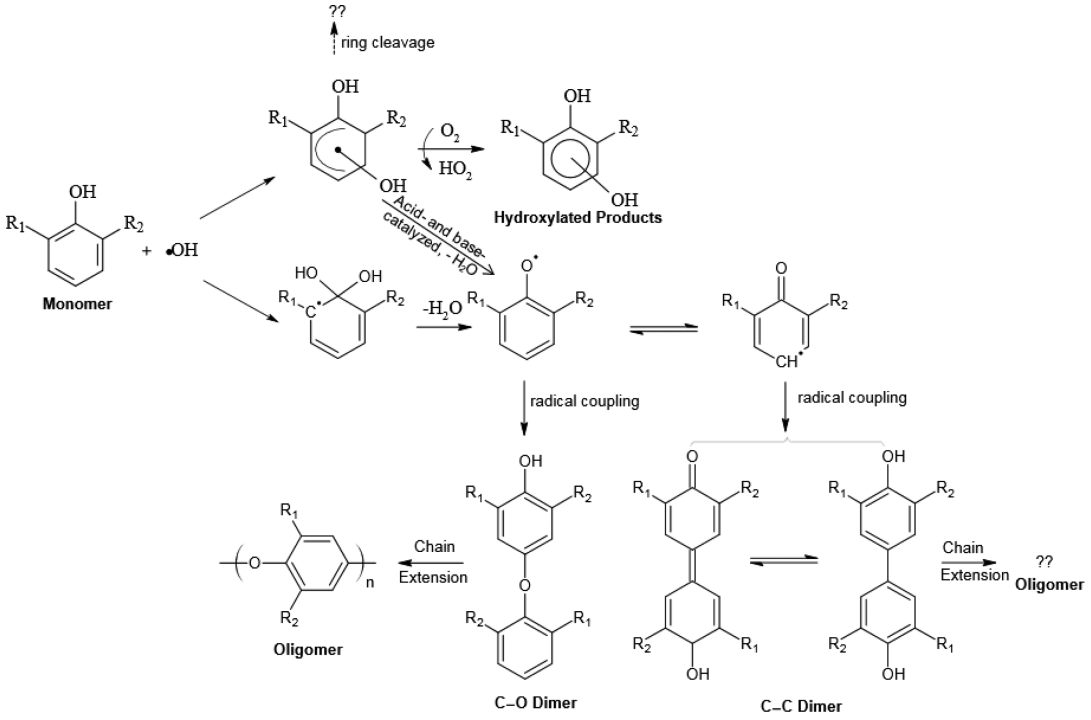

Figure 16. Reaction mechanisms for the formation of hydroxylated species and oligomers from phenolic precursors (phenol, R_1 = H, R_2 = H; guaiacol, R_1 = O−CH_3, R_2 = H; syringol, R_1 = O−CH_3, R_2 = O−CH_3). (Reprinted with permission from ref 298. Copyright 2010 Copernicus Publications.)

unidentified high-MW products, likely oligomeric compounds formed in the aqueous photonitration of guaiacol. These types of compounds can contribute to BrC in areas affected by biomass burning.

Li et al.[300] investigated the yield and chemical composition of aqSOA produced by aqueous photolysis and OH oxidation of vanillin. In that study, offline analysis of aqSOA solutions was combined with atomization and characterization of the chemical composition using AMS. Although Li et al. did not quantify the optical properties of aqSOA, they noted a yellowish color of the resulting solution in experiments with higher vanillin concentrations. Importantly, they found that the OH oxidation products were not volatile (unlike vanillin itself, which fully volatilized upon atomization and drying). The identified compounds included dimeric products of vanillin oxidation, which potentially can absorb light. Direct photolysis was found to be much less efficient in producing aqSOA from vanillin than OH oxidation.

Turpin and co-workers[301−304] examined aqSOA formation through OH oxidation of various nonaromatic isoprene oxidation products. Although they have not characterized the optical properties of aqSOA, they observed the formation of high-MW products that potentially could serve as WSOC BrC chromophores produced by photooxidation of methylglyoxal,[302,304] pyruvic acid,[301] and glycolaldehyde.[303] Laboratory experiments by Holmes and Petrucci[305] found that aqueous dark Fenton oxidation of levoglucosan (a marker of cellulose combustion) with OH results in oligomeric compounds. Acid-catalyzed oligomerization reactions also were observed in the same reaction system. Although the optical properties of the resulting products were not examined in that study, the authors suggested that products of biomass burning contain iron, hydrogen peroxide, acids, and a variety of water-soluble species, including levoglucosan, which potentially could contribute to the formation of BrC HULIS through aqueous Fenton and/or acid-catalyzed chemistry.

Rincon et al.[306] observed an interesting phenomenon that they referred to as "thermochromism" in aqueous organic matter. They found that products of aqueous photolysis of pyruvic acid developed a strong absorption with $MAC_{bulk} \sim 10^3$ cm^2/g (calculated per weight of carbon) at 532 nm after staying in solution with NH_4HSO_4 in darkness for a few hours. The resulting BrC compounds could be photolyzed with an effective half-time for the photobleaching on the order of 1 h but then would reacquire absorption if returned to darkness. This sequence could be repeated many times. The browning was attributed to alcohol dehydration leading to unsaturated compounds, while the photobleaching was ascribed to photoinduced rehydration. In a related study, Rincon et al.[251] observed similar evolution of the absorption spectra in solutions of photolyzed pyruvic acid (without added NH_4HSO_4). They noted that changes in the absorption spectra of the resulting mixture were not associated with any significant changes in the ESI mass spectra, which led them to conclude that the chromophores are supramolecular aggregates as opposed to isolated molecular compounds. This assumption is consistent with Sharpless and Blough's suggestion that optical properties of colored dissolved organic matter (CDOM) are controlled by charge-transfer interactions between molecules rather than individual chromophores[256] and with attribution of light absorption by extractable organic material from particles collected in Atlanta, GA, to charge transfer complexes.[243] However, as discussed in section 4.4.2, the formation of strong individual chromophores does not always translate into large changes in the corresponding ESI mass spectra and may be easy to miss. Regardless of the chromophores' chemical nature, the Rincon et al. experiments suggest that the optical properties of

DOI: 10.1021/cr5006167
Chem. Rev. 2015, 115, 4335−4382

BrC depend—in a complex manner—on the irradiation level, temperature, and presence of codissolved inorganic species.

In addition to OH photooxidation and direct photolysis, other types of aqueous photochemical and radical-driven processes may serve as important sources of BrC. For example, Smith et al.[307] conducted a detailed study of the photosensitized mechanism of aqSOA formation in aqueous reactions of phenol, guaiacol, and syringol with the triplet excited state of an aromatic carbonyl 3,4-dimethoxybenzaldehyde. These reactions converted phenols into aqSOA with nearly 100% yields. The authors estimated that in areas dominated by biomass combustion, these triplet state reactions can be more important than oxidation by OH. Unfortunately, they have not characterized the optical properties of the aqSOA products. It would be desirable to characterize the optical properties of the products of photosensitized reactions in all future experiments.

It is important to note that aqueous photochemical processes do not always produce oligomeric compounds. Experiments where model SOA mixtures were produced in a chamber, dissolved in water, exposed to simulated solar radiation, and analyzed by HR-MS revealed faster photodegradation of oligomeric SOA compounds compared to the smaller monomeric species.[106,107,308,309] The preferential removal of oligomeric compounds upon irradiation was observed in a range of SOA produced from biogenic (isoprene, α-pinene, β-pinene, β-myrcene, *d*-limonene, and α-humulene), anthropogenic (TMB and naphthalene), and biomass-burning (guaiacol) precursors using ozone or OH/NO_x as the oxidants. For one of these SOA types, namely, the naphthalene + OH/NO_x SOA, the effect of aqueous irradiation on MAC_{bulk} also was examined.[106] The BrC in naphthalene + OH/NO_x SOA was observed to slowly photobleach during the aqueous irradiation with an effective half-life of ~15 h (with the sun in its zenith) for the loss of its absorption coefficient. The same study demonstrated that BrC produced by aqueous reactions between *d*-limonene-derived SOA and AS (refer to section 4.4) can be bleached much faster with an effective half-time for the loss of MAC_{bulk} at 500 nm of less than 0.5 h.

In summary, depending on various conditions, aqueous photochemical processes may generate BrC compounds, e.g., by the OH-driven oxidation of certain organic molecules, or photobleach BrC via photodegradation of oligomeric, light-absorbing compounds. Therefore, for any sort of BrC aerosols, it is important not only to characterize their optical properties but also to understand how these properties may be affected by various possible aerosol aging scenarios.

4.4. Formation of BrC in Nonradical-Driven Processes

4.4.1. Chemical Aging of α-Dicarbonyls. α-Dicarbonyls, such as glyoxal (GL) and methylglyoxal (MG), form through oxidation of numerous biogenic and anthropogenic VOCs.[310−314] The estimated global sources of GL and MG are 45−56 and 140 Tg y^{-1}, respectively.[310,312] Despite the high volatility of α-dicarbonyls, they readily partition to the aqueous phase due to their high solubility (effective Henry's constant of ~3×10^5 M/atm for GL and ~3×10^3 M/atm for MG)[315] and reactivity. Enhanced GL partitioning into the particle phase has been attributed to the formation of highly soluble *gem*-diols accompanied by the formation of high-MW oligomeric products,[301,302,316−320] which was found to be a reversible process.[321] In addition, the irreversible uptake of α-dicarbonyls by aqueous aerosols and cloud droplets has been identified as an important atmospheric sink for these reactive species, contributing to a global SOA formation of 2.6 Tg C y^{-1} from GL and 8 Tg C y^{-1} from MG,[310,313] respectively.

GL and MG uptake in aerosols is significantly modified by the presence of inorganic seed.[318,322,323] Kroll et al. suggested that the observed enhancement in the effective Henry's constant for GL uptake on AS seed by a factor of ~50 is due to the high ionic strength rather than the high acidity of the seed.[323] However, bulk solution experiments by Ip et al.[324] showed that the Henry's constant of GL is specifically enhanced by the presence of sulfate anions. An increase in the concentration of NaCl (and ionic strength) actually decreased the effective Henry's constant in their experiments, unlike the case of Na_2SO_4, where the Henry's constant increased significantly with SO_4^{2-} concentration. An independent set of bulk measurements from Yu et al.[325] confirmed the strong specific effect of sulfate anions on GL partitioning into aqueous solutions. Kampf et al.[326] conducted chamber experiments on the uptake of GL into AS aerosol and concluded that the effective Henry's law constant increases exponentially with AS concentration. They were able to quantitatively describe the "salting-in" by AS with a Setschenow equation

$$\log\left(\frac{K_{H,water}}{K_{H,salt}}\right) = (0.00 \pm 0.13) + (-0.24 \pm 0.02\ m^{-1})c_{AS} \quad (23)$$

where c_{AS} is the molality of AS in the solution. Given the widespread occurrence of sulfates in the atmospheric environment, the uptake of GL by aerosols in humid air or by cloud/fog droplets containing AS is always significant.

Several aqueous-phase reactions, some of which generate light-absorbing products, contribute to the irreversible uptake of α-dicarbonyls.[327] For example, ammonium-catalyzed oligomerization and C−N bond formation were identified as key processes that contribute to the formation of light-absorbing products in reactions between GL and MG with ammonium salts.[320,321,328,329] These reactions have been observed in bulk solutions containing appropriate reactants and drying aqueous solutions representing cloud processing of SOA, as well as in the particle phase. Figure 17[321] depicts a summary of GL reactions observed in aqueous AS aerosol, while several light-absorbing products of GL + AS reactions are listed in Table 2. The following sections discuss possible pathways resulting in the formation of light-absorbing products of α-dicarbonyls.

4.4.1.1. Aqueous Oxidation and Oligomerization of α-Dicarbonyls. Oxidation of α-dicarbonyls by OH radicals results in the formation of carboxylic acids with oxalic acid being the major product of GL oxidation.[330−333] However, at typical OH concentrations and cloud droplet lifetimes (~15 min), the extent of GL oxidation is expected to be fairly low.[334] An alternative pathway involves conversion of GL-dihydrate, a dominant form of GL in bulk aqueous solutions in which both carbonyl groups are converted into *gem*-diols, into a highly reactive GL-monohydrate upon solvent evaporation.[316,321,327,334−336] The latter has been shown to form low-volatility products that remain in the condensed phase through oligomerization reactions.[301,317,321,327,337,338] For example, at concentrations of 4−1000 μM, typical for clouds and fogs, ~33% of GL and ~19% of MG are converted into oligomeric products[321,336] and remain in the aerosol phase upon droplet evaporation.[36]

Two major oligomerization pathways of α-dicarbonyls in aqueous solutions involve (1) reaction of the dicarbonyl with

DOI: 10.1021/cr5006167
Chem. Rev. 2015, 115, 4335−4382

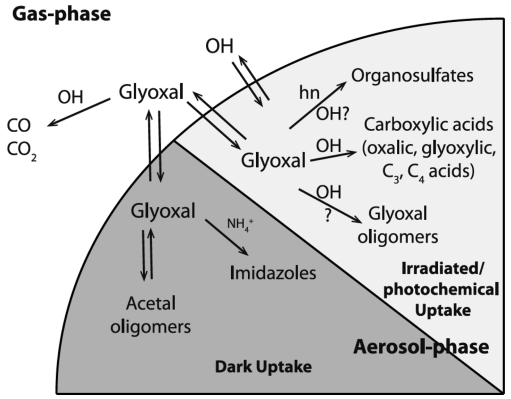

Figure 17. A summary of major glyoxal reactions within deliquesced particles and microdroplets containing ammonium sulfate. Glyoxal oligomers formed during photochemical uptake refer to any type of higher molecular weight compound. While reaction chemistry under dark conditions has been studied extensively, photochemical reactions have been examined only in limited laboratory studies using bulk samples resembling cloud-processing conditions. Overall, condensed-phase chemistry of glyoxal leads to the formation of oxidized constituents of OA. (Reprinted with permission from ref 349. Copyright 2011 Wiley-Blackwell.)

Table 2. Possible Products for the Glyoxal/Ammonium Sulfate System and Ab Initio Predictions of Their UV−Vis Absorption[a]

	Molecule	CIS			DFT (HOMO-LUMO)	
		energy (eV)	λ (nm)	oscillator strength	energy (eV)	λ (nm)
a)	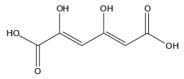	5.583	222.1	1.1331	4.057	**305.6**
b)	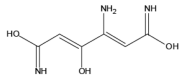	6.592 5.559	188.1 223.0	0.2552 1.1016	4.108	**301.8**
c)	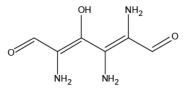	5.546	223.6	0.6557	2.663	**465.6**
d)		7.266	170.6	0.1775	5.676	218.5
e)	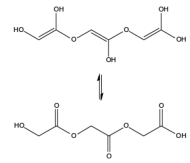	7.803 10.218 10.276	158.9 121.4 120.6	1.7168 0.1024 0.1824	5.622 7.413	220.5 167.3
f)	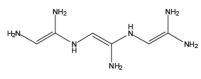	7.2183 7.0982	171.8 171.8	0.8916 0.8058	4.070	**304.6**

[a]The energy and corresponding wavelength of transitions with oscillator strength $f > 0.1$ are shown from CIS/cc-pvtz(-f) calculations, and the energy and corresponding wavelength of the HOMO−LUMO (highest occupied/lowest unoccupied molecular orbitals) transition are shown, based on DFT B3LYP/cc-pvtz(-f) calculations. (Reprinted with permission from ref 329. Copyright 2009 Copernicus Publications.)

its hydrated form, resulting in a hemiacetal followed by an intramolecular ring closure to form a cyclic hemiacetal, followed by subsequent acid-catalyzed oligomerization of the hemiactal products, and (2) acid-catalyzed aldol condensation of α-dicarbonyls. It has been demonstrated that aldol condensation is favorable at a higher pH of 4−5, while hydration/hemiacetal formation is dominant at pH 3.5.[338] Altieri et al. showed that aldol condensation does not occur in the presence of light and OH radicals, indicating that aldol condensation is important only during the nighttime.[302] Krizner et al. showed with the help of density functional theory (DFT) calculations that hydration of the aldehyde group of MG is favored over hydration of the ketone group.[339] As a result, MG-monohydrate is the dominant species in solution. In addition, calculations indicate that MG dimerization into its dimeric hemiacetal is associated with a substantial barrier of ∼25 kcal/mol, and aldol condensation is the dominant oligomerization process for this precursor.

Reactive uptake processes are not exclusive to α-dicarbonyls. Noziere and co-workers showed that, under certain conditions, oligomerization reactions of simple aldehydes and ketones may produce light-absorbing products. For example, absorption at ∼280 nm has been observed following exposure of concentrated sulfuric acid solutions to gas-phase acetone, while exposure to acetaldehyde generated light-absorbing products with absorption centered at ∼340 nm.[267] When mixed with sulfuric acid, other aldehydes and ketones also formed oligomeric products with absorption in the range of 300−400 nm.[40] The observed absorption was attributed to aldol condensation. Browning of aldehydes and ketones was observed in aqueous salt solutions of NaCl, $CaCl_2$, Na_2SO_4, and $MgSO_4$ containing the amino acids glycine, alanine, serine, arginine, and proline.[340] A transition from first-order to the second-order kinetics with respect to acetaldehyde concentration was observed with an increase in amino acid concentration. Figure 18 details the proposed mechanism of ammonium-catalyzed condensation of acetaldehyde. The reaction is initiated by the formation of an enamine intermediate, which subsequently undergoes oligomerization, forming carbonyl-containing condensation products with conjugated C−C bonds. The first-order reaction rate was attributed to enamine formation, whereas the second-order reaction rate was consistent with C−C bond formation through condensation reactions (Figure 18). Similar reactivity was observed in AS solutions containing acetaldehyde or acetone.[328]

4.4.1.2. Formation of BrC Products through Aqueous Reactions with Ammonium and Primary Amines. Several studies demonstrated the importance of ammonium, both as a catalyst and a reactant, in the formation of light-absorbing products from α-dicarbonyls and simple carbonyls in atmospheric aerosol mimics. For example, Noziere et al. studied reactions of GL with aqueous solutions of ammonium salts at room temperature.[320] They examined the reaction kinetics using UV−vis as oligomeric products formed through acid-catalyzed condensation of GL and identified several N-containing compounds using LC−MS. It has been proposed that ammonium salts act both as Brønsted acids, facilitating condensation reactions, and as reactants, forming iminium species. The iminium pathway resulted in the formation of a product absorbing at 209 nm, which was used for subsequent kinetics studies. This pathway was found to follow fairly rapid second-order kinetics, indicating that the light-absorbing

DOI: 10.1021/cr5006167
Chem. Rev. 2015, 115, 4335−4382

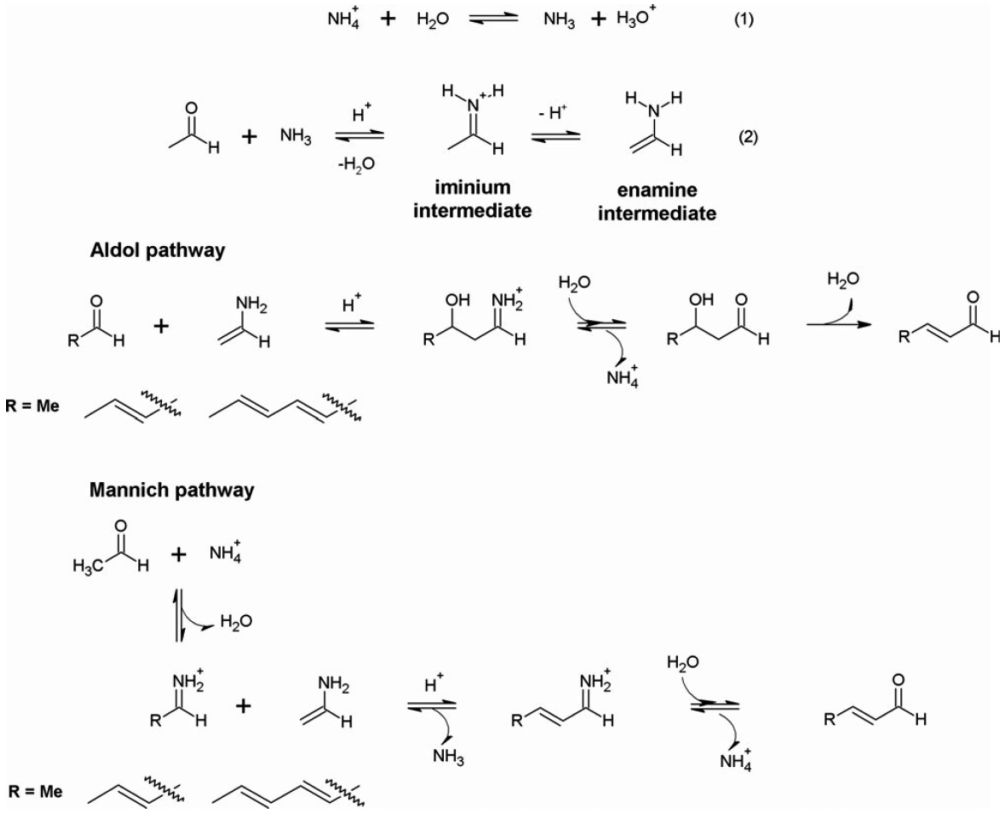

Figure 18. Mechanism of the aldol condensation of acetaldehyde catalyzed by amino acids and involving carbonyl−imine reaction chemistry. (Reprinted with permission from ref 340. Copyright 2008 American Chemical Society.)

product is a second-generation oligomer containing a C═C or C═N bond. The rate constant for this reaction increased dramatically with pH and was rather independent of the counterion at the same solution pH. A comparison between the rate constant for ammonium-catalyzed decay of GL with the rate constant for the GL reaction with OH radicals in an aqueous solution indicated that these two processes are the major sinks for GL in aqueous aerosols and cloud droplets.

Shapiro et al. proposed that reactions of GL in mildly acidic (pH 4) inorganic salt solutions generate a complex mixture of light-absorbing molecules with more than one species contributing to light absorption at a given wavelength.[329] In agreement with results reported by Noziere et al.[320] and Galloway et al.,[321] all GL−ammonium salt solutions exhibited a visible color change, while the GL−NaCl and GL−Na_2SO_4 solutions remained clear, confirming the important role of the ammonium cation in the browning chemistry of α-dicarbonyls. Similar UV−vis spectra were obtained for samples prepared in the dark and in the presence of ambient light, indicating that organosulfates formed under irradiation do not contribute to the observed light absorption. It also has been argued that both imidazole and imine pathways should be suppressed at pH 4. DFT calculations identified several π-conjugated oligomeric products of GL + AS reactions (shown in Table 2) that may be responsible for the observed absorption. These types of products may be formed through acid-catalyzed aldol condensation reactions.

In a related study, Sareen et al. used UV−vis to examine the kinetics of the formation of light-absorbing products in aqueous solutions containing MG and AS or ammonium nitrate (NH_4NO_3).[341] That study demonstrated that bimolecular reaction of MG with NH_4^+ is the rate-limiting step. DFT calculations identified light-absorbing oligomeric products of MG formed through aldol condensation reactions. The enhanced formation of light-absorbing products in the presence of NH_4^+ and H_3O^+ is consistent with the known role of these species in promoting aldol condensation. Significant surface tension depression was observed for MG in aqueous solutions with or without inorganic salts, demonstrating that oligomerization of MG results in the formation of surface-active products consistent with HULIS. In contrast, no depression was observed for GL in similar aqueous solutions of inorganic salts.[329] These observations indicate that chemical transformations resulting in browning of SOA may affect the CCN activity of the aerosol.

Reactions of GL with AS generate products with distinct absorption bands at 207 and 280 nm, with the latter band overlapping with the UV edge of the solar flux.[320] The band at 207 nm is attributed to imidazole, while 2,2′-biimidazole (BI) and imidazole-2-carboxaldehyde (IC) contribute to the band centered at 280 nm.[109] The formation of these products in bulk solutions is extremely slow. For example, Yu et al. were able to identify and quantify product concentrations at different reaction times using NMR and ESI-MS.[325] They found that 5.5 months into the reaction of 1 M GL with 1 M AS, the imidazole concentration was only 45 mM. Under these conditions, all of the observed products accounted for 4% conversion of GL after 1 week, 8.7% after a month, and 12% after 5.5 months of reaction. Formic acid was observed as another abundant product generated at about the same rate as imidazole. The formation of formic acid resulted in a strong decrease in pH (from 3.5 to <2), which slowed down all of the reaction rates by 2−3 orders of magnitude. They also proposed that IC, along with other unidentified products, contributes to

DOI: 10.1021/cr5006167
Chem. Rev. 2015, 115, 4335−4382

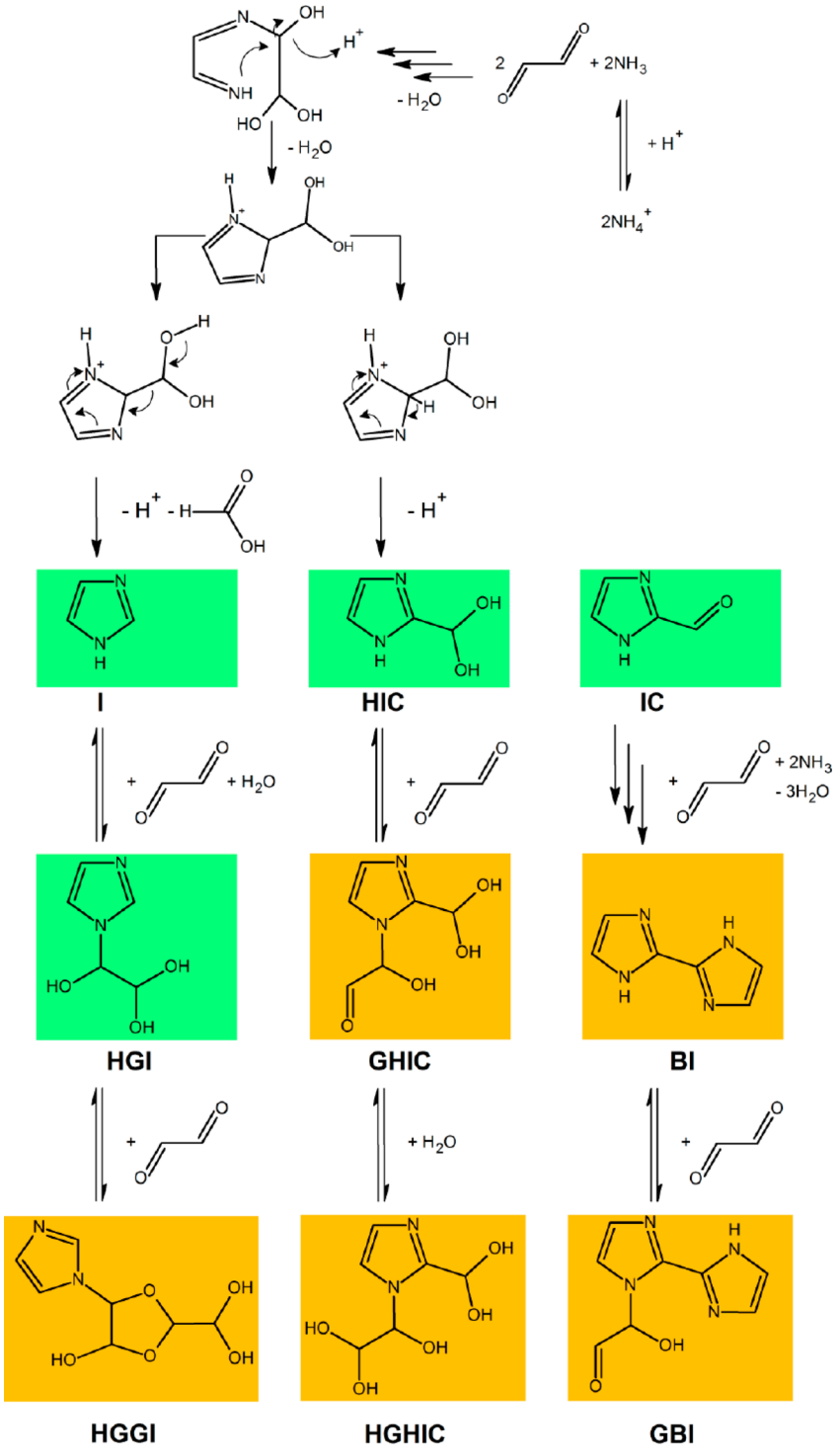

Figure 19. Reaction pathways for imidazole formation in the glyoxal and ammonium sulfate system. Green-colored compounds were described by Galloway et al.[349] (2009) and Yu et al.[325] (2011). Orange-colored compounds were identified by Kampf et al. (2012). (Reprinted with permission from ref 109. Copyright 2012 Copernicus Publications.)

the absorption band at ~280 nm. The other major product formed in aqueous aerosol mimics of GL + AS aqSOA under atmospherically relevant conditions (acidic pH 4) was identified as BI.[109] Bicyclic imidazoles and several low-polarity products with absorption in the 350−400 nm range have been observed in HPLC/ESI-MS experiments. Figure 19 provides a summary of imidazole-based products produced in reactions of GL with AS. Similar products are generated in the MG + AS system. Kampf et al.[109] suggested that although its rate of formation is 2 orders of magnitude lower than that for imidazole and IC, BI is a major molecule contributing to the 280 nm band. The high molar absorptivity of BI of 36 690 M^{-1} cm^{-1} reported by Kampf et al. makes this low-abundance product responsible for the observed light absorption of GL SOA at 280 nm. This study demonstrated that low-abundance compounds may have a significant effect on light absorption by

DOI: 10.1021/cr5006167
Chem. Rev. 2015, 115, 4335−4382

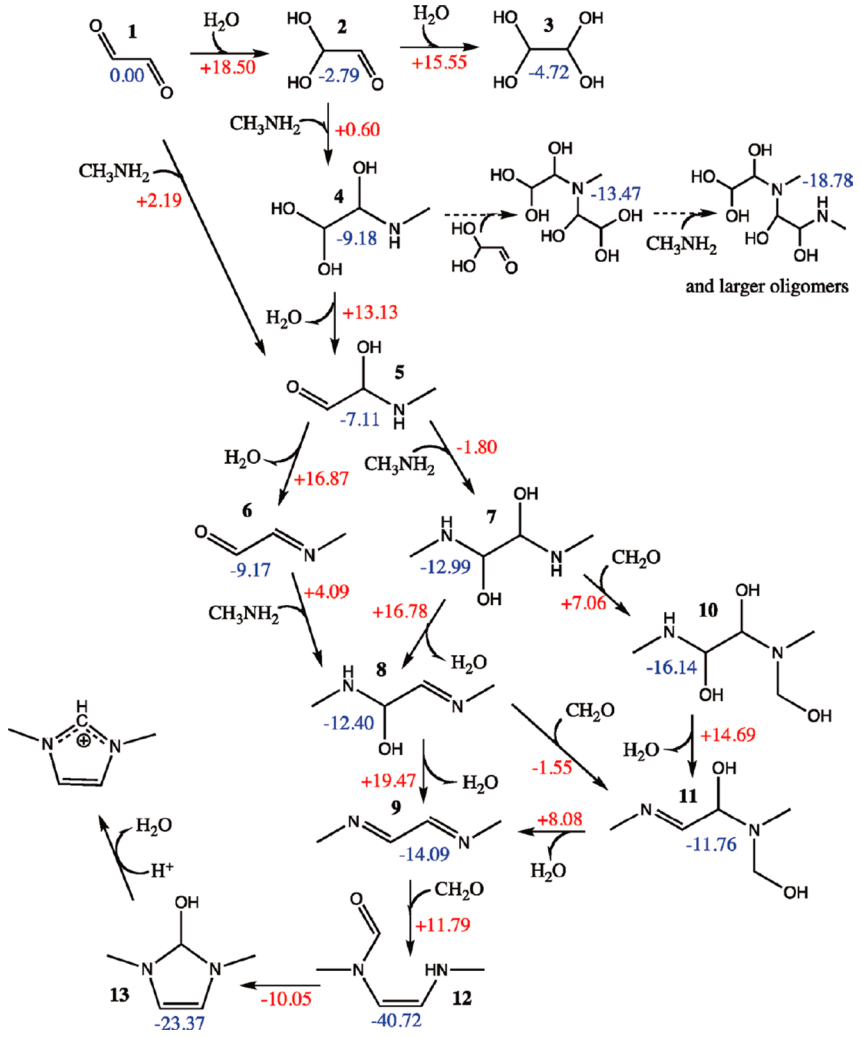

Figure 20. Free-energy landscape of neutral glyoxal, methylamine, and formaldehyde addition to form imidazole (ΔG in kcal/mol). The relative energies of the local minima relative to the neutral reactants are shown in blue, while dissociation barriers are depicted in red. (Reprinted with permission from ref 336. Copyright 2011 American Chemical Society.)

aerosol. Notably, more recent measurements by Noziere and co-workers resulted in a different molar absorptivity for BI of 18 778 M^{-1} cm^{-1}, but it is still larger than the molar absorptivities of 5000 M^{-1} cm^{-1} measured for imidazole and 13 353 M^{-1} cm^{-1} for IC.[342]

As a side note, imidazoles were found to act as photosensitizers, promoting radical chemistry in the aerosol phase.[343,344] IC is a particularly efficient photosensitizer, whereas BI and imidazole were found to be substantially less efficient. The unique effect of IC on aerosol chemistry resulting in substantial aerosol growth in flow tube experiments in the presence of limonene was attributed to hydrogen abstraction from VOCs by the IC triplet state followed by uptake and subsequent oxidation of the reactive radical intermediates. Products of the photosensitized oxidation of limonene with a surprisingly high degree of oxidation were observed by LC/ESI-MS methods.

The yield of imidazole products is a strong function of the solution pH and reagent concentrations. Kinetics experiments indicate that BI formation slows after the first few hours.[109] This decrease in BI production correlates with a decline in pH of GL + AS solutions reported by Yu et al.[325] Several studies suggested that the imidazole pathway is of minor importance under atmospherically relevant conditions.[316,321,325,345,346] Nevertheless, the strong absorption by a minor aerosol BI component reported by Kampf et al. indicates that even with fairly low production yields of strong chromophores, they may have a significant effect on light absorption by OA. Moreover, it has been suggested that BI and its derivatives may form complexes with transition metals known to efficiently absorb visible light.

DFT calculations by De Haan and co-workers provided important insights into the kinetics and mechanisms of imidazole formation in reactions of GL with methylamine with and without formaldehyde.[336] Figure 20 shows the reaction pathways involving neutral GL, methylamine, formaldehyde, and the corresponding solution-phase free energies (ΔG, kcal/mol) relative to the neutral precursors. In the figure, the relative energies of the local minima on the potential energy surface are shown in blue, while the reaction barriers are shown in red. The nucleophilic addition of methylamine to GL (**1**) is thermodynamically favorable and associated with a low barrier of 2.2 kcal/mol, forming the intermediate **5**. Similarly, the addition of CH_3NH_2 to GL-monohydrate (**2**), which is considered to be the dominant reactive glyoxal form in solution, is a downhill process associated with a very low

DOI: 10.1021/cr5006167
Chem. Rev. 2015, 115, 4335−4382

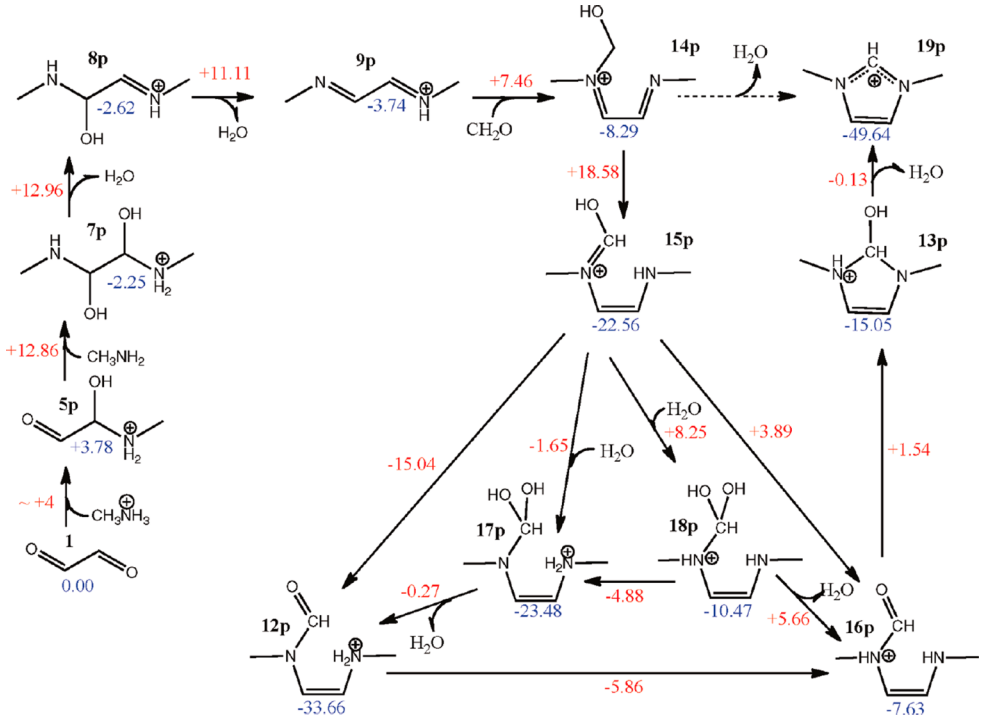

Figure 21. Free-energy landscape of glyoxal, CH_3NH_2, $CH_3NH_3^+$, and formaldehyde addition to form imidazole (ΔG in kcal/mol). The relative energies of the local minima relative to the neutral reactants are shown in blue, while dissociation barriers are shown in red. (Reprinted with permission from ref 336. Copyright 2011 American Chemical Society.)

barrier. The intermediate **4** may undergo dehydration (**4** → **5**) or oligomerization, forming a variety of nitrogen-containing oligomeric products. The addition of methylamine to **5** forming **7** is favored over dehydration. However, subsequent reactions of **7** and its products **8** and **10** that result in the formation of the stable acyclic structure **12** are associated with relatively high barriers. The high 30 kcal/mol barrier for imidazole formation from this structure suggests that in the absence of protons, the system will be trapped in this thermodynamic sink on the potential energy surface. The main pathway in the absence of protons is **1** → **5** → **7** → **8** → **9** → **12** → **13**. Figure 21 summarizes the DFT calculations of the reaction pathways in the presence of acidic compounds representing more realistic atmospheric cloudwater conditions. An index "**p**" is added to products that differ from the corresponding neutral species shown in Figure 20 by an additional proton. Somewhat lower barriers are observed along the GL → diimine (**1** → **5p** → **7p** → **8p** → **9p**) pathway, compared to the neutral analog described earlier. The most favorable diimine → imidazole pathway is **9p** → **14p** → **15p** → **12p** → **16p**→ **13p** → **19p**. The highest barrier of 18.6 kcal/mol is associated with breaking the C−H bond in **14p** to form the conjugated enol intermediate **15p**, which can tautomerize to the nonconjugated keto intermediate **16p** either directly or via the intermediate **12p**. The ring closure reaction of this intermediate forming **13p** is associated with a barrier of 9 kcal/mol. The final dehydration step has a barrier of ∼15 kcal/mol, forming a thermodynamically stable protonated imidazole, **19p**. Similar energetics were observed in the absence of formaldehyde. In this pathway, GL is added to the diimine to form an intermediate analogous to **14p**. Diimine was proposed to be an important intermediate of imidazole formation in a mildly acidic environment. In addition, it has been demonstrated that small aldehydes may be incorporated into imidazole species formed in cloud droplets and aqueous aerosols in the presence of GL and amines. DFT calculations indicated that GL self-oligomerization cannot compete with the diimine formation,[347] which is consistent with experimental observations.[337]

Similar to GL, MG forms light-absorbing products through reactions with ammonia, amines, and their ions. Sareen et al. examined browning of MG in aqueous solutions of $(NH_4)_2SO_4$ and NH_4NO_3 as mimics of tropospheric aerosol.[341] Browning was observed immediately after mixing >0.16 M MG with AS. A darker color was obtained at higher concentrations of MG and longer reaction times. At a lower MG concentration of 16.2 mM, the UV−vis spectrum was dominated by absorbance peaks at 213 and 282 nm, while absorbance bands extending into the >400 nm range were observed at higher MG concentrations. The absorbance at 282 nm showed linear dependence on both MG and AS concentration and decreased linearly with solution pH. Schwier et al. demonstrated that in mixed GL−MG solutions, absorption at 280 nm was contributed independently by products of both GL and MG reactions.[348] Aerosol chemical ionization mass spectrometry (CIMS) experiments enabled identification of nitrogen-containing compounds, aldol condensation products, and organosulfates in MG + AS aerosols. The formation of light-absorbing products was enhanced in the presence of NH_4^+ and H_3O^+, which are efficient catalysts of aldol condensation reactions. On the basis of this observation, it was proposed that aldol condensation results in the formation of light-absorbing species. Using MG concentrations in urban aerosol in the range of 0.7−7 mM and an AS concentration of 14 M, it was estimated that under these conditions, up to 86% conversion of MG would occur in 12 h, making MG + AS reaction a significant source of BrC.[341] In contrast with the GL + AS system, the significant surface tension depression expected for HULIS was observed for the MG + AS reactions

DOI: 10.1021/cr5006167
Chem. Rev. 2015, 115, 4335−4382

in aqueous solutions. Decreased surface tension may affect the CCN activity of the aerosol.

4.4.1.3. Comparison of GL and MG Browning Capacity. Powelson et al. used UV−vis and fluorescence measurements to examine browning reactions between small carbonyl compounds (MG, GL, glycolaldehyde, hydroxyacetone, and acetaldehyde) and AS, methylamine, and glycine at pH 4 and 275 K.[41] Because amino acids are more abundant in cloud droplets than primary amines, the reactivity of carbonyl compounds with glycine may be used to access the efficiency of BrC formation in cloud droplets. Table 3 shows the atmospheric concentrations of carbonyl and amine compounds examined in that study. Browning in the presence of glycine follows the order glycolaldehyde > MG > GL > hydroxyacetone ∼ acetaldehyde, with the most intense absorbance produced by the reaction of glycine with glycolaldehyde. A similar order was observed for reactions with lysine at pH 6, while browning in the presence of AS follows a slightly different order: MG > GL > glycolaldehyde ∼ hydroxyacetone ∼ acetaldehyde. The reactions of glycine, lysine, and AS with formaldehyde did not produce any colored products. In general, amines were found to be more effective at generating BrC products than AS. The MAC_{bulk} coefficients at 400 nm were in the range of 100−500 cm^2/g for MG + amine reactions and 10−200 cm^2/g for MG + AS reactions. In comparison, a MAC_{bulk} of 6×10^3 cm^2/g was reported for BrC produced through wood burning at the same wavelength. Despite the much lower MAC_{bulk} values, on the basis of the global production of MG and glycolaldehyde and the estimated uptake of these important BrC precursors into cloud droplets and particle phase, the authors estimated that aqueous reactions of carbonyl compounds with AS and amines could be responsible for up to 10% of global light absorption by BrC. We note this estimation has not accounted for rapid photobleaching, which will limit the significance of this type of BrC to early morning hours.

Table 3. Atmospheric Concentrations of Selected Carbonyl Compounds, Ammonium Sulfate, and Amino Acids[a]

reactant	cloud concn (μM)	aerosol concn (pmol/m^3)
acetaldehyde	0.2−1.5[b]	
formaldehyde	1.2−230[b,c]	
glycolaldehyde	0.3−3.6[b]	0−1300[d]
glyoxal	0.2−270[c,e]	0−1600[d]
hydroxyacetone	0.2−0.6[b]	0−1200[d]
methylglyoxal	0.1−130[c,f]	0−2600[d]
ammonium sulfate	1.2−18[g]	3200−7700[h]
glycine	0.06−1.1[g]	0.2−170[h,i]
methylamine	0.03−0.06[g]	56 ± 52[i]

[a]Reprinted with permission from ref 41. Copyright 2014 American Chemical Society. [b]van Pinxteren et al. (2005).[374] [c]Igawa et al. (1989).[375] [d]Matsunaga et al. (2004).[376] [e]Munger et al. (1995).[377] [f]Matsumoto et al. (2005).[378] [g]Mopper and Zika (1987).[379] [h]Matsumoto and Uematsu (2005).[380] [i]Zhang and Anastasio (2003).[381]

Under the experimental conditions examined by Powelson et al., browning of MG was found to be more efficient than browning of GL.[41] These results indicate that even though the atmospheric concentration of GL is often higher than the MG concentration, the faster reactivity of MG toward amines and the higher efficiency of BrC formation make it a more important source of BrC than GL in the atmosphere. Both substituted imidazoles absorbing at <300 nm and other products with absorption in the range of 300−520 nm (and even extending to 700 nm) were observed in UV−vis spectra. Although the formation of substituted imidazoles has been extensively studied by several groups (refs 36, 41, 109, 321, 325, 329, 334, 336, and 349), the formation of other products absorbing in the visible range is still poorly understood. In addition, very different UV−vis spectra were observed for AS and amines, indicating that diverse light-absorbing products likely are generated in carbonyl + AS reactions as compared to carbonyl + amine ones.

Temperature-dependent NMR studies provided valuable information regarding the kinetics of GL and MG reactions with AS and amines.[350] A more pronounced temperature dependence of the reaction rate was observed for α-dicarbonyl reactions with amines. This has been attributed to substantially lower activation energy for α-dicarbonyl + AS reactions (18 ± 8 kJ/mol) than α-dicarbonyl + amine reactions (50 ± 11 kJ/mol).[350] Low activation energies obtained for α-dicarbonyl + AS reactions are comparable to energy barriers for C−N bond formation obtained from DFT calculations, and higher energy barriers were reported for dehydration reactions.[336] These results suggest that C−N bond formation is the rate-determining step in α-dicarbonyl + AS reactions, while dehydration steps determine the rate of α-dicarbonyl + amine reactions.

Drozd and McNeil examined the effect of organic matrices, including sucrose, glucose, maltitol, sorbitol, and glycerol, on the formation of light-absorbing species from aqueous-phase reactions of GL or MG with AS in solutions with an organic-to-sulfate mass ratio of 2:1.[42] Light absorption by GL and MG solutions decreased in the order of no matrix ∼ sucrose > glucose > maltitol ≥ glycerol > sorbitol, indicating that the presence of these oxidized organic compounds has a significant effect on the overall light absorption. In contrast, no measurable change in the shape of the UV−vis spectrum was observed in the presence of organic matrices, signifying that their major effect is suppression of reactions leading to the formation of light-absorbing compounds. Changes in solution pH were found to correlate with the extent of BrC formation in the presence of an organic matrix. Specifically, matrices that significantly suppress light absorption showed smaller decreases in pH than the control solution containing GL or MG and 1 M AS. Meanwhile, matrix-containing solutions with a larger decrease in pH showed little suppression of the BrC formation. This observation is consistent with the decrease in pH during reactions of GL and AS discussed earlier.[325] Overall, the study indicated that the formation of BrC chromophores from the GL/MG reactions with AS might be substantially slower in the presence of organic matrix.

4.4.1.4. BrC Formation through Simulated Cloud Processing of α-Dicarbonyls. As previously mentioned, loss of water from an evaporating cloud or fog droplet creates special conditions that promote condensation and acid-catalyzed reactions. Reactions of GL and MG in evaporating aqueous droplets and thin films have been examined to mimic cloud processing of α-dicarbonyls in the presence of AS and amines. Lee et al. examined the formation of light-absorbing compounds in evaporating droplets containing GL and ammonium salts. Rapid reaction on a time scale of seconds was observed for the GL + AS system.[38] The resulting products showed a strong absorption band at 280 nm. Consistent with other studies, the rate of formation of light-absorbing products

DOI: 10.1021/cr5006167
Chem. Rev. 2015, 115, 4335−4382

was higher at pH 4 than at pH 3. The average N:C ratio significantly increased in the presence of sulfate anions, indicating more efficient formation of organonitrogen products in AS solutions. This was attributed to the increase in Henry's constant for glyoxal partitioning into the aqueous phase in the presence of sulfate anions (discussed earlier).[323]

Reactions of GL and MG with primary amines also resulted in the formation of light-absorbing products. For example, De Haan et al. studied cloud processing of GL through reactions with amino acids (glycine, serine, aspartic acid, ornithine, and arginine)[334] and methylamine[37,337] in aqueous evaporating droplets and bulk solutions using NMR, ESI-MS, and AMS. In the presence of amino acids or methylamine, GL typically reacted to yield 1,3-disubstituted imidazoles and oligomeric, imidazole-based light-absorbing products. Imine formation was proposed as the rate-limiting step for these reactions. The only exception was a GL reaction with arginine that involves side chain amino groups forming nonaromatic, five-membered rings. Reaction kinetics was slow (>10 days) in the bulk solution, but the reaction time was reduced to minutes in evaporating droplets containing 2−200 μM GL and 1−100 μM amino acid. Droplet evaporation resulted in preconcentration of GL from its original concentration of ∼30 μM to an estimated 5 M. However, preconcentration alone could not account for the rapid reactivity observed in drying droplets. The dramatic enhancement in the reaction rate was attributed to conversion of GL-dihydrate into GL-monohydrate—the most reactive form of GL in solution. Under atmospherically relevant conditions, GL is expected to undergo full conversion into 1,3-disubstituted imidazoles in the particle phase on a time scale of 1 day. In the experiments of Lee et al. mentioned above, the formation of BrC species in evaporating aqueous solutions of GL + AS was also observed in seconds, much faster than the corresponding reactions in the bulk solution.[38]

4.4.1.5. BrC Formation through Reactive Uptake of α-Dicarbonyls onto Particles. Several groups examined GL uptake onto AS seed aerosol under dark and photochemical conditions (refs 319, 321, 323, 326, 345, 346, 349, 351, and 352). Galloway et al. found dark uptake to be largely reversible, while irreversible uptake was found to be a minor process.[321,349] GL monomers and oligomers were the dominant compounds observed in the aerosol phase, whereas imidazole products were observed as minor species. De Haan et al. reported that drying the aerosol increases the yield of irreversible uptake.[334] Trainic et al. demonstrated that reactive uptake of GL onto AS and mixed AS/glycine seed particles occurs over a broad range of RH of 30%−90%.[345,346] Efficient reactivity observed at RH below the deliquescence point of AS (∼80% RH)[353] and glycine GL (93% RH)[354] indicated that reactions occur in a thin aqueous layer adsorbed on a particle surface, likely forming particles with a core−shell structure. Hamilton et al. examined GL uptake on AS seed particles using the large-scale European photoreactor (EUPHORE) atmospheric simulation chamber. Their experiments confirmed the presence of organic nitrogen compounds in SOA.[352] They further demonstrated that the presence of organic nitrogen compounds resulted in the enhanced ionization efficiency of SOA particles in AMS, making it a particularly useful tool for analysis of light-absorbing compounds in ambient aerosol. The EUPHORE experiments confirmed that light-absorbing imidazole products may be formed on atmospherically relevant time scales.

GL uptake under irradiated conditions results in the formation of oxidation products, including formic acid, glyoxylic acid, glycolic acid, and glycolic acid sulfate. The total amount of organic material and GL in the particle phase was lower under irradiated conditions, which could be attributed to both photochemical processing and heating of aerosol particles resulting in faster evaporation.[352] In a related study, Galloway et al. examined GL uptake on deliquesced AS particles with and without OH radicals.[349] Similar chemical composition of GL + AS aerosol, GL uptake rate, and aerosol growth were observed under dark and photochemical conditions. These results indicate that GL uptake by deliquesced AS seed aerosol is not affected by the presence of OH radicals. In contrast, Volkamer et al. reported a significant enhancement (by a factor of ∼500) of SOA formation under irradiated conditions from GL formed through OH-initiated oxidation of acetylene.[351] That study also demonstrated the reaction rate dependence on seed particle composition. Specifically, higher SOA yields were observed for mixed inorganic/organic seeds compared to pure inorganic seeds. The observed differences were attributed to different liquid water content for varied seeds.

GL uptake into solid-phase glycine aerosol at 50% RH was shown to be a reactive process, where GL is rapidly converted into 1,3-disubstituted imidazoles.[334] Similar reactive uptake was observed for other aqueous aerosol-containing nucleophilic organic compounds at RH from <5% to 50%.[355] GL uptake was found to be RH-dependent and enhanced under mildly acidic conditions. Volkamer et al. found that the GL uptake rate on seed particles was suppressed by glycine and sulfuric acid.[351] This observation was attributed to the pH dependence of the reaction kinetics. Furthermore, reactive uptake of GL was observed on supercooled H_2O/HNO_3 liquid layers and ice films. It has been proposed that GL uptake by supercooled liquid films may be a significant source of SOA (∼4%−53%) in the upper troposphere.[331]

4.4.1.6. Physical Properties of Aerosols Formed through Browning of α-Dicarbonyls. In addition to altering the chemical composition of aerosol, browning reactions were shown to have a pronounced effect on aerosol physical properties. Specifically, it has been demonstrated that the effective vapor pressure of glyoxal SOA is reduced by almost 2 orders of magnitude in the presence of ammonium at pH 7.[356] The reduced volatility of aqSOA produced by mixing GL with ammonium hydroxide results in a substantial increase in SOA yield, indicating that browning chemistry may contribute significantly to the total SOA budget. These potential effects of browning chemistry on SOA production were further supported by gas-aerosol model for mechanism analysis (GAMMA) simulations.[357]

Hawkins et al. examined the properties of aqSOA (i.e., SOA produced by aqueous chemistry pathways) formed from GL, MG, glycolaldehyde, hydroxyacetone, and small amines during simulated cloud processing.[358] Continuous hygroscopic growth of the resulting particles was observed for a range of RH, starting from ∼30%. The hygroscopic growth curves obtained in that study resemble typical hygroscopic growth curves of atmospheric HULIS, indicating the presence of a complex mixture of organic constituents in the particle phase. Particle hygroscopic growth was found to be system-dependent. For example, the largest hygroscopic growth was observed for GL + methylamine, and the least hygroscopic SOA was produced through reactions of glycolaldehyde with methylamine. These findings indicate that chemical reactions may have a pronounced effect on the physical properties of BrC material.

DOI: 10.1021/cr5006167
Chem. Rev. 2015, 115, 4335−4382

Impact-flow experiments were performed to examine phase transitions in aqSOA following brief (~10 min) drying.[358] In these experiments, SOA particles were pressed between two quartz plates. Solid particles typically shattered, while liquid particles spread out and subsequently beaded up when the top plate was removed. These experiments demonstrated that GL and MG aqSOA evaporated into a semisolid residue, whereas glycolaldehyde and hydroxyacetone particles remained liquid following 10 min of drying and became semisolid after 20 h of drying. The semisolid MG + methylamine aqSOA particles were shown to nucleate ice in the depositional freezing mode but were found to be less efficient ice nuclei than sugars.[359]

Zarzana et al. used CRD spectroscopy to measure the complex refractive indices of model SOA formed by aqueous-phase reactions between α-dicarbonyls (GL and MG) and primary amines (glycine and methylamine) at 532 nm.[104] The extinction coefficient was measured for particles with diameters in a range of 200−500 nm. The SSA of BrC particles and the relative radiative forcing were estimated on the basis of these data. Consistent with other studies, faster browning was observed for MG compared to GL. The highest absorption component of the complex refractive index (k) was obtained for the MG−methylamine system. Other model systems showed similar and lower complex refraction indices. These differences are mainly attributed to differences in pH of various dicarbonyl−amine systems. Both the absorption and the scattering components of the refractive index obtained for model SOA were higher than the values typically used in models. Figure 22 features the SSA values calculated for the four model systems compared with nonabsorbing AS aerosol. Significant absorption is observed for the MG−methylamine system, particularly at smaller SOA diameters. Radiative-forcing calculations indicate that the strongly absorbing MG−methylamine SOA causes ~25% less cooling compared to the nonabsorbing SOA.

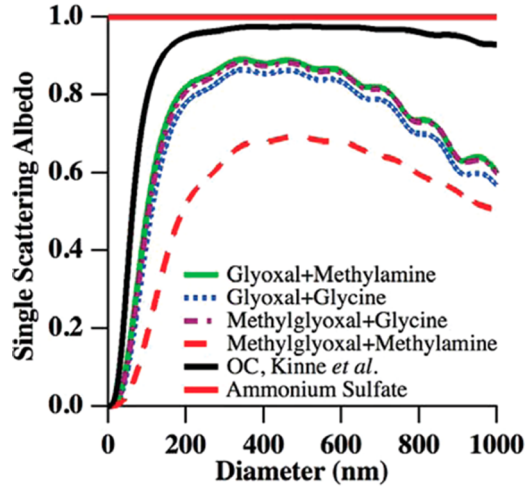

Figure 22. SSA measured at 532 nm for aerosols generated from four α-dicarbonyl−amine systems and two model values plotted as a function of particle diameter. An SSA of 1 corresponds to a nonabsorbing material. (Reprinted with permission from ref 104. Copyright 2012 American Chemical Society.)

4.4.1.7. Chemical Stability of Aerosols Formed through Browning of α-Dicarbonyls. An inventory of MG + AS reaction products was provided by Sareen et al., who examined the stability of BrC produced in MG + AS reactions with respect to solar irradiation and exposure to ozone.[360] The atmospheric lifetime of BrC with respect to photolysis was found to be remarkably short—on the order of minutes. The lifetime with respect to the O_3 reaction was on the order of hours. This important finding suggests that this type of BrC cannot survive in the atmosphere in the presence of sunlight. Therefore, it is not likely to have a strong effect on direct radiative forcing. Furthermore, this study suggested that BrC could build up during the night and trigger a cascade of photochemical reactions upon sunrise. In the context of these experimental observations, Woo et al. performed GAMMA simulations to examine the effect of browning chemistry on aerosol optical properties.[361] Consistent with field observations,[362] GAMMA predicted significant BrC formation during the night, especially under urban conditions, followed by daytime photobleaching of the chromophores. These results indicate that BrC formation is driven by the dark aqueous reactivity of GL. Moreover, the model predicted that browning chemistry has only a minor effect on particle surface tension.

4.4.2. Light-Absorbing Products in SOA Aged with Ammonia and Amino Acids. The formation of light-absorbing products through reactions with reduced nitrogen species is not limited to α-dicarbonyls. Mang et al.[268] reported that SOA produced through ozonolysis of limonene, or LSOA, undergoes browning reactions during storage in ambient air in the dark (although they could not identify the reactive component in air responsible for this browning). Subsequent characterization of aged LSOA using UV−vis revealed that browning occurs upon exposure of LSOA to ammonia, amines, and amino acids.[254] These reactions result in the formation of products with distinctive absorption bands at ~430 and ~510 nm[208,268] (illustrated in Figure 23). Apparently, even trace levels of ammonia in the laboratory air were sufficient to brown LSOA during storage in the experiments of Mang et al. In addition to LSOA, aerosols produced by ozonolysis of α-

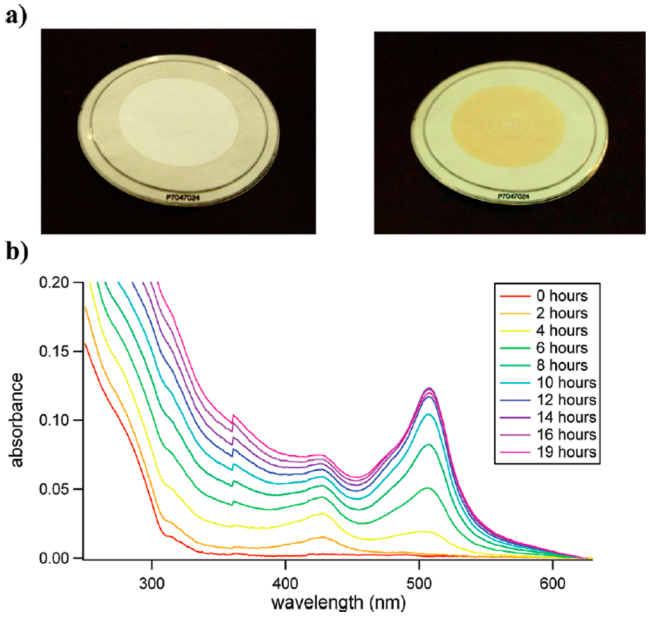

Figure 23. (a) Photographs of the fresh (left) and NH_3-aged (right) sample of SOA generated by ozonolysis of limonene (LSOA). (b) Corresponding UV−vis absorption spectra of LSOA acquired at different times during the aging process. (Reprinted with permission from ref 208. Copyright 2010 American Chemical Society.)

DOI: 10.1021/cr5006167
Chem. Rev. 2015, 115, 4335−4382

humulene, α-cedrene, cedar leaf essential oils, and γ-terpinene also showed significant browning in the presence of ammonia.[254,269] HR-MS analysis of LSOA using ESI showed no significant difference between fresh (white) and aged (brown) LSOA samples.[254] However, both DESI[208] and nano-DESI HR-MS[214] experiments, which are more suitable for the detection of chemically labile compounds, revealed the presence of nitrogen-containing products in aged LSOA. These products are chemically labile and partially decompose following solvent extraction, making them difficult to characterize using traditional ESI-MS.[208]

LSOA browning was attributed to the chemistry between carbonyl compounds and ammonia in an aqueous film formed on the particle surface. Figure 24 summarizes key reactions

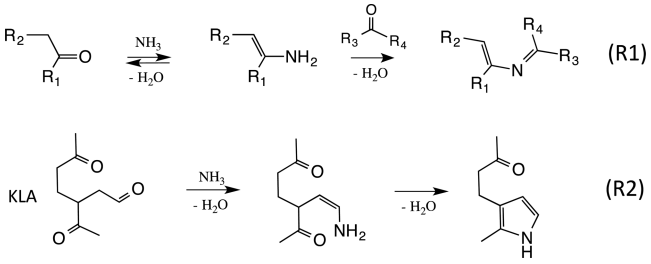

Figure 24. Initial reaction sequences of NH_3-mediated aging of OA material relevant to BrC formation. (Reprinted with permission from ref 108. Copyright 2014 American Chemical Society.)

resulting in the formation of light-absorbing species. The chemical mechanisms of this aging are complex, but the initial steps involve reactions illustrated by reaction sequences R1 and R2. NH_3 reacts with carbonyls, forming primary imines and amines, and these transient products continue to react with carbonyls, forming condensation (oligomeric) products containing more stable secondary imines (Schiff bases). Many of the SOA compounds have multiple carbonyl groups necessary for intramolecular cyclization and the formation of N-heterocyclic structures. For instance, scheme R2 in Figure 24 illustrates plausible N-heterocyclic cyclization of keto-limonon-aldehyde (KLA), a major product of *d*-limonene ozonolysis, resulting in the formation of a pyrrole derivative. KLA is selected as an example because of its critical importance to BrC formation in LSOA.[224] However, many other SOA components and their derivatives may undergo intramolecular cyclization, forming N-heterocycles of different sizes (pyridines, pyrazines, imidazoles, etc.). MS/MS experiments on selected nitrogen-containing dimers were consistent with the heterocyclic structures of these products. Reactive nano-DESI analysis of fresh and brown LSOA using the Girard's reagent T indicated that a majority of reactive carbonyl groups is consumed by the browning chemistry.[363]

Similar chemistry was observed during evaporation of aqueous LSOA extracts mixed with AS.[35] It has been demonstrated that the rate of BrC formation is enhanced by, at least, 3 orders of magnitude upon evaporation. Figure 25 shows the dependence of the UV–vis spectrum and the average MAC_{bulk} values integrated over a 300–700 nm range on the initial AS concentration in solution. The average MAC_{bulk} values initially increase with AS concentration but reach a plateau when the molar ratio AS:LSOA exceeds 0.022, indicating that only ~2% of LSOA constituents are converted into light-absorbing products. It follows that a small number of

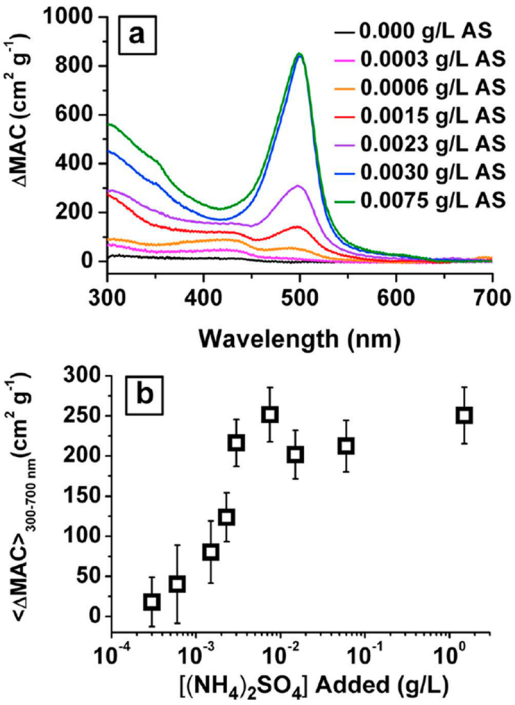

Figure 25. Effect of the initial concentration of AS on (a) the increase in MAC_{bulk} and (b) average $DMAC_{bulk}$ over the 300–700 nm range of the evaporated/redissolved LSOA + AS solutions. In all cases, the LSOA mass concentration is 0.3 g/L. The absorbance saturates above the relative AS:LSOA mass ratio of 1:100. The chromophore absorbing at 430 nm is favored at low AS concentrations, but the chromophore absorbing at 500 nm becomes dominant above this saturation ratio. (Reprinted with permission from ref 35. Copyright 2012 Wiley-Blackwell.)

strong chromophores may have a significant effect on the overall light-absorption properties of SOA. In contrast with browning of α-dicarbonyls, which is strongly pH dependent, browning of LSOA was found to be rather independent in a pH range of 4–10 but significantly suppressed at pH <4.

Mechanisms of LSOA browning chemistry were examined by comparing NH_4^+-mediated aging of limonon-aldehyde (LA), KLA, and pinon-aldehyde (PA), primary ozonolysis products of limonene and α-pinene, respectively, as illustrated by Figure 26. Figure 27 shows UV–vis spectra of LA, KLA, and PA aged in the presence of AS. KLA is the only ketoaldehyde precursor that produced colored products in reactions with AS and glycine. The UV–vis spectrum obtained for KLA is relarkably

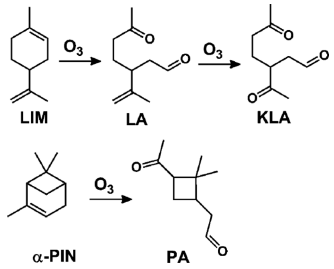

Figure 26. Products of limonene (LIM) ozonolysis [limonon-aldehyde (LA) and keto-limonon-aldehyde (KLA)] and α-pinene (α-PIN) ozonolysis [pinon-aldehyde (PA)]. KLA is a potent BrC precursor. (Reprinted with permission from ref 224. Copyright 2013 Royal Chemical Society.)

DOI: 10.1021/cr5006167
Chem. Rev. 2015, 115, 4335–4382

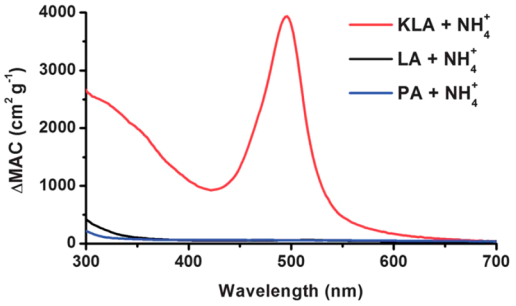

Figure 27. Comparison of the net increase in the mass absorption coefficients ($\Delta MAC_{bulk} = MAC_{bulk,sample} - MAC_{bulk,control}$) between the NH_4^+-aged keto-limonon-aldehyde (KLA), limonon-aldehyde (LA), and pinon-aldehyde (PA). (Reprinted with permission from ref 224. Copyright 2013 Royal Chemical Society.)

similar to that of aged LSOA, indicating similar browing chemistry in these systems. Similar stoichiometry was observed for both KLA + AS and KLA + GLY browning reactions. The NH_4^+:KLA effective stoichiometric ratio of 1:3 indicates that the reaction chemistry is complex and may involve up to three KLA molecules per chromophore. A large number of nitrogen-containing products of KLA + AS and KLA + GLY reactions, some of which carry positive charge, were observed using HR-MS and LC/UV−vis/ESI/HR-MS, which demonstrates a complex multistep reaction chemistry even for this simplified model system. Flores et al.,[262] who studied the effect of NH_3 uptake on LSOA in a flow reactor, confirmed the removal of the mass corresponding to KLA and the appearance of masses corresponding to larger N-containing compounds using AMS measurments.

Table 4 lists the MAC_{bulk} values reported by Updyke et al.[269] for different SOA aged under humid air containing gaseous NH_3 at mixing ratios ~100 ppb, comparable with the concentrations reported for some urban areas (up to ~200 ppb)[364] and forest fire plumes (500−1500 ppb).[365] The results of that study indicate that NH_3-mediated SOA browning produced from different biogenic and anthropogenic precursors strongly depends on the SOA precursor structure and the type of oxidant. For example, a significantly lower MAC_{bulk} value was obtained for LSOA produced through OH oxidation compared to O_3 oxidation. Furthermore, no significant browning was observed upon chemical aging of SOA produced through ozonolysis of α-pinene (PSOA),[108,224,253,254,269] a monoterpene isomeric to limonene. Comparative HR-MS analysis of LSOA and PSOA aged in the presence of gaseous NH_3 showed significant overlap in the molecular composition of these two SOA materials, indicating that both LSOA and PSOA undergo chemical aging through reactions shown in Figure 28. However, only LSOA aging generates colored products. The low browning capacity of PSOA was attributed to the rigid structures of the α-pinene oxidation products that presumably hinder chromophore formation. Several highly conjugated species containing two nitrogen atoms unique to aged LSOA were identified as potential chromophores.[108]

Table 4. Effects of NH_3-Mediated Aging Chemistry on Absorption Properties of Different SOA Samples[a]

VOC precursor[b]	oxidant	initial VOC (ppb)	initial NO (ppb)	$\langle\Delta MAC_{bulk}\rangle$ ($cm^2\ g^{-1}$)	ΔMAC_{bulk} peak value ($cm^2\ g^{-1}$)
LIM	O_3	–	–	400	1200
LIM	OH	250	<1	170	80
CED	O_3	–	–	260	700
HUM	O_3	–	–	300	800
FAR	O_3	–	–	60	10
APIN	O_3	–	–	50	50
APIN	OH	250	<1	100	40
PLO	O_3	–	–	100	60
CLO	O_3	–	–	500	1000
ISO	OH	250	–	50	20
ISO	O_3	–	–	10	5
TET	OH	250	–	80	60
TMB	OH	250	<1	20	40
TMB	OH/NO_x	250	300	70	10
NAP	OH	100	<1	200	100
NAP	OH/NO_x	100	300	1000	400

[a]The value of ΔMAC_{bulk} refers to an increase in MAC experienced upon exposure of SOA material to NH_3, and $\langle\Delta MAC_{bulk}\rangle$ is an average of ΔMAC_{bulk} over the 300−700 nm wavelength range. (Reprinted with permission from ref 269. Copyright 2012 Elsevier Ltd.) [b]Precursors are abbreviated as follows: APIN, α-pinene; CED, α-cedrene; CLO, cedar leaf essential oils; FAR, farnesene; HUM, α-humulene; ISO, isoprene; LIM, *d*-limonene; NAP, naphthalene; PLO, pine leaf essential oils; TET, tetradecane; TMB, 1,3,5-trimethylbenzene.

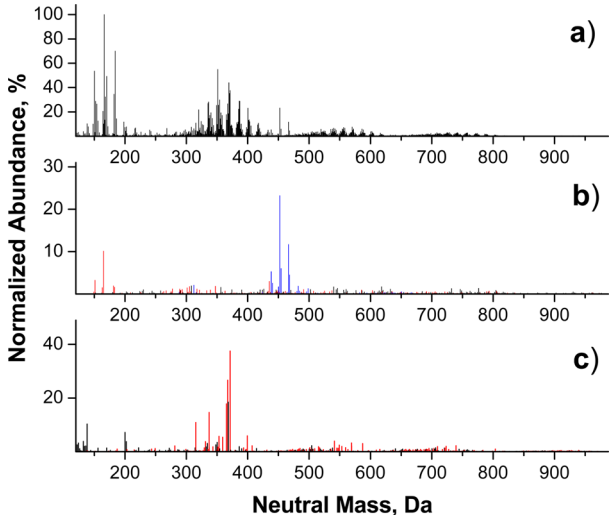

Figure 28. (a) Assigned peaks observed in both NH_3-aged limonene/O_3 SOA (LSOA) and NH_3-aged α-pinene/O_3 SOA (PSOA) samples (combined data sets). (b) Peaks unique to NH_3-aged LSOA. (c) Peaks unique to NH_3-aged PSOA. To facilitate comparison, normalized abundances of the peaks are plotted against the corresponding neutral masses. In panels b and c, mass spectral features containing no nitrogen atoms (CHO) are shown in black, and species containing one and two nitrogen atoms ($CHON_1$ and $CHON_2$) are shown in red and blue, respectively. The distinctive presence of $CHON_2$ products in the brown LSOA sample and their absence in the white PSOA sample indicate their relevance to BrC formation. (Reprinted with permission from ref 108. Copyright 2014 American Chemical Society.)

5. SUMMARY AND FUTURE DIRECTIONS

5.1. Summary of the Known Types of Chromophoric Compounds

BrC is now recognized as an important component in the atmosphere that affects climate forcing through a combination of direct effects on the transmission of solar and terrestrial radiation and indirect effects resulting from changes in cloud formation and microphysics. In addition, long-range transport and deposition of BrC most likely play a role in carbon and

DOI: 10.1021/cr5006167
Chem. Rev. 2015, 115, 4335−4382

nitrogen cycling between atmosphere, land, and water and contribute to the formation of CDOM. Understanding the environmental effects of BrC, its sources, formation, and atmospheric aging mechanisms requires adequate description of the relationship between its molecular composition and light-absorption properties. The existing evidence suggests that even a very small weight fraction of strongly absorbing BrC chromophores may have a distinct effect on OA optical properties. Because of the low concentrations of light-absorbing molecules in complex organic mixtures composing both laboratory-generated and ambient OA, identification of BrC chromophores is a very challenging task. Studies reviewed in this paper indicate that a variety of BrC chromophores may be present in both POA and SOA originating from different sources. However, present knowledge of their chemical identity, specific light-absorbing properties, concentrations, and atmospheric stability is still in its infancy, and more studies are needed to better understand and predict the regional and global importance of BrC with explicit attributions to POA and SOA emissions.

Despite the analytical difficulties, several classes of compounds have been identified as potential contributors to light absorption by BrC. These include nitroaromatic compounds, such as nitrophenols, imidazole-based and other N-heterocyclic compounds, and quinones. Less is known about the molecular composition of light-absorbing oligomers produced through condensation reactions and HULIS. Additionally, it has been proposed that supramolecular aggregates and complexes of organic molecules with transition metals may be responsible for the observed optical properties of BrC. Still, it is unclear if typical BrC is composed of a few strong chromophores or is a mixture of a large number of weak chromophores. The latter would be more consistent with the featureless UV−vis spectra of BrC observed in the majority of field studies. However, UV−vis spectra showing clear peaks in the visible range also have been reported for BrC observed in several field studies,[69,158,159] indicating that both molecular and supramolecular chromophores may coexist in ambient BrC. Several laboratory proxies of BrC, despite their molecular complexity, also have been shown to exhibit distinct absorption spectra (such as the 510 nm band in the aged LSOA shown in Figure 23). The identification and structural characterization of BrC chromophores clearly require highly sensitive molecular characterization approaches capable of detecting both strongly and weakly absorbing species.

5.2. Chemical Processes Involving BrC Requiring Further Study

The dynamic nature of BrC and nonabsorbing OA presents a significant challenge to chemical characterization. Some examples of the physical and chemical transformations summarized in this review include photolysis by solar radiation; oxidation by NO_3, O_3, H_2O_2, OH, chlorine atoms, and other oxidants; photosensitized reactions involving electronically excited states; acid- or base-catalyzed condensation reactions; reactions between carbonyl compounds and reduced nitrogen species; evaporation-driven processes; and other reactions that remain to be explored. These atmospheric aging processes may have both positive and negative effects on light absorption by BrC. For example, chromophores may decompose and photobleach following direct photolysis, but on the other hand, they may be regenerated from smaller molecular building blocks through numerous atmospheric reactions. Moreover, water evaporation from cloud droplets may result in dramatic enhancement of reaction rates for condensation and other browning reactions, while water uptake may promote hydrolysis of BrC compounds. In addition, the uptake and evaporation of water by particles and droplets are known to alter the pH and shift the equilibria of acid-catalyzed reactions with potential effects on chromophores containing either weakly acidic or basic groups. For example, the acid−base equilibria involving nitrophenols, important chromophores identified in BrC field studies, are well-known to strongly affect their absorption spectra.

Changes in the particle morphology and internal heterogeneity (mixing state) could potentially affect light absorption by BrC. Understanding the effect of particle internal structure and the location of chromophores within individual particles on the overall absorption characteristics of BrC requires a combination of comprehensive chemical imaging and molecular characterization on a single-particle basis, which presently is not possible due to the limitations of existing analytical techniques. It also is important to understand how hydration and drying cycles affect particle morphology, the distribution of light-absorbing species within the particle, and chemical equilibrium between BrC chromophores and nonabsorbing OA constituents. Temperature- and RH-induced transformations of organic particles between solid, semisolid, and aqueous phases[366] and relevant solid−liquid and liquid−liquid phase separations[367] would have additional impacts on BrC light-absorbing properties. Furthermore, it is essential to understand the contribution of reactions at gas−water interfaces to the formation and decomposition of BrC chromophores.

Interactions between individual chromophores in BrC may affect its optical properties. Presently, little is known about the role of noncovalent complexes and supramolecular assemblies in BrC formation. A recent review by Sharpless and Blough[256] on light absorption by aquatic CDOM indicates that absorption spectra of CDOM cannot be adequately described as a superposition of noninteracting chromophores. Instead, it has been suggested that CDOM optical properties are controlled by charge-transfer interactions between chromophores in CDOM. It remains to be seen to which extent these ideas may be applicable to the interpretation of absorption spectra and photochemical behavior of atmospheric BrC in general because it contains smaller molecular systems than aquatic CDOM. A recent study by Phillips and Smith[243] showed that charge transfer complexes do contribute to the absorption by the organic fraction of ambient particles. They observed a decrease in light absorption by the water-extracted ambient particulate matter upon chemical reduction of the solution with $NaBH_4$, which selectively reduces carbonyl groups that act as acceptors in charge-transfer processes. Experiments of this type should be carried out for a broad range of aerosols, including model laboratory systems.

As discussed in section 4.4, imidazoles were found to act as photosensitizers promoting radical chemistry in the aerosol phase and offering an alternative mechanism of SOA generation that does not involve traditional oxidants.[343,344] This implies that, at least, some of the BrC compounds may act as efficient photosensitizers. The photosensitized reactions may produce additional BrC compounds, both in aerosol particles and aqueous droplets. For example, Yu et al.[368] demonstrated the formation of light-absorbing products via the aqueous-phase reaction of syringol with the photochemically excited triplet state of an aromatic carbonyl. Therefore, the atmospheric

DOI: 10.1021/cr5006167
Chem. Rev. 2015, 115, 4335−4382

photosensitized processes, which are only beginning to be explored,[369,370] are inherently related to BrC atmospheric chemistry and should have high priority in the research.

Despite the fact that almost every publication on atmospheric aerosols diligently mentions the health effects of aerosols in the introduction, there have been no systematic experiments probing BrC toxicity. A few of the recent studies have assessed the effects of wood smoke inhalation on human volunteers.[371−373] These studies indicated only mild effects causing irritation of nose and throat and suggested that biomass-burning smoke may be less toxic than diesel exhaust, for instance. However, long-term chronic effects of smoke inhalation are likely significant. The biomass-burning smoke, which serves as a major source of BrC, feasibly shares some similarities to cigarette smoke, the adverse health effects of which have been extensively documented. Therefore, it would be interesting to compare the biological effect of cigarette tar to that of the material in biomass-burning tar balls. Given that a significant fraction of the Earth's population uses indoor biomass burning for cooking purposes, studies probing the health effects of BrC should be given high priority by the international research community.

To better understand and mitigate the effects of BrC on climate and the environment, more experimental, theoretical chemistry, and atmospheric modeling studies are required. These investigations should involve fundamental molecular-level studies of BrC chromophores, including characterization of their chemical composition and optical properties, sources and mechanisms of their formation, and atmospheric degradation. While some phenomenological knowledge in these areas has been accumulated over the past decade from laboratory studies, the overall level of our understanding is insufficient for practical parametrization of BrC properties in atmospheric and climate models. Presently, only limited data exist providing an explicit chemical description of BrC characteristics for different atmospheric environments and emission sources. A common understanding of the most important BrC constituents still is lacking. Before successful BrC parametrization for atmospheric and climate models can be developed, more basic research on BrC chemistry must be conducted to obtain a good grasp of the most important properties and parameters necessary to include in the models. Furthermore, extensive experimental data from both field and laboratory studies are necessary to provide sufficient observations and scientific knowledge for constraining and validating future models.

AUTHOR INFORMATION

Corresponding Authors

*A.L.: e-mail, alexander.laskin@pnnl.gov; phone, +1 509 376-6129; fax, +1 509 376-6139.
*J.L.: e-mail, julia.laskin@pnnl.gov; phone, +1 509 376-6136; fax, +1 509 376-6139.
*S.A.N.: e-mail, nizkorod@uci.edu; phone, +1 949 824-1262; fax, +1 949 824-2420.

Notes

The authors declare no competing financial interest.

Biographies

Alexander Laskin received his undergraduate degree from the Polytechnical Institute, St. Petersburg, Russia, in 1991 in physics and his Ph.D. degree in physical chemistry from the Hebrew University of Jerusalem, in 1998. Following postdoctoral research appointments at the University of Delaware, Princeton University, and Pacific Northwest National Laboratory (PNNL), he became a research scientist at PNNL in 2001. His present and past research interests include the physical and analytical chemistry of aerosols, the environmental and atmospheric effects of aerosols, the chemical imaging and molecular level studies of aerosols, the microspectroscopy and high-resolution mass spectrometry of aerosols, the study of combustion-related aerosols, combustion chemistry, and chemical kinetics.

Julia Laskin received her undergraduate degree in physics from the Polytechnical Institute, St. Petersburg, Russia, in 1990 and her Ph.D. degree in physical chemistry from the Hebrew University of Jerusalem (1998). She was a postdoctoral fellow at the University of Delaware (1998−1999) and PNNL (2000−2002). She became a research scientist at PNNL in 2002. Her research is focused on understanding the activation and dissociation following collisions of complex ions with surfaces, selective surface modification using ion beams, and development of new approaches for characterization of the chemical composition of organic aerosols and imaging of biological materials using mass spectrometry.

DOI: 10.1021/cr5006167
Chem. Rev. 2015, 115, 4335−4382

Sergey Nizkorodov received his undergraduate degree in biochemistry from Novosibirsk State University, Novosibirsk, Russia, in 1993 and graduate degree in chemical physics from Basel University, Basel, Switzerland, in 1997. After doing his postdoctoral research in chemical kinetics and reaction dynamics at the University of Colorado at Boulder and in atmospheric chemistry at the California Institute of Technology, he joined the faculty of the Department of Chemistry, University of California, Irvine, in 2002. He teaches analytical, physical, and atmospheric chemistry courses and does research on the chemistry of particulate matter in the ambient atmosphere and in indoor environments using state-of-the art spectroscopic and mass spectrometric techniques. His primary areas of expertise are molecular spectroscopy, high-resolution mass spectrometry, chemical reaction dynamics, and photochemistry.

ACKNOWLEDGMENTS

The authors gratefully thank the U.S. Department of Commerce, National Oceanic and Atmospheric Administration through the Climate Program Office's AC4 program, awards NA13OAR4310066 (PNNL) and NA13OAR4310062 (UCI), for research support at the time of the manuscript's compilation. Additional support for previous and ongoing research projects in the authors' groups described in this review has been provided by the U.S. Department of Energy's (DOE) Office of Biological and Environmental Research (BER) through its sponsorship of the William R. Wiley Environmental Molecular Sciences Laboratory (EMSL); DOE-BER Atmospheric System Research program (A.L.); DOE's Office of Basic Energy Sciences, Division of Chemical Sciences, Geosciences and Biosciences (J.L.); U.S. National Science Foundation grants AGS-1227579, CHE-0909227, and MRI-0923323 (S.A.N.); Laboratory Directed Research and Development funds of PNNL (A.L.).

GLOSSARY

aqSOA	SOA produced via aqueous chemistry reactions
AAE	absorption Angström exponent
AAOD	absorption aerosol optical depth
ABC	atmospheric brown clouds
AERONET	Aerosol Robotic Network
AMS	aerosol mass spectrometer
AOD	aerosol optical depth
APCI	atmospheric pressure chemical ionization
APPI	atmospheric pressure photoionization
AS	ammonium sulfate
ASAP-MS	atmospheric solids analysis probe mass spectrometry
BBCES	broadband cavity-enhanced spectroscopy
BC	black carbon
BrC	brown carbon
BI	2,2′-biimidazole
CCN	cloud condensation nuclei
CDOM	chromophoric dissolved organic matter
CES	cavity-enhanced spectroscopy
CRD	cavity ring-down
DESI	desorption electrospray ionization
DFT	density functional theory
EC	elemental carbon
EDX	energy-dispersive X-ray (spectroscopy)
EELS	electron energy-loss spectroscopy
EEM	excitation−emission matrix (spectroscopy)
EELS	electron energy loss spectroscopy
EESI	extractive electrospray ionization
EF	emission factor
ESI	electrospray ionization
ELVOC	extremely low volatility organic compound
FTIR	Fourier transform infrared (spectroscopy or spectrometer)
GAMMA	gas−aerosol model for mechanism analysis
GL	glyoxal
GLY	glycine
HPLC	high-performance liquid chromatography
HR-MS	high-resolution mass spectrometry
HULIS	humic-like substances
IBBCEAS	incoherent broadband cavity-enhanced absorption spectroscopy
IC	imidazole carbonyl
IM	imidazole
KLA	keto-limonon-aldehyde
LA	limonon-aldehyde
LC-MS	liquid chromatography mass spectrometry
LSOA	SOA produced by ozonolysis of *d*-limonene
$m = n + ik$	complex refractive index
MAC_{bulk}	mass absorption coefficient (typically measured from solution extracts of PM)
MAC_a	mass-normalized absorption cross section (typically measured using aerosolized particles or particles collected on filters. section 3 explains the difference between MAC_{bulk} and MAC_a)
MAE	mass absorption efficiency, synonym of MAC_a
MG	methyl glyoxal
MSC_a	mass scattering coefficient and mass-normalized scattering cross section
MSE	mass scattering efficiency, synonym of MSC_a
MW	molecular weight
NEXAFS	near-edge fine structure absorption spectroscopy
NMR	nuclear magnetic resonance
OA	organic aerosol
OC	organic carbon
PA	pinon-aldehyde
PAS	photoacoustic spectroscopy
PAM	potential aerosol mass (reactor)
PILS	particle-into-liquid sampler
PM	particulate matter
POA	primary organic aerosol
PSOA	SOA produced by ozonolysis of α-pinene
RH	relative humidity
RFE	radiative-forcing efficiency (closely related to SFE)
SAOD	scattering aerosol optical depth
SFE	simple forcing efficiency (closely related to RFE)

DOI: 10.1021/cr5006167
Chem. Rev. 2015, 115, 4335−4382

SOA	secondary organic aerosol
SOM	secondary organic material
SSA	single scattering albedo
STXM	scanning transmission X-ray microscopy
SVOC	semivolatile organic compound
TEM	transmission electron microscope (or microscopy)
TMB	1,3,5-trimethylbenzene
TOC	total organic carbon
UV−vis	ultraviolet−visible
VOC	volatile organic compound
WSOC	water-soluble organic carbon
WIOC	water-insoluble organic carbon

REFERENCES

(1) Ervens, B.; Turpin, B. J.; Weber, R. J. *Atmos. Chem. Phys.* **2011**, *11*, 11069.
(2) Hallquist, M.; Wenger, J. C.; Baltensperger, U.; Rudich, Y.; Simpson, D.; Claeys, M.; Dommen, J.; Donahue, N. M.; George, C.; Goldstein, A. H.; Hamilton, J. F.; Herrmann, H.; Hoffmann, T.; Iinuma, Y.; Jang, M.; Jenkin, M. E.; Jimenez, J. L.; Kiendler-Scharr, A.; Maenhaut, W.; McFiggans, G.; Mentel, T. F.; Monod, A.; Prevot, A. S. H.; Seinfeld, J. H.; Surratt, J. D.; Szmigielski, R.; Wildt, J. *Atmos. Chem. Phys.* **2009**, *9*, 5155.
(3) Herckes, P.; Valsaraj, K. T.; Collett, J. L. *Atmos. Res.* **2013**, *132*, 434.
(4) Carlton, A. G.; Wiedinmyer, C.; Kroll, J. H. *Atmos. Chem. Phys.* **2009**, *9*, 4987.
(5) Kroll, J. H.; Seinfeld, J. H. *Atmos. Environ.* **2008**, *42*, 3593.
(6) Rudich, Y.; Donahue, N. M.; Mentel, T. F. *Annu. Rev. Phys. Chem.* **2007**, *58*, 321.
(7) Kanakidou, M.; Seinfeld, J. H.; Pandis, S. N.; Barnes, I.; Dentener, F. J.; Facchini, M. C.; Van Dingenen, R.; Ervens, B.; Nenes, A.; Nielsen, C. J.; Swietlicki, E.; Putaud, J. P.; Balkanski, Y.; Fuzzi, S.; Horth, J.; Moortgat, G. K.; Winterhalter, R.; Myhre, C. E. L.; Tsigaridis, K.; Vignati, E.; Stephanou, E. G.; Wilson, J. *Atmos. Chem. Phys.* **2005**, *5*, 1053.
(8) Moosmueller, H.; Chakrabarty, R. K.; Arnott, W. P. *J. Quant. Spectr. Rad. Transfer* **2009**, *110*, 844.
(9) Satheesh, S. K.; Moorthy, K. K. *Atmos. Environ.* **2005**, *39*, 2089.
(10) Yu, H.; Kaufman, Y. J.; Chin, M.; Feingold, G.; Remer, L. A.; Anderson, T. L.; Balkanski, Y.; Bellouin, N.; Boucher, O.; Christopher, S.; DeCola, P.; Kahn, R.; Koch, D.; Loeb, N.; Reddy, M. S.; Schulz, M.; Takemura, T.; Zhou, M. *Atmos. Chem. Phys.* **2006**, *6*, 613.
(11) Bond, T.; Bergstrom, R. *Aerosol Sci. Technol.* **2006**, *40*, 27.
(12) Bond, T. C.; Doherty, S. J.; Fahey, D. W.; Forster, P. M.; Berntsen, T.; DeAngelo, B. J.; Flanner, M. G.; Ghan, S.; Kaercher, B.; Koch, D.; Kinne, S.; Kondo, Y.; Quinn, P. K.; Sarofim, M. C.; Schultz, M. G.; Schulz, M.; Venkataraman, C.; Zhang, H.; Zhang, S.; Bellouin, N.; Guttikunda, S. K.; Hopke, P. K.; Jacobson, M. Z.; Kaiser, J. W.; Klimont, Z.; Lohmann, U.; Schwarz, J. P.; Shindell, D.; Storelvmo, T.; Warren, S. G.; Zender, C. S. *J. Geophys. Res.: Atmos.* **2013**, *118*, 5380.
(13) Venkataraman, C.; Habib, G.; Eiguren-Fernandez, A.; Miguel, A. H.; Friedlander, S. K. *Science* **2005**, *307*, 1454.
(14) Menon, S.; Hansen, J.; Nazarenko, L.; Luo, Y. *Science* **2002**, *297*, 2250.
(15) Ramanathan, V.; Li, F.; Ramana, M. V.; Praveen, P. S.; Kim, D.; Corrigan, C. E.; Nguyen, H.; Stone, E. A.; Schauer, J. J.; Carmichael, G. R.; Adhikary, B.; Yoon, S. C. *J. Geophys. Res.: Atmos.* **2007**, *112*, D22S21.
(16) Feng, Y.; Ramanathan, V.; Kotamarthi, V. R. *Atmos. Chem. Phys.* **2013**, *13*, 8607.
(17) Andreae, M. O.; Gelencser, A. *Atmos. Chem. Phys.* **2006**, *6*, 3131.
(18) Hansen, J.; Sato, M.; Ruedy, R. *J. Geophys. Res.: Atmos.* **1997**, *102*, 6831.
(19) Poschl, U. *Angew. Chem., Int. Ed.* **2005**, *44*, 7520.
(20) Wang, H. *Proc. Combust. Inst.* **2011**, *33*, 41.
(21) Lack, D. A.; Langridge, J. M. *Atmos. Chem. Phys.* **2013**, *13*, 10535.
(22) Moosmueller, H.; Chakrabarty, R. K.; Ehlers, K. M.; Arnott, W. P. *Atmos. Chem. Phys.* **2011**, *11*, 1217.
(23) Bond, T. C.; Zarzycki, C.; Flanner, M. G.; Koch, D. M. *Atmos. Chem. Phys.* **2011**, *11*, 1505.
(24) Ma, X.; Yu, F.; Luo, G. *Atmos. Chem. Phys.* **2012**, *12*, 5563.
(25) Bahadur, R.; Praveen, P. S.; Xu, Y.; Ramanathan, V. *Proc. Natl. Acad. Sci. U. S. A.* **2012**, *109*, 17366.
(26) Chung, C. E.; Ramanathan, V.; Decremer, D. *Proc. Natl. Acad. Sci. U. S. A.* **2012**, *109*, 11624.
(27) Kirchstetter, T. W.; Novakov, T.; Hobbs, P. V. *J. Geophys. Res.: Atmos.* **2004**, *109*, D21208.
(28) Yang, M.; Howell, S. G.; Zhuang, J.; Huebert, B. J. *Atmos. Chem. Phys.* **2009**, *9*, 2035.
(29) Chakrabarty, R. K.; Moosmueller, H.; Chen, L. W. A.; Lewis, K.; Arnott, W. P.; Mazzoleni, C.; Dubey, M. K.; Wold, C. E.; Hao, W. M.; Kreidenweis, S. M. *Atmos. Chem. Phys.* **2010**, *10*, 6363.
(30) Lack, D. A.; Richardson, M. S.; Law, D.; Langridge, J. M.; Cappa, C. D.; McLaughlin, R. J.; Murphy, D. M. *Aerosol Sci. Technol.* **2012**, *46*, 555.
(31) Bond, T. C. *Geophys. Res. Lett.* **2001**, *28*, 4075.
(32) Andreae, M. O.; Crutzen, P. J. *Science* **1997**, *276*, 1052.
(33) Rizzo, L. V.; Artaxo, P.; Mueller, T.; Wiedensohler, A.; Paixao, M.; Cirino, G. G.; Arana, A.; Swietlicki, E.; Roldin, P.; Fors, E. O.; Wiedemann, K. T.; Leal, L. S. M.; Kulmala, M. *Atmos. Chem. Phys.* **2013**, *13*, 2391.
(34) Rizzo, L. V.; Correia, A. L.; Artaxo, P.; Procopio, A. S.; Andreae, M. O. *Atmos. Chem. Phys.* **2011**, *11*, 8899.
(35) Nguyen, T. B.; Lee, P. B.; Updyke, K. M.; Bones, D. L.; Laskin, J.; Laskin, A.; Nizkorodov, S. A. *J. Geophys. Res.: Atmos.* **2012**, *117*, D01207.
(36) De Haan, D. O.; Corrigan, A. L.; Tolbert, M. A.; Jimenez, J. L.; Wood, S. E.; Turley, J. J. *Environ. Sci. Technol.* **2009**, *43*, 8184.
(37) De Haan, D. O.; Hawkins, L. N.; Kononenko, J. A.; Turley, J. J.; Corrigan, A. L.; Tolbert, M. A.; Jimenez, J. L. *Environ. Sci. Technol.* **2011**, *45*, 984.
(38) Lee, A. K. Y.; Zhao, R.; Li, R.; Liggio, J.; Li, S.-M.; Abbatt, J. P. D. *Environ. Sci. Technol.* **2013**, *47*, 12819.
(39) Noziere, B.; Dziedzic, P.; Cordova, A. *Geophys. Res. Lett.* **2007**, *34*, L21812.
(40) Noziere, B.; Esteve, W. *Atmos. Environ.* **2007**, *41*, 1150.
(41) Powelson, M. H.; Espelien, B. M.; Hawkins, L. N.; Galloway, M. M.; De Haan, D. O. *Environ. Sci. Technol.* **2014**, *48*, 985.
(42) Drozd, G. T.; McNeil, V. F. *Environ. Sci.: Processes Impacts* **2014**, *16*, 741.
(43) Bergstrom, R. W.; Russell, P. B.; Hignett, P. *J. Atmos. Sci.* **2002**, *59*, 567.
(44) Lack, D. A.; Cappa, C. D. *Atmos. Chem. Phys.* **2010**, *10*, 4207.
(45) Fuller, K. A.; Malm, W. C.; Kreidenweis, S. M. *J. Geophys. Res.: Atmos.* **1999**, *104*, 15941.
(46) Shiraiwa, M.; Kondo, Y.; Iwamoto, T.; Kita, K. *Aerosol Sci. Technol.* **2010**, *44*, 46.
(47) Adler, G.; Flores, J. M.; Riziq, A. A.; Borrmann, S.; Rudich, Y. *Atmos. Chem. Phys.* **2011**, *11*, 1491.
(48) Wang, X.; Heald, C. L.; Ridley, D. A.; Schwarz, J. P.; Spackman, J. R.; Perring, A. E.; Coe, H.; Liu, D.; Clarke, A. D. *Atmos. Chem. Phys.* **2014**, *14*, 10989.
(49) Jethva, H.; Torres, O. *Atmos. Chem. Phys.* **2011**, *11*, 10541.
(50) Arola, A.; Schuster, G.; Myhre, G.; Kazadzis, S.; Dey, S.; Tripathi, S. N. *Atmos. Chem. Phys.* **2011**, *11*, 215.
(51) Wang, L.; Li, Z.; Tian, Q.; Ma, Y.; Zhang, F.; Zhang, Y.; Li, D.; Li, K.; Li, L. *J. Geophys. Res.: Atmos.* **2013**, *118*, 6534.
(52) Lin, G.; Penner, J. E.; Flanner, M. G.; Sillman, S.; Xu, L.; Zhou, C. *J. Geophys. Res.: Atmos.* **2014**, *119*, 7453.
(53) Jiang, X.; Wiedinmyer, C.; Carlton, A. G. *Environ. Sci. Technol.* **2012**, *46*, 11878.
(54) Li, G.; Bei, N.; Tie, X.; Molina, L. T. *Atmos. Chem. Phys.* **2011**, *11*, 5169.

DOI: 10.1021/cr5006167
Chem. Rev. 2015, 115, 4335−4382

(55) Burling, I. R.; Yokelson, R. J.; Akagi, S. K.; Urbanski, S. P.; Wold, C. E.; Griffith, D. W. T.; Johnson, T. J.; Reardon, J.; Weise, D. R. *Atmos. Chem. Phys.* **2011**, *11*, 12197.
(56) Geron, C.; Hays, M. *Atmos. Environ.* **2013**, *64*, 192.
(57) Hays, M. D.; Geron, C. D.; Linna, K. J.; Smith, N. D.; Schauer, J. J. *Environ. Sci. Technol.* **2002**, *36*, 2281.
(58) McMeeking, G. R.; Kreidenweis, S. M.; Baker, S.; Carrico, C. M.; Chow, J. C.; Collett, J. L., Jr.; Hao, W. M.; Holden, A. S.; Kirchstetter, T. W.; Malm, W. C.; Moosmueller, H.; Sullivan, A. P.; Wold, C. E. *J. Geophys. Res.: Atmos.* **2009**, *114*, D19210.
(59) Aurell, J.; Gullett, B. K. *Environ. Sci. Technol.* **2013**, *47*, 8443.
(60) Saleh, R.; Hennigan, C. J.; McMeeking, G. R.; Chuang, W. K.; Robinson, E. S.; Coe, H.; Donahue, N. M.; Robinson, A. L. *Atmos. Chem. Phys.* **2013**, *13*, 7683.
(61) Graber, E. R.; Rudich, Y. *Atmos. Chem. Phys.* **2006**, *6*, 729.
(62) Mukai, H.; Ambe, Y. *Atmos. Environ.* **1986**, *20*, 813.
(63) Fuzzi, S.; Facchini, M. C.; Decesari, S.; Matta, E.; Mircea, M. *Atmos. Res.* **2002**, *64*, 89.
(64) Claeys, M.; Vermeylen, R.; Yasmeen, F.; Gomez-Gonzalez, Y.; Chi, X. G.; Maenhaut, W.; Meszaros, T.; Salma, I. *Environ. Chem.* **2012**, *9*, 273.
(65) Kahnt, A.; Behrouzi, S.; Vermeylen, R.; Shalamzari, M. S.; Vercauteren, J.; Roekens, E.; Claeys, M.; Maenhaut, W. *Atmos. Environ.* **2013**, *81*, 561.
(66) Lin, P.; Engling, G.; Yu, J. Z. *Atmos. Chem. Phys.* **2010**, *10*, 6487.
(67) Lin, P.; Yu, J. Z.; Engling, G.; Kalberer, M. *Environ. Sci. Technol.* **2012**, *46*, 13118.
(68) Zheng, G. J.; He, K. B.; Duan, F. K.; Cheng, Y.; Ma, Y. L. *Environ. Pollut.* **2013**, *181*, 301.
(69) Liu, J.; Bergin, M.; Guo, H.; King, L.; Kotra, N.; Edgerton, E.; Weber, R. J. *Atmos. Chem. Phys.* **2013**, *13*, 12389.
(70) Capel, P. D.; Gunde, R.; Zurcher, F.; Giger, W. *Environ. Sci. Technol.* **1990**, *24*, 722.
(71) Hoffer, A.; Gelencser, A.; Guyon, P.; Kiss, G.; Schmid, O.; Frank, G. P.; Artaxo, P.; Andreae, M. O. *Atmos. Chem. Phys.* **2006**, *6*, 3563.
(72) Hecobian, A.; Zhang, X.; Zheng, M.; Frank, N.; Edgerton, E. S.; Weber, R. J. *Atmos. Chem. Phys.* **2010**, *10*, 5965.
(73) Paglione, M.; Kiendler-Scharr, A.; Mensah, A. A.; Finessi, E.; Giulianelli, L.; Sandrini, S.; Facchini, M. C.; Fuzzi, S.; Schlag, P.; Piazzalunga, A.; Tagliavini, E.; Henzing, J. S.; Decesari, S. *Atmos. Chem. Phys.* **2014**, *14*, 25.
(74) Salma, I.; Meszaros, T.; Maenhaut, W.; Vass, E.; Majer, Z. *Atmos. Chem. Phys.* **2010**, *10*, 1315.
(75) Lin, P.; Rincon, A. G.; Kalberer, M.; Yu, J. Z. *Environ. Sci. Technol.* **2012**, *46*, 7454.
(76) Stone, E. A.; Hedman, C. J.; Sheesley, R. J.; Shafer, M. M.; Schauer, J. J. *Atmos. Environ.* **2009**, *43*, 4205.
(77) Gao, S.; Surratt, J. D.; Knipping, E. M.; Edgerton, E. S.; Shahgholi, M.; Seinfeld, J. H. *J. Geophys. Res.: Atmos.* **2006**, *111*, D14314.
(78) Cavalli, F.; Facchini, M. C.; Decesari, S.; Mircea, M.; Emblico, L.; Fuzzi, S.; Ceburnis, D.; Yoon, Y. J.; O'Dowd, C. D.; Putaud, J. P.; Dell'Acqua, A. *J. Geophys. Res.: Atmos.* **2004**, *109*, D24215.
(79) Salma, I.; Ocskay, R.; Lang, G. G. *Atmos. Chem. Phys.* **2008**, *8*, 2243.
(80) Dinar, E.; Riziq, A. A.; Spindler, C.; Erlick, C.; Kiss, G.; Rudich, Y. *Faraday Discuss.* **2008**, *137*, 279.
(81) Bergstrom, R. W.; Pilewskie, P.; Russell, P. B.; Redemann, J.; Bond, T. C.; Quinn, P. K.; Sierau, B. *Atmos. Chem. Phys.* **2007**, *7*, 5937.
(82) Sandradewi, J.; Prevot, A. S. H.; Szidat, S.; Perron, N.; Alfarra, M. R.; Lanz, V. A.; Weingartner, E.; Baltensperger, U. *Environ. Sci. Technol.* **2008**, *42*, 3316.
(83) Kirchstetter, T. W.; Thatcher, T. L. *Atmos. Chem. Phys.* **2012**, *12*, 6067.
(84) Chen, Y.; Bond, T. C. *Atmos. Chem. Phys.* **2010**, *10*, 1773.
(85) Schmid, O.; Chand, D.; Karg, E.; Guyon, P.; Frank, G. P.; Swietlicki, E.; Andreae, M. O. *Environ. Sci. Technol.* **2009**, *43*, 1166.
(86) Zhang, X.; Lin, Y.-H.; Surratt, J. D.; Weber, R. J. *Environ. Sci. Technol.* **2013**, *47*, 3685.
(87) Lang-Yona, N.; Abo-Riziq, A.; Erlick, C.; Segre, E.; Trainic, M.; Rudich, Y. *Phys. Chem. Chem. Phys.* **2010**, *12*, 21.
(88) Adachi, K.; Buseck, P. R. *J. Geophys. Res.: Atmos.* **2011**, *116*, D05204.
(89) Alexander, D. T. L.; Crozier, P. A.; Anderson, J. R. *Science* **2008**, *321*, 833.
(90) Chakrabarty, R. K.; Arnold, I. J.; Francisco, D. M.; Hatchett, B.; Hosseinpour, F.; Loria, M.; Pokharel, A.; Woody, B. M. *J. Quant. Spectrosc. Radiat. Transfer* **2013**, *122*, 25.
(91) China, S.; Mazzoleni, C.; Gorkowski, K.; Aiken, A. C.; Dubey, M. K. *Nat. Commun.* **2013**, *4*, 2122.
(92) Hand, J.; Malm, W.; Laskin, A.; Day, D.; Lee, T.; Wang, C.; Carrico, C.; Carrillo, J.; Cowin, J.; Collett, J.; Iedema, M. *J. Geophys. Res.: Atmos.* **2005**, *110*, D21210.
(93) Zhu, J.; Crozier, P. A.; Anderson, J. R. *Atmos. Chem. Phys.* **2013**, *13*, 6359.
(94) Posfai, M.; Gelencser, A.; Simonics, R.; Arato, K.; Li, J.; Hobbs, P. V.; Buseck, P. R. *J. Geophys. Res.: Atmos.* **2004**, *109*, D06213.
(95) Hopkins, R. J.; Tivanski, A. V.; Marten, B. D.; Gilles, M. K. *J. Aerosol Sci.* **2007**, *38*, 573.
(96) Tivanski, A. V.; Hopkins, R. J.; Tyliszczak, T.; Gilles, M. K. *J. Phys. Chem. A* **2007**, *111*, 5448.
(97) Saleh, R.; Robinson, E. S.; Tkacik, D. S.; Ahern, A. T.; Liu, S.; Aiken, A. C.; Sullivan, R. C.; Presto, A. A.; Dubey, M. K.; Yokelson, R. J.; Donahue, N. M.; Robinson, A. L. *Nat. Geosci.* **2014**, *7*, 647.
(98) Donahue, N. M.; Kroll, J. H.; Pandis, S. N.; Robinson, A. L. *Atmos. Chem. Phys.* **2012**, *12*, 615.
(99) Cappa, C. D.; Onasch, T. B.; Massoli, P.; Worsnop, D. R.; Bates, T. S.; Cross, E. S.; Davidovits, P.; Hakala, J.; Hayden, K. L.; Jobson, B. T.; Kolesar, K. R.; Lack, D. A.; Lerner, B. M.; Li, S.-M.; Mellon, D.; Nuaaman, I.; Olfert, J. S.; Petaja, T.; Quinn, P. K.; Song, C.; Subramanian, R.; Williams, E. J.; Zaveri, R. A. *Science* **2012**, *337*, 1078.
(100) Lack, D. A.; Langridge, J. M.; Bahreini, R.; Cappa, C. D.; Middlebrook, A. M.; Schwarz, J. P. *Proc. Natl. Acad. Sci. U. S. A.* **2012**, *109*, 14802.
(101) Lewis, K. A.; Arnott, W. P.; Moosmueller, H.; Chakrabarty, R. K.; Carrico, C. M.; Kreidenweis, S. M.; Day, D. E.; Malm, W. C.; Laskin, A.; Jimenez, J. L.; Ulbrich, I. M.; Huffman, J. A.; Onasch, T. B.; Trimborn, A.; Liu, L.; Mishchenko, M. I. *Atmos. Chem. Phys.* **2009**, *9*, 8949.
(102) Lack, D. A.; Bahreni, R.; Langridge, J. M.; Gilman, J. B.; Middlebrook, A. M. *Atmos. Chem. Phys.* **2013**, *13*, 2415.
(103) Langridge, J. M.; Lack, D.; Brock, C. A.; Bahreini, R.; Middlebrook, A. M.; Neuman, J. A.; Nowak, J. B.; Perring, A. E.; Schwarz, J. P.; Spackman, J. R.; Holloway, J. S.; Pollack, I. B.; Ryerson, T. B.; Roberts, J. M.; Warneke, C.; de Gouw, J. A.; Trainer, M. K.; Murphy, D. M. *J. Geophys. Res.: Atmos.* **2012**, *117*, D00V11.
(104) Zarzana, K. J.; De Haan, D. O.; Freedman, M. A.; Hasenkopf, C. A.; Tolbert, M. A. *Environ. Sci. Technol.* **2012**, *46*, 4845.
(105) Lambe, A. T.; Cappa, C. D.; Massoli, P.; Onasch, T. B.; Forestieri, S. D.; Martin, A. T.; Cummings, M. J.; Croasdale, D. R.; Brune, W. H.; Worsnop, D. R.; Davidovits, P. *Environ. Sci. Technol.* **2013**, *47*, 6349.
(106) Lee, H. J. J.; Aiona, P. K.; Laskin, A.; Laskin, J.; Nizkorodov, S. A. *Environ. Sci. Technol.* **2014**, *48*, 10217.
(107) Romonosky, D.; Laskin, A.; Laskin, J.; Nizkorodov, S. A. *J. Phys. Chem. A* **2015**, article ASAP, DOI:10.1021/jp509476r.
(108) Laskin, J.; Laskin, A.; Nizkorodov, S. A.; Roach, P. J.; Eckert, P.; Gilles, M. K.; Wang, B.; Lee, J.; Hu, Q. *Environ. Sci. Technol.* **2014**, *48*, 12047.
(109) Kampf, C. J.; Jakob, R.; Hoffmann, T. *Atmos. Chem. Phys.* **2012**, *12*, 6323.
(110) Thompson, J. E.; Hayes, P. L.; Jimenez, J. L.; Adachi, K.; Zhang, X.; Liu, J.; Weber, R. J.; Buseck, P. R. *Atmos. Environ.* **2012**, *55*, 190.
(111) Zhong, M.; Jang, M. *Atmos. Chem. Phys.* **2014**, *14*, 1517.

DOI: 10.1021/cr5006167
Chem. Rev. 2015, 115, 4335−4382

(112) Vakkari, V.; Kerminen, V.-M.; Beukes, J. P.; Tiitta, P.; van Zyl, P. G.; Josipovic, M.; Venter, A. D.; Jaars, K.; Worsnop, D. R.; Kulmala, M.; Laakso, L. *Geophys. Res. Lett.* **2014**, *41*, 2644.
(113) Moosmuller, H.; Chakrabarty, R. K. *Atmos. Chem. Phys.* **2011**, *11*, 10677.
(114) Gustafsson, O.; Krusa, M.; Zencak, Z.; Sheesley, R. J.; Granat, L.; Engstrom, E.; Praveen, P. S.; Rao, P. S. P.; Leck, C.; Rodhe, H. *Science* **2009**, *323*, 495.
(115) Ramanathan, V.; Ramana, M. V.; Roberts, G.; Kim, D.; Corrigan, C.; Chung, C.; Winker, D. *Nature* **2007**, *448*, 575.
(116) Ten Hoeve, J. E.; Jacobson, M. Z.; Remer, L. A. *J. Geophys. Res.: Atmos.* **2012**, *117*, D08203.
(117) Park, R. J.; Kim, M. J.; Jeong, J. I.; Youn, D.; Kim, S. *Atmos. Environ.* **2010**, *44*, 1414.
(118) Bonasoni, P.; Laj, P.; Marinoni, A.; Sprenger, M.; Angelini, F.; Arduini, J.; Bonafe, U.; Calzolari, F.; Colombo, T.; Decesari, S.; Di Biagio, C.; di Sarra, A. G.; Evangelisti, F.; Duchi, R.; Facchini, M. C.; Fuzzi, S.; Gobbi, G. P.; Maione, M.; Panday, A.; Roccato, F.; Sellegri, K.; Venzac, H.; Verza, G. P.; Villani, P.; Vuillermoz, E.; Cristofanelli, P. *Atmos. Chem. Phys.* **2010**, *10*, 7515.
(119) Decesari, S.; Facchini, M. C.; Carbone, C.; Giulianelli, L.; Rinaldi, M.; Finessi, E.; Fuzzi, S.; Marinoni, A.; Cristofanelli, P.; Duchi, R.; Bonasoni, P.; Vuillermoz, E.; Cozic, J.; Jaffrezo, J. L.; Laj, P. *Atmos. Chem. Phys.* **2010**, *10*, 4583.
(120) Engling, G.; Zhang, Y.-N.; Chan, C.-Y.; Sang, X.-F.; Lin, M.; Ho, K.-F.; Li, Y.-S.; Lin, C.-Y.; Lee, J. J. *Tellus, Ser. B* **2011**, *63*, 117.
(121) Ram, K.; Sarin, M. M.; Hegde, P. *Atmos. Chem. Phys.* **2010**, *10*, 11791.
(122) Stone, E. A.; Lough, G. C.; Schauer, J. J.; Praveen, P. S.; Corrigan, C. E.; Ramanathan, V. *J. Geophys. Res.: Atmos.* **2007**, *112*, D22S23.
(123) Andreae, M. O.; Schmid, O.; Yang, H.; Chand, D.; Yu, J. Z.; Zeng, L.-M.; Zhang, Y.-H. *Atmos. Environ.* **2008**, *42*, 6335.
(124) Srinivas, B.; Sarin, M. M. *Environ. Res. Lett.* **2013**, *8*, 1748.
(125) Srinivas, B.; Sarin, M. M. *Atmos. Environ.* **2014**, *89*, 835.
(126) Srinivas, B.; Sarin, M. M. *Sci. Total Environ.* **2014**, *487*, 196.
(127) Kirillova, E. N.; Andersson, A.; Han, J.; Lee, M.; Gustafsson, O. *Atmos. Chem. Phys.* **2014**, *14*, 1413.
(128) Kirillova, E. N.; Andersson, A.; Sheesley, R. J.; Krusa, M.; Praveen, P. S.; Budhavant, K.; Safai, P. D.; Rao, P. S. P.; Gustafsson, O. *J. Geophys. Res.: Atmos.* **2013**, *118*, 614.
(129) Mishra, A. K.; Shibata, T. *Atmos. Environ.* **2012**, *57*, 205.
(130) Chakrabarty, R. K.; Pervez, S.; Chow, J. C.; Watson, J. G.; Dewangan, S.; Robles, J.; Tian, G. *Environ. Sci. Technol. Lett.* **2014**, *1*, 44.
(131) Miyazaki, Y.; Kondo, Y.; Han, S.; Koike, M.; Kodama, D.; Komazaki, Y.; Tanimoto, H.; Matsueda, H. *J. Geophys. Res.: Atmos.* **2007**, *112*, D22S30.
(132) Chung, C. E.; Kim, S. W.; Lee, M.; Yoon, S. C.; Lee, S. *Atmos. Chem. Phys.* **2012**, *12*, 6173.
(133) Du, Z.; He, K.; Cheng, Y.; Duan, F.; Ma, Y.; Liu, J.; Zhang, X.; Zheng, M.; Weber, R. *Atmos. Environ.* **2014**, *92*, 514.
(134) Du, Z.; He, K.; Cheng, Y.; Duan, F.; Ma, Y.; Liu, J.; Zhang, X.; Zheng, M.; Weber, R. *Atmos. Environ.* **2014**, *89*, 235.
(135) Cheng, Y.; Engling, G.; He, K. B.; Duan, F. K.; Ma, Y. L.; Du, Z. Y.; Liu, J. M.; Zheng, M.; Weber, R. J. *Atmos. Chem. Phys.* **2013**, *13*, 7765.
(136) Cheng, Y.; He, K. B.; Zheng, M.; Duan, F. K.; Du, Z. Y.; Ma, Y. L.; Tan, J. H.; Yang, F. M.; Liu, J. M.; Zhang, X. L.; Weber, R. J.; Bergin, M. H.; Russell, A. G. *Atmos. Chem. Phys.* **2011**, *11*, 11497.
(137) Cheng, Y.; He, K.-b.; Duan, F.-k.; Du, Z.-y.; Zheng, M.; Ma, Y.-l. *Atmos. Environ.* **2012**, *59*, 551.
(138) Fuzzi, S.; Decesari, S.; Facchini, M. C.; Cavalli, F.; Emblico, L.; Mircea, M.; Andreae, M. O.; Trebs, I.; Hoffer, A.; Guyon, P.; Artaxo, P.; Rizzo, L. V.; Lara, L. L.; Pauliquevis, T.; Maenhaut, W.; Raes, N.; Chi, X.; Mayol-Bracero, O. L.; Soto-Garcia, L. L.; Claeys, M.; Kourtchev, I.; Rissler, J.; Swietlicki, E.; Tagliavini, E.; Schkolnik, G.; Falkovich, A. H.; Rudich, Y.; Fisch, G.; Gatti, L. V. *J. Geophys. Res.: Atmos.* **2007**, *112*, D01201.
(139) Hoffer, A.; Gelencser, A.; Blazso, M.; Guyon, P.; Artaxo, P.; Andreae, M. O. *Atmos. Chem. Phys.* **2006**, *6*, 3505.
(140) Marley, N. A.; Gaffney, J. S.; Castro, T.; Salcido, A.; Frederick, J. *Atmos. Chem. Phys.* **2009**, *9*, 189.
(141) Duong, H. T.; Sorooshian, A.; Craven, J. S.; Hersey, S. P.; Metcalf, A. R.; Zhang, X.; Weber, R. J.; Jonsson, H.; Flagan, R. C.; Seinfeld, J. H. *J. Geophys. Res.: Atmos.* **2011**, *116*, D00V04.
(142) Verma, V.; Rico-Martinez, R.; Kotra, N.; King, L.; Liu, J.; Snell, T. W.; Weber, R. J. *Environ. Sci. Technol.* **2012**, *46*, 11384.
(143) Zhang, X.; Lin, Y.-H.; Surratt, J. D.; Zotter, P.; Prevot, A. S. H.; Weber, R. J. *Geophys. Res. Lett.* **2011**, *38*, L21810.
(144) Zhang, X.; Liu, Z.; Hecobian, A.; Zheng, M.; Frank, N. H.; Edgerton, S.; Weber, R. J. *Atmos. Chem. Phys.* **2012**, *12*, 6593.
(145) Liu, J.; Scheuer, E.; Dibb, J.; Ziemba, L. D.; Thornhill, K. L.; Anderson, B. E.; Wisthaler, A.; Mikoviny, T.; Devi, J. J.; Bergin, M.; Weber, R. J. *Geophys. Res. Lett.* **2014**, *41*, 2191.
(146) Genberg, J.; van der Gon, H. A. C. D.; Simpson, D.; Swietlicki, E.; Areskoug, H.; Beddows, D.; Ceburnis, D.; Fiebig, M.; Hansson, H. C.; Harrison, R. M.; Jennings, S. G.; Saarikoski, S.; Spindler, G.; Visschedijk, A. J. H.; Wiedensohler, A.; Yttri, K. E.; Bergstrom, R. *Atmos. Chem. Phys.* **2013**, *13*, 8719.
(147) Utry, N.; Ajtai, T.; Filep, A.; Pinter, M.; Toeroek, Z.; Bozoki, Z.; Szabo, G. *Atmos. Environ.* **2014**, *91*, 52.
(148) Utry, N.; Ajtai, T.; Filep, A.; Pinter, M. D.; Hoffer, A.; Bozoki, Z.; Szabo, G. *Atmos. Environ.* **2013**, *69*, 321.
(149) Costabile, F.; Barnaba, F.; Angelini, F.; Gobbi, G. P. *Atmos. Chem. Phys.* **2013**, *13*, 2455.
(150) Mladenov, N.; Alados-Arboledas, L.; Olmo, F. J.; Lyamani, H.; Delgado, A.; Molina, A.; Reche, I. *Atmos. Environ.* **2011**, *45*, 1960.
(151) Mogo, S.; Cachorro, V. E.; de Frutos, A. M. *J. Environ. Manage.* **2012**, *111*, 267.
(152) Mogo, S.; Cachorro, V. E.; de Frutos, A.; Rodrigues, A. *J. Environ. Monit.* **2012**, *14*, 3174.
(153) Mohr, C.; Lopez-Hilfiker, F. D.; Zotter, P.; Prevot, A. S. H.; Xu, L.; Ng, N. L.; Herndon, S. C.; Williams, L. R.; Franklin, J. P.; Zahniser, M. S.; Worsnop, D. R.; Knighton, W. B.; Aiken, A. C.; Gorkowski, K. J.; Dubey, M. K.; Allan, J. D.; Thornton, J. A. *Environ. Sci. Technol.* **2013**, *47*, 6316.
(154) McNaughton, C. S.; Clarke, A. D.; Freitag, S.; Kapustin, V. N.; Kondo, Y.; Moteki, N.; Sahu, L.; Takegawa, N.; Schwarz, J. P.; Spackman, J. R.; Watts, L.; Diskin, G.; Podolske, J.; Holloway, J. S.; Wisthaler, A.; Mikoviny, T.; de Gouw, J.; Warneke, C.; Jimenez, J.; Cubison, M.; Howell, S. G.; Middlebrook, A.; Bahreini, R.; Anderson, B. E.; Winstead, E.; Thornhill, K. L.; Lack, D.; Cozic, J.; Brock, C. A. *Atmos. Chem. Phys.* **2011**, *11*, 7561.
(155) Dash, J. G.; Rempel, A. W.; Wettlaufer, J. S. *Rev. Modern Phys.* **2006**, *78*, 695.
(156) Domine, F.; Bock, J.; Voisin, D.; Donaldson, D. J. *J. Phys. Chem. A* **2013**, *117*, 4733.
(157) Domine, F.; Shepson, P. B. *Science* **2002**, *297*, 1506.
(158) Corr, C. A.; Hall, S. R.; Ullmann, K.; Anderson, B. E.; Beyersdorf, A. J.; Thornhill, K. L.; Cubison, M. J.; Jimenez, J. L.; Wisthaler, A.; Dibb, J. E. *Atmos. Chem. Phys.* **2012**, *12*, 10505.
(159) Doherty, S. J.; Warren, S. G.; Grenfell, T. C.; Clarke, A. D.; Brandt, R. E. *Atmos. Chem. Phys.* **2010**, *10*, 11647.
(160) Hegg, D. A.; Warren, S. G.; Grenfell, T. C.; Doherty, S. J.; Clarke, A. D. *Atmos. Chem. Phys.* **2010**, *10*, 10923.
(161) Bohren, C. F.; Huffman, D. R. *Absorption and Scattering of Light by Small Particles*; John Wiley and Sons: New York, 1998.
(162) Lignell, H.; Hinks, M. L.; Nizkorodov, S. A. *Proc. Natl. Acad. Sci. U. S. A.* **2014**, *111*, 13780.
(163) Liu, P.; Zhang, Y.; Martin, S. T. *Environ. Sci. Technol.* **2013**, *47*, 13594.
(164) Weber, R. J.; Orsini, D.; Daun, Y.; Lee, Y. N.; Klotz, P. J.; Brechtel, F. *Aerosol Sci. Technol.* **2001**, *35*, 718.
(165) Sun, H.; Biedermann, L.; Bond, T. C. *Geophys. Res. Lett.* **2007**, *34*, L17813.

DOI: 10.1021/cr5006167
Chem. Rev. 2015, 115, 4335−4382

(166) Finlayson-Pitts, B. J.; Pitts, J. N., Jr. *Chemistry of the Upper and Lower Atmosphere: Theory, Experiments, and Applications*; Academic Press: San Diego, CA, 2000.
(167) Bond, T. C.; Anderson, T. L.; Campbell, D. *Aerosol Sci. Technol.* **1999**, *30*, 582.
(168) Nakayama, T.; Sato, K.; Matsumi, Y.; Imamura, T.; Yamazaki, A.; Uchiyama, A. *Atmos. Chem. Phys.* **2013**, *13*, 531.
(169) Hansen, A. D. A.; Rosen, H.; Novakov, T. *Sci. Total Environ.* **1984**, *36*, 191.
(170) Petzold, A.; Schönlinner, M. *J. Aerosol Sci.* **2004**, *35*, 421.
(171) Massabo, D.; Bernardoni, V.; Bove, M. C.; Brunengo, A.; Cuccia, E.; Piazzalunga, A.; Prati, P.; Valli, G.; Vecchi, R. *J. Aerosol Sci.* **2013**, *60*, 34.
(172) Subramanian, R.; Roden, C. A.; Boparai, P.; Bond, T. C. *Aerosol Sci. Technol.* **2007**, *41*, 630.
(173) Cappa, C. D.; Lack, D. A.; Burkholder, J. B.; Ravishankara, A. R. *Aerosol Sci. Technol.* **2008**, *42*, 1022.
(174) Hitzenberger, R.; Dusek, U.; Berner, A. *J. Geophys. Res.: Atmos.* **1996**, *101*, 19601.
(175) Wonaschütz, A.; Hitzenberger, R.; Bauer, H.; Pouresmaeil, P.; Klatzer, B.; Caseiro, A.; Puxbaum, H. *Environ. Sci. Technol.* **2009**, *43*, 1141.
(176) Zhong, M.; Jang, M. *Atmos. Environ.* **2011**, *45*, 4263.
(177) Montilla, E.; Mogo, S.; Cachorro, V.; de Frutos, A. *J. Aerosol Sci.* **2011**, *42*, 204.
(178) O'Keefe, A.; Scherer, J. J.; Paul, J. B.; Saykally, R. J. *ACS Symp. Ser.* **1999**, *720*, 71.
(179) Sappey, A. D.; Hill, E. S.; Settersten, T.; Linne, M. A. *Opt. Lett.* **1998**, *23*, 954.
(180) Smith, J. D.; Atkinson, D. B. *Analyst* **2001**, *126*, 1216.
(181) Walker, J. S.; Carruthers, A. E.; Orr-Ewing, A. J.; Reid, J. P. *J. Phys. Chem. Lett.* **2013**, *4*, 1748.
(182) Moosmueller, H.; Varma, R.; Arnott, W. *Aerosol Sci. Technol.* **2005**, *39*, 30.
(183) Washenfelder, R. A.; Flores, J. M.; Brock, C. A.; Brown, S. S.; Rudich, Y. *Atmos. Meas. Tech.* **2013**, *6*, 861.
(184) Zhao, W.; Dong, M.; Chen, W.; Gu, X.; Hu, C.; Gao, X.; Huang, W.; Zhang, W. *Anal. Chem.* **2013**, *85*, 2260.
(185) Varma, R. M.; Ball, S. M.; Brauers, T.; Dorn, H. P.; Heitmann, U.; Jones, R. L.; Platt, U.; Pöhler, D.; Ruth, A. A.; Shillings, A. J. L.; Thieser, J.; Wahner, A.; Venables, D. S. *Atmos. Meas. Technol.* **2013**, *6*, 3115.
(186) Heintzenberg, J.; Charlson, R. J. *J. Atmos. Ocean. Technol.* **1996**, *13*, 987.
(187) Ma, L.; Thompson, J. E. *Anal. Chem.* **2012**, *84*, 5611.
(188) Dial, K. D.; Hiemstra, S.; Thompson, J. E. *Anal. Chem.* **2010**, *82*, 7885.
(189) Arnott, W. P.; Moosmüller, H.; Sheridan, P. J.; Ogren, J. A.; Raspet, R.; Slaton, W. V.; Hand, J. L.; Kreidenweis, S. M.; Collett, J. L. *J. Geophys. Res.: Atmos.* **2003**, *108*, 4034.
(190) Lack, D. A.; Lovejoy, E. R.; Baynard, T.; Pettersson, A.; Ravishankara, A. R. *Aerosol Sci. Technol.* **2006**, *40*, 697.
(191) Cross, E. S.; Onasch, T. B.; Ahern, A.; Wrobel, W.; Slowik, J. G.; Olfert, J.; Lack, D. A.; Massoli, P.; Cappa, C. D.; Schwarz, J. P.; Spackman, J. R.; Fahey, D. W.; Sedlacek, A.; Trimborn, A.; Jayne, J. T.; Freedman, A.; Williams, L. R.; Ng, N. L.; Mazzoleni, C.; Dubey, M.; Brem, B.; Kok, G.; Subramanian, R.; Freitag, S.; Clarke, A.; Thornhill, D.; Marr, L. C.; Kolb, C. E.; Worsnop, D. R.; Davidovits, P. *Aerosol Sci. Technol.* **2010**, *44*, 592.
(192) Havey, D. K.; Bueno, P. A.; Gillis, K. A.; Hodges, J. T.; Mulholland, G. W.; van Zee, R. D.; Zachariah, M. R. *Anal. Chem.* **2010**, *82*, 7935.
(193) Langridge, J. M.; Richardson, M. S.; Lack, D. A.; Brock, C. A.; Murphy, D. M. *Aerosol Sci. Technol.* **2013**, *47*, 1163.
(194) Riziq, A. A.; Trainic, M.; Erlick, C.; Segre, E.; Rudich, Y. *Atmos. Chem. Phys.* **2008**, *8*, 1823.
(195) Duarte, R.; Duarte, A. C. *TrAC, Trends Anal. Chem.* **2011**, *30*, 1659.
(196) Laskin, A.; Laskin, J.; Nizkorodov, S. A. *Environ. Chem.* **2012**, *9*, 163.
(197) Laskin, J.; Laskin, A.; Nizkorodov, S. A. *Int. Rev. Phys. Chem.* **2013**, *32*, 128.
(198) Mopper, K.; Stubbins, A.; Ritchie, J. D.; Bialk, H. M.; Hatcher, P. G. *Chem. Rev.* **2007**, *107*, 419.
(199) Nizkorodov, S. A.; Laskin, J.; Laskin, A. *Phys. Chem. Chem. Phys.* **2011**, *13*, 3612.
(200) Pratt, K. A.; Prather, K. A. *Mass Spectrom. Rev.* **2012**, *31*, 1.
(201) Pratt, K. A.; Prather, K. A. *Mass Spectrom. Rev.* **2012**, *31*, 17.
(202) Reemtsma, T. *J. Chromatogr. A* **2009**, *1216*, 3687.
(203) Nozière, B.; Kalberer, M.; Claeys, M.; Allan, J.; D'Anna, B.; Decesari, S.; Finessi, E.; Glasius, M.; Grgić, I.; Hamilton, J.; Hoffmann, T.; Iinuma, Y.; Jaoui, M.; Kahnt, A.; Kampf, K. J.; Kourtchev, I.; Maenhaut, W.; Marsden, N.; Saarikoski, S.; Schnelle-Kreis, J.; Surratt, J. D.; Szidat, S.; Szmigielski, R.; Wisthaler, A. *Chem. Rev.* **2015**, DOI: 10.1021/cr5003485, (accompanying paper in this issue).
(204) Fenn, J. B.; Mann, M.; Meng, C. K.; Wong, S. F.; Whitehouse, C. M. *Mass Spectrom. Rev.* **1990**, *9*, 37.
(205) Byrdwell, W. C. *Lipids* **2001**, *36*, 327.
(206) Robb, D. B.; Covey, T. R.; Bruins, A. P. *Anal. Chem.* **2000**, *72*, 3653.
(207) Takáts, Z.; Wiseman, J. M.; Cooks, R. G. *J. Mass Spectrom.* **2005**, *40*, 1261.
(208) Laskin, J.; Laskin, A.; Roach, P. J.; Slysz, G. W.; Anderson, G. A.; Nizkorodov, S. A.; Bones, D. L.; Nguyen, L. Q. *Anal. Chem.* **2010**, *82*, 2048.
(209) Li, M.; Chen, H.; Wang, B. F.; Yang, X.; Lian, J. J.; Chen, J. M. *Int. J. Mass Spectrom.* **2009**, *281*, 31.
(210) Li, M.; Chen, H.; Yang, X.; Chen, J. M.; Li, C. L. *Atmos. Environ.* **2009**, *43*, 2717.
(211) McEwen, C. N.; McKay, R. G.; Larsen, B. S. *Anal. Chem.* **2005**, *77*, 7826.
(212) Bruns, E. A.; Perraud, V.; Greaves, J.; Finlayson-Pitts, B. J. *Anal. Chem.* **2010**, *82*, 5922.
(213) Roach, P. J.; Laskin, J.; Laskin, A. *Analyst* **2010**, *135*, 2233.
(214) Roach, P. J.; Laskin, J.; Laskin, A. *Anal. Chem.* **2010**, *82*, 7979.
(215) Fuller, S. J.; Zhao, Y.; Cliff, S. S.; Wexler, A. S.; Kalberer, M. *Anal. Chem.* **2012**, *84*, 9858.
(216) Doezema, L. A.; Longin, T.; Cody, W.; Perraud, V.; Dawson, M. L.; Ezell, M. J.; Greaves, J.; Johnson, K. R.; Finlayson-Pitts, B. J. *RSC Adv.* **2012**, *2*, 2930.
(217) Gallimore, P. J.; Kalberer, M. *Environ. Sci. Technol.* **2013**, *47*, 7324.
(218) Kendrick, E. *Anal. Chem.* **1963**, *35*, 2146.
(219) Kind, T.; Fiehn, O. *BMC Bioinf.* **2007**, *8*, 1.
(220) Roach, P. J.; Laskin, J.; Laskin, A. *Anal. Chem.* **2011**, *83*, 4924.
(221) Jayne, J. T.; Leard, D. C.; Zhang, X.; Davidovits, P.; Smith, K. A.; Kolb, C. E.; Worsnop, D. R. *Aerosol Sci. Technol.* **2000**, *33*, 49.
(222) Desyaterik, Y.; Sun, Y.; Shen, X.; Lee, T.; Wang, X.; Wang, T.; Collett, J. L., Jr. *J. Geophys. Res.: Atmos.* **2013**, *118*, 7389.
(223) Kitanovski, Z.; Grgic, I.; Vermeylen, R.; Claeys, M.; Maenhaut, W. *J. Chromatogr. A* **2012**, *1268*, 35.
(224) Nguyen, T. B.; Laskin, A.; Laskin, J.; Nizkorodov, S. A. *Faraday Discuss.* **2013**, *165*, 473.
(225) Iinuma, Y.; Böge, O.; Gräfe, R.; Herrmann, H. *Environ. Sci. Technol.* **2010**, *44*, 8453.
(226) Kitanovski, Z.; Grgic, I.; Yasmeen, F.; Claeys, M.; Cusak, A. *Rapid Commun. Mass Spectrom.* **2012**, *26*, 793.
(227) Yokelson, R. J.; Burling, I. R.; Urbanski, S. P.; Atlas, E. L.; Adachi, K.; Buseck, P. R.; Wiedinmyer, C.; Akagi, S. K.; Toohey, D. W.; Wold, C. E. *Atmos. Chem. Phys.* **2011**, *11*, 6787.
(228) Yokelson, R. J.; Crounse, J. D.; DeCarlo, P. F.; Karl, T.; Urbanski, S.; Atlas, E.; Campos, T.; Shinozuka, Y.; Kapustin, V.; Clarke, A. D.; Weinheimer, A.; Knapp, D. J.; Montzka, D. D.; Holloway, J.; Weibring, P.; Flocke, F.; Zheng, W.; Toohey, D.; Wennberg, P. O.; Wiedinmyer, C.; Mauldin, L.; Fried, A.; Richter, D.; Walega, J.; Jimenez, J. L.; Adachi, K.; Buseck, P. R.; Hall, S. R.; Shetter, R. *Atmos. Chem. Phys.* **2009**, *9*, 5785.

DOI: 10.1021/cr5006167
Chem. Rev. 2015, 115, 4335−4382

(229) Posfai, M.; Buseck, P. R. *Annu. Rev. Earth Planet. Sci.* **2010**, *38*, 17.
(230) Buseck, P. R.; Anderson, J. R. In *Advanced Minerology*; Marfunin, A. S., Ed.; Springer-Verlag: Berlin, 1998; Vol. 3, p 292.
(231) Moffet, R. C.; Roedel, T. C.; Kelly, S. T.; Yu, X. Y.; Carroll, G. T.; Fast, J.; Zaveri, R. A.; Laskin, A.; Gilles, M. K. *Atmos. Chem. Phys.* **2013**, *13*, 10445.
(232) Posfai, M.; Anderson, J. R.; Buseck, P. R.; Sievering, H. *J. Geophys. Res.: Atmos.* **1999**, *104*, 21685.
(233) Moffet, R. C.; Tivanski, A. V.; Gilles, M. K. In *Fundamentals and Applications in Aerosol Spectroscopy*; Signorell, R., Reid, J. P., Eds.; Taylor and Francis Books, Inc.: Philadelphia, PA, 2010; p 419.
(234) Moffet, R. C.; Henn, T. R.; Laskin, A.; Gilles, M. K. *Anal. Chem.* **2010**, *82*, 7906.
(235) Moffet, R. C.; Henn, T. R.; Tivanski, A. V.; Hopkins, R. J.; Desyaterik, Y.; Kilcoyne, A. L. D.; Tyliszczak, T.; Fast, J.; Barnard, J.; Shutthanandan, V.; Cliff, S. S.; Perry, K. D.; Laskin, A.; Gilles, M. K. *Atmos. Chem. Phys.* **2010**, *10*, 961.
(236) Hopkins, R. J.; Lewis, K.; Desyaterik, Y.; Wang, Z.; Tivanski, A. V.; Arnott, W. P.; Laskin, A.; Gilles, M. K. *Geophys. Res. Lett.* **2007**, *34*, L18806.
(237) Hudson, N.; Baker, A.; Reynolds, D. *River Res. Appl.* **2007**, *23*, 631.
(238) Abbt-Braun, G.; Lankes, U.; Frimmel, F. H. *Aquat. Sci.* **2004**, *66*, 151.
(239) Pöhlker, C.; Huffman, J. A.; Pöschl, U. *Atmos. Meas. Technol.* **2012**, *5*, 37.
(240) Birdwell, J. E.; Valsaraj, K. T. *Atmos. Environ.* **2010**, *44*, 3246.
(241) Duarte, R. M. B. O.; Pio, C. A.; Duarte, A. C. *J. Atmos. Chem.* **2004**, *48*, 157.
(242) Nakajima, H.; Okada, K.; Kuroki, Y.; Nakama, Y.; Handa, D.; Arakaki, T.; Tanahara, A. *Atmos. Environ.* **2008**, *42*, 3046.
(243) Phillips, S. M.; Smith, G. D. *Environ. Sci. Technol. Lett.* **2014**, *1*, 382.
(244) Wang, C.; Pan, Y.-L.; James, D.; Wetmore, A. E.; Redding, B. *Anal. Chim. Acta* **2014**, *820*, 119.
(245) Hirst, E.; Kaye, P. H.; Foot, V. E.; Clark, J. M.; Withers, P. B. *Proc. SPIE-Int. Soc. Opt. Eng.* **2004**, *5617*, 416.
(246) Jonsson, P.; Kullander, F.; Vahlberg, C.; Jelger, P.; Tiihonen, M.; Waesterby, P.; Tjaernhage, T.; Lindgren, M. *Proc. SPIE-Int. Soc. Opt. Eng.* **2006**, *6398*, 63980F/1.
(247) Pinnick, R. G.; Hill, S. C.; Nachman, P.; Videen, G.; Chen, G.; Chang, R. K. *Aerosol Sci. Technol.* **1998**, *28*, 95.
(248) Pan, Y.-L.; Hill, S. C.; Pinnick, R. G.; Huang, H.; Bottiger, J. R.; Chang, R. K. *Opt. Express* **2010**, *18*, 12436.
(249) Pinnick, R. G.; Fernandez, E.; Rosen, J. M.; Hill, S. C.; Wang, Y.; Pan, Y. L. *Atmos. Environ.* **2013**, *65*, 195.
(250) Hegglin, M. I.; Krieger, U. K.; Koop, T.; Peter, T. *Aerosol Sci. Technol.* **2002**, *36*, 510.
(251) Rincon, A. G.; Guzman, M. I.; Hoffmann, M. R.; Colussi, A. J. *J. Phys. Chem. A* **2009**, *113*, 10512.
(252) Chang, J. L.; Thompson, J. E. *Atmos. Environ.* **2010**, *44*, 541.
(253) Lee, H. J.; Laskin, A.; Laskin, J.; Nizkorodov, S. A. *Environ. Sci. Technol.* **2013**, *47*, 5763.
(254) Bones, D. L.; Henricksen, D. K.; Mang, S. A.; Gonsior, M.; Bateman, A. P.; Nguyen, T. B.; Cooper, W. J.; Nizkorodov, S. A. *J. Geophys. Res.: Atmos.* **2010**, *115*, D05203.
(255) Lee, H. J.; Aiona, P. K.; Laskin, A.; Laskin, J.; Nizkorodov, S. A. *Environ. Sci. Technol.* **2014**, *48*, 10217.
(256) Sharpless, C. M.; Blough, N. V. *Environ. Sci.: Processes Impacts* **2014**, *16*, 654.
(257) Havers, N.; Burba, P.; Lambert, J.; Klockow, D. *J. Atmos. Chem.* **1998**, *29*, 45.
(258) Varga, B.; Kiss, G.; Ganszky, I.; Gelencsér, A.; Krivácsy, Z. *Talanta* **2001**, *55*, 561.
(259) Duarte, R. M. B. O.; Santos, E. B. H.; Duarte, A. C. *Water Res.* **2003**, *37*, 4073.
(260) Perkampus, H.-H. *UV−VIS Atlas of Organic Compounds*; Wiley & Sons, Inc.: New York, 1996.
(261) Hand, J. L.; Day, D. E.; McMeeking, G. M.; Levin, E. J. T.; Carrico, C. M.; Kreidenweis, S. M.; Malm, W. C.; Laskin, A.; Desyaterik, Y. *Atmos. Chem. Phys.* **2010**, *10*, 6179.
(262) Flores, J. M.; Washenfelder, R. A.; Adler, G.; Lee, H. J.; Segev, L.; Laskin, J.; Laskin, A.; Nizkorodov, S. A.; Brown, S. S.; Rudich, Y. *Phys. Chem. Chem. Phys.* **2014**, *16*, 10629.
(263) Kim, H.; Paulson, S. E. *Atmos. Chem. Phys.* **2013**, *13*, 7711.
(264) Nakayama, T.; Matsumi, Y.; Sato, K.; Imamura, T.; Yamazaki, A.; Uchiyama, A. *J. Geophys. Res.: Atmos.* **2010**, *115*, D24204.
(265) Nakayama, T.; Sato, K.; Matsumi, Y.; Imamura, T.; Yamazaki, A.; Uchiyama, A. *Sola* **2012**, *8*, 1349.
(266) Song, C.; Gyawali, M.; Zaveri, R. A.; Shilling, J. E.; Arnott, W. P. *J. Geophys. Res.: Atmos.* **2013**, *118*, 11.
(267) Noziere, B.; Esteve, W. *Geophys. Res. Lett.* **2005**, *32*, L03812.
(268) Mang, S. A.; Henricksen, D. K.; Bateman, A. P.; Andersen, M. P. S.; Blake, D. R.; Nizkorodov, S. A. *J. Phys. Chem. A* **2008**, *112*, 8337.
(269) Updyke, K. M.; Nguyen, T. B.; Nizkorodov, S. A. *Atmos. Environ.* **2012**, *63*, 22.
(270) Paulot, F.; Crounse, J. D.; Kjaergaard, H. G.; Kuerten, A.; St. Clair, J. M.; Seinfeld, J. H.; Wennberg, P. O. *Science* **2009**, *325*, 730.
(271) Lin, Y.-H.; Zhang, Z.; Docherty, K. S.; Zhang, H.; Budisulistiorini, S. H.; Rubitschun, C. L.; Shaw, S. L.; Knipping, E. M.; Edgerton, E. S.; Kleindienst, T.; Gold, A.; Surratt, J. D. *Environ. Sci. Technol.* **2012**, *46*, 250.
(272) Surratt, J. D.; Chan, A. W. H.; Eddingsaas, N. C.; Chan, M.; Loza, C. L.; Kwan, A. J.; Hersey, S. P.; Flagan, R. C.; Wennberg, P. O.; Seinfeld, J. H. *Proc. Natl. Acad. Sci. U. S. A.* **2010**, *107*, 6640.
(273) Lin, Y.-H.; Budisulistiorini, S. H.; Chu, K.; Siejack, R. A.; Zhang, H.; Riva, M.; Zhang, Z.; Gold, A.; Kautzman, K. E.; Surratt, J. D. *Environ. Sci. Technol.* **2014**, *48*, 12012.
(274) Zhong, M.; Jang, M.; Oliferenko, A.; Pillai, G. G.; Katritzky, A. R. *Phys. Chem. Chem. Phys.* **2012**, *14*, 9058.
(275) Liu, S.; Shilling, J. E.; Song, C.; Hiranuma, N.; Zaveri, R. A.; Russell, L. M. *Aerosol Sci. Technol.* **2012**, *46*, 1359.
(276) Clemitshaw, K. C.; Williams, J.; Rattigan, O. V.; Shallcross, D. E.; Law, K. S.; Cox, R. A. *J. Photochem. Photobiol., A Chem.* **1997**, *102*, 117.
(277) Liu, P. F.; Abdelmalki, N.; Hung, H. M.; Wang, Y.; Brune, W. H.; Martin, S. T. *Atmos. Chem. Phys.* **2015**, *15*, 1435.
(278) Li, K.; Wang, W.; Ge, M.; Li, J.; Wang, D. *Sci. Rep.* **2014**, *4*, 2045.
(279) Ofner, J.; Krueger, H. U.; Grothe, H.; Schmitt-Kopplin, P.; Whitmore, K.; Zetzsch, C. *Atmos. Chem. Phys.* **2011**, *11*, 1.
(280) Ofner, J.; Balzer, N.; Buxmann, J.; Grothe, H.; Schmitt-Kopplin, P.; Platt, U.; Zetzsch, C. *Atmos. Chem. Phys.* **2012**, *12*, 5787.
(281) Jacobson, M. Z. *J. Geophys. Res.: Atmos.* **1999**, *104*, 3527.
(282) Chen, J.; Wenger, J. C.; Venables, D. S. *J. Phys. Chem. A* **2011**, *115*, 12235.
(283) Berndt, T.; Boge, O. *Phys. Chem. Chem. Phys.* **2003**, *5*, 342.
(284) Jang, M. S.; Kamens, R. M. *Environ. Sci. Technol.* **2001**, *35*, 3626.
(285) Sato, K.; Hatakeyama, S.; Imamura, T. *J. Phys. Chem. A* **2007**, *111*, 9796.
(286) Forstner, H. J. L.; Flagan, R. C.; Seinfeld, J. H. *Environ. Sci. Technol.* **1997**, *31*, 1345.
(287) Nishino, N.; Atkinson, R.; Arey, J. *Environ. Sci. Technol.* **2008**, *42*, 9203.
(288) Koch, R.; Knispel, R.; Elend, M.; Siese, M.; Zetzsch, C. *Atmos. Chem. Phys.* **2007**, *7*, 2057.
(289) Zimmermann, K.; Jariyasopit, N.; Simonich, S. L. M.; Tao, S.; Atkinson, R.; Arey, J. *Environ. Sci. Technol.* **2013**, *47*, 8434.
(290) Lu, J. W.; Flores, J. M.; Lavi, A.; Abo-Riziq, A.; Rudich, Y. *Phys. Chem. Chem. Phys.* **2011**, *13*, 6484.
(291) Jaoui, M.; Edney, E. O.; Kleindienst, T. E.; Lewandowski, M.; Offenberg, J. H.; Surratt, J. D.; Seinfeld, J. H. *J. Geophys. Res.: Atmos.* **2008**, *113*, D09303.
(292) Sato, K.; Takami, A.; Kato, Y.; Seta, T.; Fujitani, Y.; Hikida, T.; Shimono, A.; Imamura, T. *Atmos. Chem. Phys.* **2012**, *12*, 4667.
(293) Jang, M.; Kamens, R. M. *Environ. Sci. Technol.* **2001**, *35*, 4758.

DOI: 10.1021/cr5006167
Chem. Rev. 2015, 115, 4335−4382

(294) White, S. J.; Jamie, I. M.; Angove, D. E. *Atmos. Environ.* **2014**, *83*, 237.
(295) Herrmann, H.; Schaefer, T.; Tilgner, A.; Weller, C.; Teich, M.; Styler, S. A. *Chem. Rev.* **2015**, DOI: 10.1021/cr500447k, (accompanying paper in this issue).
(296) Gelencser, A.; Hoffer, A.; Kiss, G.; Tombacz, E.; Kurdi, R.; Bencze, L. *J. Atmos. Chem.* **2003**, *45*, 25.
(297) Hoffer, A.; Kiss, G.; Blazso, M.; Gelencser, A. *Geophys. Res. Lett.* **2004**, *31*, L06115.
(298) Sun, Y. L.; Zhang, Q.; Anastasio, C.; Sun, J. *Atmos. Chem. Phys.* **2010**, *10*, 4809.
(299) Kitanovski, Z.; Čusak, A.; Grgić, I.; Claeys, M. *Atmos. Meas. Technol.* **2014**, *7*, 2457.
(300) Li, Y. J.; Huang, D. D.; Cheung, H. Y.; Lee, A. K. Y.; Chan, C. K. *Atmos. Chem. Phys.* **2014**, *14*, 2871.
(301) Altieri, K. E.; Carlton, A. G.; Lim, H.-J.; Turpin, B. J.; Seitzinger, S. P. *Environ. Sci. Technol.* **2006**, *40*, 4956.
(302) Altieri, K. E.; Seitzinger, S. P.; Carlton, A. G.; Turpin, B. J.; Klein, G. C.; Marshall, A. G. *Atmos. Environ.* **2008**, *42*, 1476.
(303) Perri, M. J.; Seitzinger, S.; Turpin, B. J. *Atmos. Environ.* **2009**, *43*, 1487.
(304) Tan, Y.; Perri, M. J.; Seitzinger, S. P.; Turpin, B. J. *Environ. Sci. Technol.* **2009**, *43*, 8105.
(305) Holmes, B. J.; Petrucci, G. A. *Environ. Sci. Technol.* **2006**, *40*, 4983.
(306) Rincon, A. G.; Guzman, M. I.; Hoffmann, M. R.; Colussi, A. J. *J. Phys. Chem. Lett.* **2010**, *1*, 368.
(307) Smith, J. D.; Sio, V.; Yu, L.; Zhang, Q.; Anastasio, C. *Environ. Sci. Technol.* **2014**, *48*, 1049.
(308) Bateman, A. P.; Nizkorodov, S. A.; Laskin, J.; Laskin, A. *Phys. Chem. Chem. Phys.* **2011**, *13*, 12199.
(309) Nguyen, T. B.; Laskin, A.; Laskin, J.; Nizkorodov, S. A. *Phys. Chem. Chem. Phys.* **2012**, *14*, 9702.
(310) Fu, T.-M.; Jacob, D. J.; Wittrock, F.; Burrows, J. P.; Vrekoussis, M.; Henze, D. K. *J. Geophys. Res.: Atmos.* **2008**, *113*, D15303.
(311) Kawamura, K.; Kasukabe, H.; Barrie, L. A. *Atmos. Environ.* **1996**, *30*, 1709.
(312) Myriokefalitakis, S.; Vrekoussis, M.; Tsigaridis, K.; Wittrock, F.; Richter, A.; Bruehl, C.; Volkamer, R.; Burrows, J. P.; Kanakidou, M. *Atmos. Chem. Phys.* **2008**, *8*, 4965.
(313) Volkamer, R.; Martini, F. S.; Molina, L. T.; Salcedo, D.; Jimenez, J. L.; Molina, M. J. *Geophys. Res. Lett.* **2007**, *34*, L19807.
(314) Volkamer, R.; Platt, U.; Wirtz, K. *J. Phys. Chem. A* **2001**, *105*, 7865.
(315) Betterton, E. A.; Hoffmann, M. R. *Environ. Sci. Technol.* **1988**, *22*, 1415.
(316) Ervens, B.; Volkamer, R. *Atmos. Chem. Phys.* **2010**, *10*, 8219.
(317) Hastings, W. P.; Koehler, C. A.; Bailey, E. L.; De Haan, D. O. *Environ. Sci. Technol.* **2005**, *39*, 8728.
(318) Liggio, J.; Li, S. M.; McLaren, R. *Environ. Sci. Technol.* **2005**, *39*, 1532.
(319) Liggio, J.; Li, S. M.; McLaren, R. *J. Geophys. Res.: Atmos.* **2005**, *110*, D10304.
(320) Noziere, B.; Dziedzic, P.; Cordova, A. *J. Phys. Chem. A* **2009**, *113*, 231.
(321) Galloway, M. M.; Chhabra, P. S.; Chan, A. W. H.; Surratt, J. D.; Flagan, R. C.; Seinfeld, J. H.; Keutsch, F. N. *Atmos. Chem. Phys.* **2009**, *9*, 3331.
(322) Zhou, X.; Mopper, K. *Environ. Sci. Technol.* **1990**, *24*, 1864.
(323) Kroll, J. H.; Ng, N. L.; Murphy, S. M.; Varutbangkul, V.; Flagan, R. C.; Seinfeld, J. H. *J. Geophys. Res.: Atmos.* **2005**, *110*, D23207.
(324) Ip, H. S. S.; Huang, X. H. H.; Yu, J. Z. *Geophys. Res. Lett.* **2009**, *36*, L01802.
(325) Yu, G.; Bayer, A. R.; Galloway, M. M.; Korshavn, K. J.; Fry, C. G.; Keutsch, F. N. *Environ. Sci. Technol.* **2011**, *45*, 6336.
(326) Kampf, C. J.; Waxman, E. M.; Slowik, J. G.; Dommen, J.; Pfaffenberger, L.; Praplan, A. P.; Prevot, A. S. H.; Baltensperger, U.; Hoffmann, T.; Volkamer, R. *Environ. Sci. Technol.* **2013**, *47*, 4236.
(327) Loeffler, K. W.; Koehler, C. A.; Paul, N. M.; De Haan, D. O. *Environ. Sci. Technol.* **2006**, *40*, 6318.
(328) Noziere, B.; Dziedzic, P.; Cordova, A. *Phys. Chem. Chem. Phys.* **2010**, *12*, 3864.
(329) Shapiro, E. L.; Szprengiel, J.; Sareen, N.; Jen, C. N.; Giordano, M. R.; McNeill, V. F. *Atmos. Chem. Phys.* **2009**, *9*, 2289.
(330) Carlton, A. G.; Turpin, B. J.; Altieri, K. E.; Seitzinger, S.; Reff, A.; Lim, H.-J.; Ervens, B. *Atmos. Environ.* **2007**, *41*, 7588.
(331) Connelly, B. M.; De Haan, D. O.; Tolbert, M. A. *J. Phys. Chem. A* **2012**, *116*, 6180.
(332) Crahan, K. K.; Hegg, D.; Covert, D. S.; Jonsson, H. *Atmos. Environ.* **2004**, *38*, 3757.
(333) Ervens, B.; Feingold, G.; Frost, G. J.; Kreidenweis, S. M. *J. Geophys. Res.: Atmos.* **2004**, *109*, D15205.
(334) De Haan, D. O.; Corrigan, A. L.; Smith, K. W.; Stroik, D. R.; Turley, J. J.; Lee, F. E.; Tolbert, M. A.; Jimenez, J. L.; Cordova, K. E.; Ferrell, G. R. *Environ. Sci. Technol.* **2009**, *43*, 2818.
(335) Tong, C. H.; Blanco, M.; Goddard, W. A.; Seinfeld, J. H. *Environ. Sci. Technol.* **2006**, *40*, 2333.
(336) Kua, J.; Krizner, H. E.; De Haan, D. O. *J. Phys. Chem. A* **2011**, *115*, 1667.
(337) De Haan, D. O.; Tolbert, M. A.; Jimenez, J. L. *Geophys. Res. Lett.* **2009**, *36*, L11819.
(338) Yasmeen, F.; Sauret, N.; Gal, J. F.; Maria, P. C.; Massi, L.; Maenhaut, W.; Claeys, M. *Atmos. Chem. Phys.* **2010**, *10*, 3803.
(339) Krizner, H. E.; De Haan, D. O.; Kua, J. *J. Phys. Chem. A* **2009**, *113*, 6994.
(340) Noziere, B.; Cordova, A. *J. Phys. Chem. A* **2008**, *112*, 2827.
(341) Sareen, N.; Schwier, A. N.; Shapiro, E. L.; Mitroo, D.; McNeill, V. F. *Atmos. Chem. Phys.* **2010**, *10*, 997.
(342) Maxut, A.; Fenet, B.; Mechakra, H.; Noziere, B. *Green Chem.* **2014**, submitted.
(343) Aregahegn, K. Z.; Noziere, B.; George, C. *Faraday Discuss.* **2013**, *165*, 123.
(344) Rossignol, S.; Aregahegn, K. Z.; Tinel, L.; Fine, L.; Noziere, B.; George, C. *Environ. Sci. Technol.* **2014**, *48*, 3218.
(345) Trainic, M.; Riziq, A. A.; Lavi, A.; Flores, J. M.; Rudich, Y. *Atmos. Chem. Phys.* **2011**, *11*, 9697.
(346) Trainic, M.; Riziq, A. A.; Lavi, A.; Rudich, Y. *J. Phys. Chem. A* **2012**, *116*, 5948.
(347) Kua, J.; Hanley, S. W.; De Haan, D. O. *J. Phys. Chem. A* **2008**, *112*, 66.
(348) Schwier, A. N.; Sareen, N.; Mitroo, D.; Shapiro, E. L.; McNeill, V. F. *Environ. Sci. Technol.* **2010**, *44*, 6174.
(349) Galloway, M. M.; Loza, C. L.; Chhabra, P. S.; Chan, A. W. H.; Yee, L. D.; Seinfeld, J. H.; Keutsch, F. N. *Geophys. Res. Lett.* **2011**, *38*, L17811.
(350) Sedehi, N.; Takano, H.; Blasic, V. A.; Sullivan, K. A.; De Haan, D. O. *Atmos. Environ.* **2013**, *77*, 656.
(351) Volkamer, R.; Ziemann, P. J.; Molina, M. J. *Atmos. Chem. Phys.* **2009**, *9*, 1907.
(352) Hamilton, J. F.; Baeza-Romero, M. T.; Finessi, E.; Rickard, A. R.; Healy, R. M.; Peppe, S.; Adams, T. J.; Daniels, M. J. S.; Ball, S. M.; Goodall, I. C. A.; Monks, P. S.; Borras, E.; Munoz, A. *Faraday Discuss.* **2013**, *165*, 447.
(353) Tang, I. N.; Munkelwitz, H. R. *J. Geophys. Res.: Atmos.* **1994**, *99*, 18801.
(354) Chan, M. N.; Choi, M. Y.; Ng, N. L.; Chan, C. K. *Environ. Sci. Technol.* **2005**, *39*, 1555.
(355) Corrigan, A. L.; Hanley, S. W.; De Haan, D. O. *Environ. Sci. Technol.* **2008**, *42*, 4428.
(356) Ortiz-Montalvo, D. L.; Hakkinen, S. A. K.; Schwier, A. N.; Lim, Y. B.; McNeill, V. F.; Turpin, B. J. *Environ. Sci. Technol.* **2014**, *48*, 255.
(357) McNeill, V. F.; Woo, J. L.; Kim, D. D.; Schwier, A. N.; Wannell, N. J.; Sumner, A. J.; Barakat, J. M. *Environ. Sci. Technol.* **2012**, *46*, 8075.
(358) Hawkins, L. N.; Baril, M. J.; Sedehi, N.; Galloway, M. M.; De Haan, D. O.; Schill, G. P.; Tolbert, M. A. *Environ. Sci. Technol.* **2014**, *48*, 2273.

DOI: 10.1021/cr5006167
Chem. Rev. 2015, 115, 4335−4382

(359) Schill, G. P.; De Haan, D. O.; Tolbert, M. A. *Environ. Sci. Technol.* **2014**, *48*, 1675.
(360) Sareen, N.; Moussa, S. G.; McNeill, V. F. *J. Phys. Chem. A* **2013**, *117*, 2987.
(361) Woo, J. L.; Kim, D. D.; Schwier, A. N.; Li, R. Z.; McNeill, V. F. *Faraday Discuss.* **2013**, *165*, 357.
(362) Paredes-Miranda, G.; Arnott, W. P.; Jimenez, J. L.; Aiken, A. C.; Gaffney, J. S.; Marley, N. A. *Atmos. Chem. Phys.* **2009**, *9*, 3721.
(363) Laskin, J.; Eckert, P. A.; Roach, P. J.; Heath, B. S.; Nizkorodov, S. A.; Laskin, A. *Anal. Chem.* **2012**, *84*, 7179.
(364) Li, Y. Q.; Schwab, J. J.; Demerjian, K. L. *J. Geophys. Res.: Atmos.* **2006**, *111*, D10s02.
(365) Griffith, D. W. T.; Mankin, W. G.; Coffey, M. T.; Ward, D. E.; Riebau, A. In *Global Biomass Burning: Atmospheric, Climatic and Biospheric Implications*; Levine, J. S., Ed.; MIT Press: Cambridge, MA, 1991; p 230.
(366) Koop, T.; Bookhold, J.; Shiraiwa, M.; Poeschl, U. *Phys. Chem. Chem. Phys.* **2011**, *13*, 19238.
(367) You, Y.; Smith, M. L.; Song, M.; Martin, S. T.; Bertram, A. K. *Int. Rev. Phys. Chem.* **2014**, *33*, 43.
(368) Yu, L.; Smith, J.; Laskin, A.; Anastasio, C.; Laskin, J.; Zhang, Q. *Atmos. Chem. Phys.* **2014**, *14*, 13801.
(369) George, C.; D'Anna, B.; Herrmann, H.; Weller, C.; Vaida, V.; Donaldson, D. J.; Bartels-Rausch, T.; Ammann, M. In *Atmospheric and Aerosol Chemistry*; McNeill, V. F., Ariya, P. A., Eds.; Springer: New York, 2014; Vol. *339*, p 1.
(370) George, C.; Ammann, M.; D'Anna, B.; Donaldson, D. J.; Nizkorodov, S. A. *Chem. Rev.* **2015**, DOI: 10.1021/cr500648z, (accompanying paper in this issue).
(371) Bonlokke, J. H.; Riddervold, I. S.; Gronborg, T. K.; Skogstrand, K.; Hougaard, D. M.; Barregard, L.; Sigsgaard, T. *J. Occup. Environ. Med.* **2014**, *56*, 177.
(372) Forchhammer, L.; M?ller, P.; Riddervold, I. S.; Bonlokke, J.; Massling, A.; Sigsgaard, T.; Loft, S. *Part. Fibre Toxicol.* **2012**, *9*, 1743.
(373) Riddervold, I. S.; Bonlokke, J. H.; Olin, A.-C.; Gronborg, T. K.; Schlunssen, V.; Skogstrand, K.; Hougaard, D.; Massling, A.; Sigsgaard, T. *Part. Fibre Toxicol.* **2012**, *9*, 1743.
(374) van Pinxteren, D.; Plewka, A.; Hofmann, D.; Muller, K.; Kramberger, H.; Svrcina, B.; Bachmann, K.; Jaeschke, W.; Mertes, S.; Collett, J. L.; Herrmann, H. *Atmos. Environ.* **2005**, *39*, 4305.
(375) Igawa, M.; Munger, J. W.; Hoffmann, M. R. *Environ. Sci. Technol.* **1989**, *23*, 556.
(376) Matsunaga, S.; Mochida, M.; Kawamura, K. *J. Geophys. Res.: Atmos.* **2004**, *109*, D04302.
(377) Munger, J. W.; Jacob, D. J.; Daube, B. C.; Horowitz, L. W.; Keene, W. C.; Heikes, B. G. *J. Geophys. Res.: Atmos.* **1995**, *100*, 9325.
(378) Matsumoto, K.; Kawai, S.; Igawa, M. *Atmos. Environ.* **2005**, *39*, 7321.
(379) Mopper, K.; Zika, R. G. *Nature* **1987**, *325*, 246.
(380) Matsumoto, K.; Uematsu, M. *Atmos. Environ.* **2005**, *39*, 2163.
(381) Zhang, Q.; Anastasio, C. *Atmos. Environ.* **2003**, *37*, 2247.

DOI: 10.1021/cr5006167
Chem. Rev. 2015, 115, 4335−4382